



ISSN 2686-7575 (Online)

ТОНКИЕ ХИМИЧЕСКИЕ ТЕХНОЛОГИИ

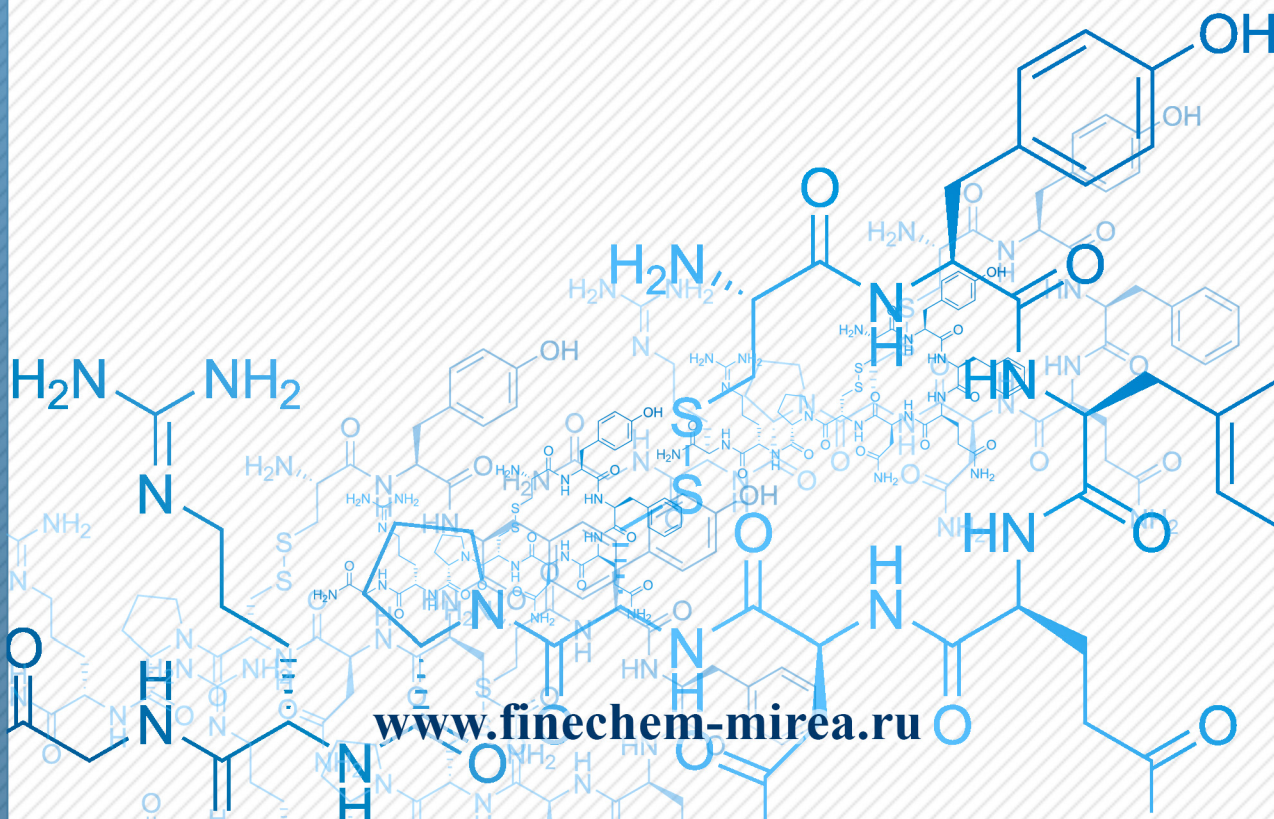
Fine Chemical Technologies

- | Theoretical Bases of Chemical Technology
- | Chemistry and Technology of Organic Substances
- | Chemistry and Technology of Medicinal Compounds and Biologically Active Substances
- | Biochemistry and Biotechnology
- | Synthesis and Processing of Polymers and Polymeric Composites
- | Chemistry and Technology of Inorganic Materials
- | Analytical Methods in Chemistry and Chemical Technology
- | Mathematical Methods and Information Systems in Chemical Technology

18(6)

2023

www.finechem-mirea.ru





ISSN 2686-7575 (Online)

ТОНКИЕ ХИМИЧЕСКИЕ ТЕХНОЛОГИИ

Fine Chemical Technologies

- | Theoretical Bases of Chemical Technology
- | Chemistry and Technology of Organic Substances
- | Chemistry and Technology of Medicinal Compounds and Biologically Active Substances
- | Biochemistry and Biotechnology
- | Synthesis and Processing of Polymers and Polymeric Composites
- | Chemistry and Technology of Inorganic Materials
- | Analytical Methods in Chemistry and Chemical Technology
- | Mathematical Methods and Information Systems in Chemical Technology

Tonkie Khimicheskie Tekhnologii =
Fine Chemical Technologies
Vol. 18, No. 6, 2023

Тонкие химические технологии =
Fine Chemical Technologies
Том 18, № 6, 2023

<https://doi.org/10.32362/2410-6593-2023-18-6>
www.finechem-mirea.ru

The peer-reviewed scientific and technical journal *Fine Chemical Technologies* highlights the modern achievements of fundamental and applied research in the field of fine chemical technologies, including theoretical bases of chemical technology, chemistry and technology of medicinal compounds and biologically active substances, organic substances and inorganic materials, biochemistry and biotechnology, synthesis and processing of polymers and polymeric composites, analytical and mathematical methods and information systems in chemistry and chemical technology.

Founder and Publisher

Federal State Budget
Educational Institution of Higher Education
“MIREA – Russian Technological University”
78, Vernadskogo pr., Moscow, 119454, Russian Federation.
Publication frequency: bimonthly.
The journal was founded in 2006. The name was *Vestnik MITHT* until 2015 (ISSN 1819-1487).

The journal is included into the List of peer-reviewed science press of the State Commission for Academic Degrees and Titles of the Russian Federation.

The journal is indexed:
SCOPUS, DOAJ, Chemical Abstracts, Science Index, RSCI, Ulrich's International Periodicals Directory

Editor-in-Chief:

Andrey V. Timoshenko – Dr. Sci. (Eng.), Cand. Sci. (Chem.),
Professor, MIREA – Russian Technological University,
Moscow, Russian Federation. Scopus Author ID 56576076700,
ResearcherID Y-8709-2018,
<https://orcid.org/0000-0002-6511-7440>,
timoshenko@mirea.ru

Deputy Editor-in-Chief:

Valery V. Fomichev – Dr. Sci. (Chem.), Professor,
MIREA – Russian Technological University, Moscow,
Russian Federation. Scopus Author ID 57196028937,
<http://orcid.org/0000-0003-4840-0655>,
fomichev@mirea.ru

Executive Editor:

Sergey A. Durakov – Cand. Sci. (Chem.), Associate Professor,
MIREA – Russian Technological University, Moscow,
Russian Federation, Scopus Author ID 57194217518,
ResearcherID AAS-6578-2020, <http://orcid.org/0000-0003-4842-3283>,
durakov@mirea.ru

Editorial staff:

Managing Editor Cand. Sci. (Eng.) Galina D. Seredina
Science editors Dr. Sci. (Chem.), Prof. Tatyana M. Buslaeva
Dr. Sci. (Chem.), Prof. Anatolii A. Ischenko
Dr. Sci. (Eng.), Prof. Anatolii V. Markov
Dr. Sci. (Chem.), Prof. Yuri P. Miroshnikov
Dr. Sci. (Chem.), Prof. Vladimir A. Tverskoy
Desktop publishing Larisa G. Semernya

86, Vernadskogo pr., Moscow, 119571, Russian Federation.
Phone: +7 (499) 600-80-80 (#31288)
E-mail: seredina@mirea.ru

The registration number ПИ № ФС 77–74580 was issued in December 14, 2018 by the Federal Service for Supervision of Communications, Information Technology, and Mass Media of Russia.

The subscription index of *Pressa Rossii*: **36924**

Научно-технический рецензируемый журнал «Тонкие химические технологии» освещает современные достижения фундаментальных и прикладных исследований в области тонких химических технологий, включая теоретические основы химической технологии, химию и технологию лекарственных препаратов и биологически активных соединений, органических веществ и неорганических материалов, биохимию и биотехнологию, синтез и переработку полимеров и композитов на их основе, аналитические и математические методы и информационные системы в химии и химической технологии.

Учредитель и издатель

федеральное государственное бюджетное
образовательное учреждение высшего образования
«МИРЭА – Российский технологический университет»
119454, РФ, Москва, пр-т Вернадского, д. 78.
Периодичность: один раз в два месяца.
Журнал основан в 2006 году. До 2015 года издавался под названием «Вестник МИТХТ» (ISSN 1819-1487).

Журнал входит в Перечень ведущих рецензируемых научных журналов ВАК РФ.

Индексируется:

SCOPUS, DOAJ, Chemical Abstracts,
РИНЦ (Science Index), RSCI,
Ulrich's International Periodicals Directory

Главный редактор:

Тимошенко Андрей Всеволодович – д.т.н., к.х.н.,
профессор, МИРЭА – Российский технологический университет,
Москва, Российская Федерация. Scopus Author ID 56576076700,
ResearcherID Y-8709-2018,
<https://orcid.org/0000-0002-6511-7440>,
timoshenko@mirea.ru

Заместитель главного редактора:

Фомичёв Валерий Вячеславович – д.х.н., профессор,
МИРЭА – Российский технологический университет, Москва,
Российская Федерация. Scopus Author ID 57196028937,
<http://orcid.org/0000-0003-4840-0655>,
fomichev@mirea.ru

Выпускающий редактор:

Дураков Сергей Алексеевич – к.х.н., доцент,
МИРЭА – Российский технологический университет, Москва,
Российская Федерация, Scopus Author ID 57194217518,
ResearcherID AAS-6578-2020, <http://orcid.org/0000-0003-4842-3283>,
durakov@mirea.ru

Редакция:

Зав. редакцией к.т.н. Г.Д. Середина
Научные редакторы д.х.н., проф. Т.М. Буслаева
д.х.н., проф. А.А. Ищенко
д.т.н., проф. А.В. Марков
д.х.н., проф. Ю.П. Мирошников
д.х.н., проф. В.А. Тверской

Компьютерная верстка Л.Г. Семерня

119571, Москва, пр. Вернадского, 86, оф. Л-119.
Тел.: +7 (499) 600-80-80 (#31288)
E-mail: seredina@mirea.ru

Регистрационный номер и дата принятия решения о регистрации СМИ: ПИ № ФС 77-74580 от 14.12.2018 г. СМИ зарегистрировано Федеральной службой по надзору в сфере связи, информационных технологий и массовых коммуникаций (Роскомнадзор).

Индекс по Объединенному каталогу «Пресса России»: **36924**

Editorial Board

Andrey V. Blokhin – Dr. Sci. (Chem.), Professor, Belarusian State University, Minsk, Belarus. Scopus Author ID 7101971167, ResearcherID AAF-8122-2019 <https://orcid.org/0000-0003-4778-5872> blokhin@bsu.by.

Sergey P. Verevkin – Dr. Sci. (Eng.), Professor, University of Rostock, Rostock, Germany. Scopus Author ID 7006607848, ResearcherID G-3243-2011, <https://orcid.org/0000-0002-0957-5594>, sergey.verevkin@uni-rostock.de.

Konstantin Yu. Zhizhin – Corresponding Member of the Russian Academy of Sciences (RAS), Dr. Sci. (Chem.), Professor, N.S. Kurnakov Institute of General and Inorganic Chemistry of the RAS, Moscow, Russian Federation. Scopus Author ID 6701495620, ResearcherID C-5681-2013, <http://orcid.org/0000-0002-4475-124X>, kyuzhizhin@igic.ras.ru.

Igor V. Ivanov – Dr. Sci. (Chem.), Professor, MIREA – Russian Technological University, Moscow, Russian Federation. Scopus Author ID 34770109800, ResearcherID I-5606-2016, <http://orcid.org/0000-0003-0543-2067>, ivanov_i@mirea.ru.

Carlos A. Cardona – PhD (Eng.), Professor, National University of Columbia, Manizales, Colombia. Scopus Author ID 7004278560, <http://orcid.org/0000-0002-0237-2313>, ccardonaal@unal.edu.co.

Oskar I. Koifman – Academician at the RAS, Dr. Sci. (Chem.), Professor, President of the Ivanovo State University of Chemistry and Technology, Ivanovo, Russian Federation. Scopus Author ID 6602070468, ResearcherID R-1020-2016, <http://orcid.org/0000-0002-1764-0819>, president@isuct.ru.

Elvira T. Krut'ko – Dr. Sci. (Eng.), Professor, Belarusian State Technological University, Minsk, Belarus. Scopus Author ID 6602297257, ela_krutko@mail.ru.

Anatolii I. Miroshnikov – Academician at the RAS, Dr. Sci. (Chem.), Professor, M.M. Shemyakin and Yu.A. Ovchinnikov Institute of Bioorganic Chemistry of the RAS, Member of the Presidium of the RAS, Chairman of the Presidium of the RAS Pushchino Research Center, Moscow, Russian Federation. Scopus Author ID 7006592304, ResearcherID G-5017-2017, aiv@ibch.ru.

Aziz M. Muzafarov – Academician at the RAS, Dr. Sci. (Chem.), Professor, A.N. Nesmeyanov Institute of Organoelement Compounds of the RAS, Moscow, Russian Federation. Scopus Author ID 7004472780, ResearcherID G-1644-2011, <https://orcid.org/0000-0002-3050-3253>, aziz@ineos.ac.ru.

Редакционная коллегия

Блохин Андрей Викторович – д.х.н., профессор Белорусского государственного университета, Минск, Беларусь. Scopus Author ID 7101971167, ResearcherID AAF-8122-2019 <https://orcid.org/0000-0003-4778-5872> blokhin@bsu.by.

Верёвкин Сергей Петрович – д.т.н., профессор Университета г. Росток, Росток, Германия. Scopus Author ID 7006607848, ResearcherID G-3243-2011, <https://orcid.org/0000-0002-0957-5594>, sergey.verevkin@uni-rostock.de.

Жижин Константин Юрьевич – член-корр. Российской академии наук (РАН), д.х.н., профессор, Институт общей и неорганической химии им. Н.С. Курнакова РАН, Москва, Российская Федерация. Scopus Author ID 6701495620, ResearcherID C-5681-2013, <http://orcid.org/0000-0002-4475-124X>, kyuzhizhin@igic.ras.ru.

Иванов Игорь Владимирович – д.х.н., профессор, МИРЭА – Российский технологический университет, Москва, Российская Федерация. Scopus Author ID 34770109800, ResearcherID I-5606-2016, <http://orcid.org/0000-0003-0543-2067>, ivanov_i@mirea.ru.

Кардона Карлос Ариэль – PhD, профессор Национального университета Колумбии, Манизалес, Колумбия. Scopus Author ID 7004278560, <http://orcid.org/0000-0002-0237-2313>, ccardonaal@unal.edu.co.

Койфман Оскар Иосифович – академик РАН, д.х.н., профессор, президент Ивановского государственного химико-технологического университета, Иваново, Российская Федерация. Scopus Author ID 6602070468, ResearcherID R-1020-2016, <http://orcid.org/0000-0002-1764-0819>, president@isuct.ru.

Крутько Эльвира Тихоновна – д.т.н., профессор Белорусского государственного технологического университета, Минск, Беларусь. Scopus Author ID 6602297257, ela_krutko@mail.ru.

Мирошников Анатолий Иванович – академик РАН, д.х.н., профессор, Институт биоорганической химии им. академиков М.М. Шемякина и Ю.А. Овчинникова РАН, член Президиума РАН, председатель Президиума Пушкинского научного центра РАН, Москва, Российская Федерация. Scopus Author ID 7006592304, ResearcherID G-5017-2017, aiv@ibch.ru.

Музафаров Азиз Мансурович – академик РАН, д.х.н., профессор, Институт элементоорганических соединений им. А.Н. Несмеянова РАН, Москва, Российская Федерация. Scopus Author ID 7004472780, ResearcherID G-1644-2011, <https://orcid.org/0000-0002-3050-3253>, aziz@ineos.ac.ru.

Ivan A. Novakov – Academician at the RAS, Dr. Sci. (Chem.), Professor, President of the Volgograd State Technical University, Volgograd, Russian Federation. Scopus Author ID 7003436556, ResearcherID I-4668-2015, <http://orcid.org/0000-0002-0980-6591>, president@vstu.ru.

Alexander N. Ozerin – Corresponding Member of the RAS, Dr. Sci. (Chem.), Professor, Enikolopov Institute of Synthetic Polymeric Materials of the RAS, Moscow, Russian Federation. Scopus Author ID 7006188944, ResearcherID J-1866-2018, <https://orcid.org/0000-0001-7505-6090>, ozerin@ispm.ru.

Tapani A. Pakkanen – PhD, Professor, Department of Chemistry, University of Eastern Finland, Joensuu, Finland. Scopus Author ID 7102310323, tapani.pakkanen@uef.fi.

Armando J.L. Pombeiro – Academician at the Academy of Sciences of Lisbon, PhD, Professor, President of the Center for Structural Chemistry of the Higher Technical Institute of the University of Lisbon, Lisbon, Portugal. Scopus Author ID 7006067269, ResearcherID I-5945-2012, <https://orcid.org/0000-0001-8323-888X>, pombeiro@ist.utl.pt.

Dmitrii V. Pyshnyi – Corresponding Member of the RAS, Dr. Sci. (Chem.), Professor, Institute of Chemical Biology and Fundamental Medicine, Siberian Branch of the RAS, Novosibirsk, Russian Federation. Scopus Author ID 7006677629, ResearcherID F-4729-2013, <https://orcid.org/0000-0002-2587-3719>, pyshnyi@niboch.nsc.ru.

Alexander S. Sigov – Academician at the RAS, Dr. Sci. (Phys. and Math.), Professor, President of MIREA – Russian Technological University, Moscow, Russian Federation. Scopus Author ID 35557510600, ResearcherID L-4103-2017, sigov@mirea.ru.

Alexander M. Toikka – Dr. Sci. (Chem.), Professor, Institute of Chemistry, Saint Petersburg State University, St. Petersburg, Russian Federation. Scopus Author ID 6603464176, ResearcherID A-5698-2010, <http://orcid.org/0000-0002-1863-5528>, a.toikka@spbu.ru.

Andrzej W. Trochimczuk – Dr. Sci. (Chem.), Professor, Faculty of Chemistry, Wrocław University of Science and Technology, Wrocław, Poland. Scopus Author ID 7003604847, andrzej.trochimczuk@pwr.edu.pl.

Aslan Yu. Tsivadze – Academician at the RAS, Dr. Sci. (Chem.), Professor, A.N. Frumkin Institute of Physical Chemistry and Electrochemistry of the RAS, Moscow, Russian Federation. Scopus Author ID 7004245066, ResearcherID G-7422-2014, tsiv@phych.ac.ru.

Новаков Иван Александрович – академик РАН, д.х.н., профессор, президент Волгоградского государственного технического университета, Волгоград, Российская Федерация. Scopus Author ID 7003436556, ResearcherID I-4668-2015, <http://orcid.org/0000-0002-0980-6591>, president@vstu.ru.

Озерин Александр Никифорович – член-корр. РАН, д.х.н., профессор, Институт синтетических полимерных материалов им. Н.С. Ениколопова РАН, Москва, Российская Федерация. Scopus Author ID 7006188944, ResearcherID J-1866-2018, <https://orcid.org/0000-0001-7505-6090>, ozerin@ispm.ru.

Пакканен Тапани – PhD, профессор, Департамент химии, Университет Восточной Финляндии, Йоенсуу, Финляндия. Scopus Author ID 7102310323, tapani.pakkanen@uef.fi.

Помбейро Армандо – академик Академии наук Лиссабона, PhD, профессор, президент Центра структурной химии Высшего технического института университета Лиссабона, Португалия. Scopus Author ID 7006067269, ResearcherID I-5945-2012, <https://orcid.org/0000-0001-8323-888X>, pombeiro@ist.utl.pt.

Пышный Дмитрий Владимирович – член-корр. РАН, д.х.н., профессор, Институт химической биологии и фундаментальной медицины Сибирского отделения РАН, Новосибирск, Российская Федерация. Scopus Author ID 7006677629, ResearcherID F-4729-2013, <https://orcid.org/0000-0002-2587-3719>, pyshnyi@niboch.nsc.ru.

Сигов Александр Сергеевич – академик РАН, д.ф.-м.н., профессор, президент МИРЭА – Российского технологического университета, Москва, Российская Федерация. Scopus Author ID 35557510600, ResearcherID L-4103-2017, sigov@mirea.ru.

Тойкка Александр Матвеевич – д.х.н., профессор, Институт химии, Санкт-Петербургский государственный университет, Санкт-Петербург, Российская Федерация. Scopus Author ID 6603464176, ResearcherID A-5698-2010, <http://orcid.org/0000-0002-1863-5528>, a.toikka@spbu.ru.

Трохимчук Анджей – д.х.н., профессор, Химический факультет Вроцлавского политехнического университета, Вроцлав, Польша. Scopus Author ID 7003604847, andrzej.trochimczuk@pwr.edu.pl.

Цивадзе Аслан Юсупович – академик РАН, д.х.н., профессор, Институт физической химии и электрохимии им. А.Н. Фрумкина РАН, Москва, Российская Федерация. Scopus Author ID 7004245066, ResearcherID G-7422-2014, tsiv@phych.ac.ru.

CONTENTS

СОДЕРЖАНИЕ

**Chemistry and Technology
of Organic Substances**

*Kurganova E.A., Frolov A.S., Kanaev S.A.,
Koshel G.N., Petukhov A.A., Rybina G.V.,
Plakhtinskii V.V., Kabanova V.S., Smurova A.A.* **505**
Epoxidation of cyclohexene
with cyclohexyl hydroperoxide

*Stepanov G.O., Rodionova N.N.,
Konstantinov R.R., Subbotin K.A.* **517**
Effect of adding technologically processed
antibodies to interferon-gamma
into a parent solution on the structural
features of triglycine sulfate crystals
grown from this solution

**Synthesis and Processing of Polymers
and Polymeric Composites**

*Mikhailova S.T., Reznichenko S.V.,
Krasnikov E.A., Tsygankov P.Yu.,
Menshutina N.V., Simonov-Emel'yanov I.D.* **534**
Swelling of rubbers of different
chemical natures in supercritical
carbon dioxide

**Химия и технология
органических веществ**

*Курганова Е.А., Фролов А.С., Канаев С.А.,
Кошель Г.Н., Петухов А.А., Рыбина Г.В.,
Плахтинский В.В., Кабанова В.С., Смунова А.А.*
Эпоксидирование циклогексена
гидропероксидом циклогексила

*Степанов Г.О., Родионова Н.Н.,
Константинов Р.Р., Субботин К.А.*
Влияние добавления в маточный раствор
технологически отработанных антител
к интерферону-гамма на структурные
особенности выращиваемых из этого
раствора кристаллов триглицинсульфата

**Синтез и переработка полимеров
и композитов на их основе**

*Михайлова С.Т., Резниченко С.В.,
Красников Е.А., Цыганков П.Ю.,
Меньшутина Н.В., Симонов-Емельянов И.Д.*
Исследование набухания каучуков различной
химической природы в сверхкритическом
диоксиде углерода

*Romanov S.V., Botvinova O.A., Timakov E.A.,
Rashchupkina D.A., Panov Yu.T.*
High-performance slow-curing
polyurea compositions

549

**Chemistry and Technology
of Inorganic Materials**

*Absalan Ya., Alabada R., Razavi M.R.,
Gholizadeh M., Avramenko O.V., Bychkova I.N.,
Kovalchukova O.V.*

A green synthetic method
for cobalt(II,III) oxide nanoparticles
with high surface activity

559

D'yachenko A.N.

Fluorination of titanomagnetite
concentrate with ammonium
bifluoride

572

*Savinkina E.V., Karavaev I.A., Bettels E.K.,
Buzanov G.A., Kubasov A.S.*

Coordination compounds of indium,
gadolinium, and erbium nitrates
with low urea content

583

*Романов С.В., Ботвинова О.А., Тимаков Е.А.,
Ращупкина Д.А., Панов Ю.Т.*

Медленные полимочевинные композиции
с высокими эксплуатационными свойствами

**Химия и технология
неорганических материалов**

*Абсалан Я., Алабада Р., Разави М.Р.,
Голизадех М., Авраменко О.В., Бычкова И.Н.,
Ковальчукова О.В.*

«Зеленый» метод синтеза наночастиц
оксида кобальта(II,III) с улучшенной
поверхностной активностью

Дьяченко А.Н.

Исследование процесса фторирования
титаномагнетитового концентрата
дифторидом аммония

*Савинкина Е.В., Караваев И.А., Беттельс Е.К.,
Бузанов Г.А., Кубасов А.С.*

Координационные соединения нитратов
индия, гадолиния и эрбия с низким
содержанием мочевины

CHEMISTRY AND TECHNOLOGY OF ORGANIC SUBSTANCES

ХИМИЯ И ТЕХНОЛОГИЯ ОРГАНИЧЕСКИХ ВЕЩЕСТВ

ISSN 2686-7575 (Online)

<https://doi.org/10.32362/2410-6593-2023-18-6-505-516>

UDC 547.592/.595:547-311



RESEARCH ARTICLE

Epoxidation of cyclohexene with cyclohexyl hydroperoxide

Ekaterina A. Kurganova^{1,✉}, Aleksandr S. Frolov¹, Sergei A. Kanaev², Georgiy N. Koshel¹, Aleksandr A. Petukhov³, Galina V. Rybina¹, Vladimir V. Plakhtinskii¹, Viktoriya S. Kabanova¹, Alina A. Smurova¹

¹Yaroslavl State Technical University, Yaroslavl, 150023 Russia

²KuibyshevAzot, Togliatti, 445007 Russia

³Kazan National Research Technological University, Kazan, 420015 Russia

✉ Corresponding author, e-mail: kurganova@ystu.ru

Abstract

Objectives. To investigate the regularities of the process of joint production of epoxycyclohexane, cyclohexanol, and cyclohexanone using the cyclohexene epoxidation reaction with cyclohexyl hydroperoxide in the presence of an ammonium paramolybdate catalyst, representing an alternative to the method of cyclohexanol and cyclohexanone synthesis by alkaline catalytic decomposition of cyclohexyl hydroperoxide.

Methods. The qualitative and quantitative analysis of the obtained intermediate and target compounds was determined using modern physicochemical research methods: gas-liquid chromatography using the Chromatec-Crystal 5000.2 hardware and software complex with a flame ionization detector and infrared spectroscopy on an RX-1 infrared Fourier spectrometer. The content of hydroperoxide in the oxidation products was determined using iodometric titration, while the carboxylic acid content was determined by the titrimetric method based on the neutralization reaction.

Results. The presented method for obtaining cyclohexanol and cyclohexanone together with epoxycyclohexane by the reaction of cyclohexene epoxidation with cyclohexyl hydroperoxide containing cyclohexane in the products of high-temperature liquid-phase

oxidation is experimentally substantiated. The influence of various technological parameters on the process of liquid-phase oxidation of cyclohexane to hydroperoxide is described. The conditions for carrying out this reaction are determined to ensure the achievement of a content of cyclohexyl hydroperoxide of 1.5 wt % in the products of oxidation. The regularities of the epoxidation reaction of the synthesized cyclohexyl hydroperoxide with cyclohexene in the presence of an ammonium paramolybdate catalyst are analyzed.

Conclusions. Epoxidation of cyclohexene with cyclohexyl hydroperoxide produced epoxycyclohexane at a yield of 80–90% and a conversion of cyclohexane hydroperoxide of 85%.

Keywords: cyclohexene, cyclohexane, cyclohexyl hydroperoxide, cyclohexanone, cyclohexanol, liquid phase oxidation, epoxidation

For citation: Kurganova E.A., Frolov A.S., Kanaev S.A., Koshel G.N., Petukhov A.A., Rybina G.V., Plakhtinskii V.V., Kabanova V.S., Smurova A.A. Epoxidation of cyclohexene with cyclohexyl hydroperoxide. *Tonk. Khim. Tekhnol. = Fine Chem. Technol.* 2023;18(6):505–516. <https://doi.org/10.32362/2410-6593-2023-18-6-505-516>

НАУЧНАЯ СТАТЬЯ

Эпоксидирование циклогексена гидропероксидом циклогексила

Е.А. Курганова^{1,✉}, А.С. Фролов¹, С.А. Канаев², Г.Н. Кошель¹, А.А. Петухов³, Г.В. Рыбина¹, В.В. Плахтинский¹, В.С. Кабанова¹, А.А. Смурова¹

¹Ярославский государственный технический университет, Ярославль, 150023 Россия

²КуйбышевАзот, Тольятти, 445007 Россия

³Казанский национальный исследовательский технологический университет, Казань, 420015 Россия

✉ Автор для переписки, e-mail: kurganova@ystu.ru

Аннотация

Цели. Исследование закономерностей процесса совместного получения эпоксициклогексана, циклогексанола, циклогексанона реакцией эпоксидирования циклогексена гидропероксидом циклогексила в присутствии катализатора — парамolibдата аммония. Разрабатываемый процесс является альтернативой способу синтеза циклогексанола и циклогексанона щелочно-каталитическим разложением гидропероксида циклогексила.

Методы. Определение качественного и количественного анализа полученных промежуточных и целевых соединений осуществлялось с применением газожидкостной хроматографии на аппаратно-программном комплексе «Хроматек-Кристалл 5000.2» с пламенно-ионизационным детектором, инфракрасной спектроскопией на приборе

ИК Фурье RX-1. Содержание гидропероксида в продуктах окисления проводилось с использованием йодометрического титрования, а содержание карбоновых кислот — титриметрическим методом на основе реакции нейтрализации.

Результаты. Экспериментально обоснован метод получения циклогексанола и циклогексанона совместно с эпоксициклогексаном реакцией эпоксидирования циклогексена гидропероксидом циклогексила, содержащимся в продуктах высокотемпературного жидкофазного окисления циклогексана. Исследовано влияние различных технологических параметров на процесс жидкофазного окисления циклогексана до гидропероксида. Определены условия проведения данной реакции, обеспечивающие достижение содержания гидропероксида циклогексила 1.5 мас. % в продуктах окисления. Изучены закономерности реакции эпоксидирования синтезированного гидропероксида циклогексила с циклогексеном в присутствии парамолибдата аммония в качестве катализатора.

Выводы. Эпоксидированием циклогексена гидропероксидом циклогексила получен эпоксициклогексан с выходом 80–90% при конверсии гидропероксида циклогексана 85%.

Ключевые слова: циклогексен, циклогексан, гидропероксид циклогексила, циклогексанон, циклогексанола, жидкофазное окисление, эпоксидирование

Для цитирования: Курганова Е.А., Фролов А.С., Канаев С.А., Кошель Г.Н., Петухов А.А., Рыбина Г.В., Плахтинский В.В., Кабанова В.С., Смурова А.А. Эпоксидирование циклогексена гидропероксидом циклогексила. *Тонкие химические технологии*. 2023;18(6):505–516. <https://doi.org/10.32362/2410-6593-2023-18-6-505-516>

INTRODUCTION

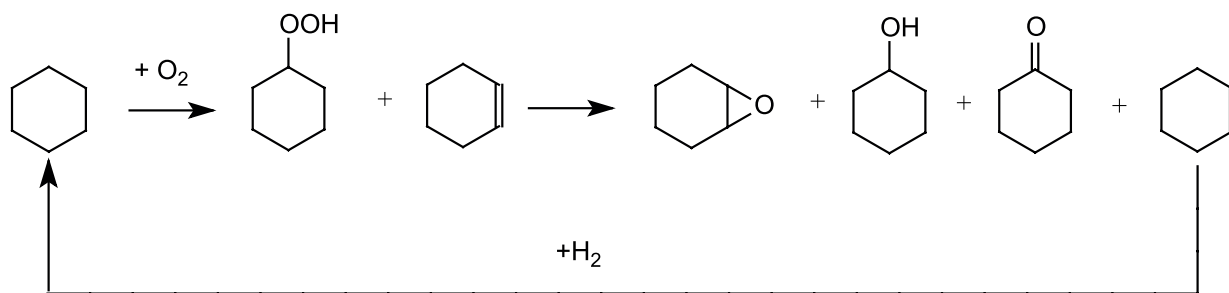
The selective oxidation of cyclohexane to cyclohexanone and cyclohexanol is a key stage in the process of producing nyolone-6 and nylon-6,6 polyamides, whose global production of which reaches more than 6 mln t/year.

Two main methods are implemented for the industrial production of cyclohexanol and cyclohexanone both in Russia and abroad. A one-step method for the synthesis of these compounds is based on the catalytic liquid-phase oxidation of cyclohexane with air oxygen at 150–170°C to a cyclohexane conversion of 5–7% and a selectivity for cyclohexanone and cyclohexanol formation of 70–75% in the presence of cobalt-containing catalysts [1]. A two-stage method for the production of cyclohexanone and cyclohexanol includes autocatalytic liquid-phase oxidation of cyclohexane to cyclohexyl hydroperoxide containing 3–5 wt % and subsequent homogeneous catalytic decomposition of cyclohexyl hydroperoxide to the target products in an alkaline medium in the presence of cobalt

salts [2]. The scientific basis of the chemistry and technology of the latter method for producing cyclohexanone and cyclohexanol were developed at the Research and Design Institute of Nitrogen Industry and Products of Organic Synthesis (GIAP, Russia) by V.V. Lipes and his colleagues during the 1980s [3–4].

A distinctive feature of the two-stage process is the higher selectivity of target product formation (97–99%), achieving a 94–96% conversion of cyclohexyl hydroperoxide. However, among the significant disadvantages of this cyclohexane oxidation method are included the formation of a large amount of alkaline waste as a result of neutralization of acids contained in the oxidation products, as well as the irreversible loss of oxygen (up to 50%) contained in the hydroperoxide fragment.

In order to improve the economic and technological efficiency of this approach for cyclohexanol and cyclohexanone production the alkali-catalytic cleavage of cyclohexyl hydroperoxide can be replaced with the use of hydroperoxide to epoxidate olefins, among which cyclohexene is of greatest interest (Scheme).



Scheme. Reaction of cyclohexene epoxidation with hydroperoxide.

Epoxycyclohexane formed along with cyclohexanol and cyclohexanone as a result of the epoxidation reaction is used in the production of epoxy resins and photoreactive polymers, pesticide acaricides, surfactants, and rubber additives [5–7]. A promising use of cyclohexane epoxide lies in its enantioselective transformation into chiral 1,2-aminocyclohexanol or 1,2-diaminocyclohexane, representing chemical building blocks for the preparation of natural and synthetic biologically active molecules, including amino acids [8, 9]. The epoxide can be used as such or converted into cyclohexanol or cyclohexanone for subsequent processing into adipic acid or ϵ -caprolactam [10–12]. Unreacted cyclohexene following hydrogenation can be sent for oxidation.

The aim of the present work is to study the regularities of cyclohexene epoxidation with cyclohexyl hydroperoxide.

MATERIALS AND METHODS

The following reagents were used in this study: cyclohexanol (reagent grade, TU-2632-185-44493179-2017) and cyclohexane (reagent grade, TU 2631-204-44493179-2016, *EKOS-I*, Russia), sulfuric acid (reagent grade, GOST 4204-77¹, *Sigma Tek*, Russia), ammonium molybdate tetrahydrate (reagent grade, GOST 3765-78², *Khimsintez*, Russia), propylene glycol (TU 2632-146-44493179-11, *EKOS-I*, Russia), acetic acid (reagent grade, GOST 61-75³) and potassium iodide (reagent grade, GOST 4232-74⁴,

Spektr Khim, Russia), sodium hyposulfite (analytical grade, GOST 27068-86⁵, *Uralkhiminvest*, Russia), sodium hydroxide (analytical grade, GOST 4328-77⁶, *Kaustik*, Russia), phenolphthalein (analytical grade, TU 6-09-5360-88, *Spektr Khim*, Russia).

The main method for analyzing the reaction mass was gas-liquid chromatography (GLC) carried out on a Chromatec-Crystal 5000.2 chromatograph (*Chromatec*, Russia) with a flame ionization detector. A 30-m capillary column SK-5 having a diameter of 0.32 mm was filled with 5% phenyl/95% dimethylpolysiloxane. Nitrogen was used as a carrier gas at a flow rate 2 cm³/min. The programmed temperature rise was from 80 to 200°C at a rate of 8°C/min.

The identification of the obtained compounds was carried out by infrared (IR) spectroscopy on a Spectrum RX-1 Fourier transform IR spectrometer (*PerkinElmer*, USA). Mathematical processing of the spectra was carried out using the IBM Spectrum Scale, v.5.0.1 program provided by *PerkinElmer*. Spectra were recorded in the range of 4000–400 cm^{–1} in the form of a microlayer between potassium bromide glasses and in a potassium bromide cuvette with a layer thickness $d = 0.0011$.

The hydroperoxide content in the oxidation products was determined by the iodometric titration method [13] based on hydroperoxide reduction with potassium iodide in an acidic medium. The amount of iodine released as a result of the reaction was titrated with a solution of sodium thiosulfate.

The content of carboxylic acids formed along with hydroperoxide in the process of cyclohexane oxidation was determined by the titrimetric method

¹ GOST 4204-77. State Standard of the USSR. Reagents. Sulphuric acid. Specifications. Moscow: Standartinform; 2006.

² GOST 3765-78. State Standard of the USSR. Reagents. Ammonium molybdate acid. Specifications. Moscow: IPK Izdatelstvo standartov; 1998.

³ GOST 61-75. Interstate Standard. Reagents. Acetic acid. Specifications. Moscow: Standartinform; 2006.

⁴ GOST 4232-74. Interstate Standard. Reagents. Potassium iodide. Specifications. Moscow: Standartinform; 2006.

⁵ GOST 27068-86. Interstate Standard. Reagents. Sodium thiosulphate, 5-aqueous. Specifications. Moscow: IPK Izdatelstvo standartov; 1998.

⁶ GOST 4328-77. Interstate standard. Reagents. Sodium hydroxide. Specifications. Moscow: IPK Izdatelstvo standartov; 1978.

based on the neutralization of an aqueous extract obtained from a certain organic layer mass using a solution of sodium hydroxide in the presence of the indicator phenolphthalein according to the method described by *KuibyshevAzot*, Russia.

EXPERIMENTAL

Cyclohexene was obtained by cyclohexanol dehydration in the presence of concentrated sulfuric acid at 110–120°C for 1.5 h. The process was carried out in a Wurtz flask placed in a glycerol bath and equipped with a Weigel–Liebig refrigerator. Water and cyclohexene formed during the reaction were evaporated, condensed in a direct refrigerator, and collected in the receiver. The target product was isolated from the reaction mass by vacuum rectification at a temperature of 83–85°C and a residual pressure of 0.8–0.9 atm. The yield of cyclohexene was about 80%; its structure was confirmed by GLC and IR spectroscopy. The IR spectrum of the synthesized cyclohexene displays the characteristic bands of stretching vibrations of C–H bonds with bands at 3022 and 2925 cm^{-1} . The presence of a C=C bond in the structure is confirmed by the band at 1652.93 cm^{-1} . Deformation vibrations of the $-\text{CH}_2$ bond are characterized by bands at 1446.15 and 1437.73 cm^{-1} .

Liquid-phase oxidation of cyclohexane to hydroperoxide with air oxygen at a system pressure of 25 atm was carried out at 160–170°C in a steel reactor set up for the oxidation of liquefied hydrocarbon gases (Fig. 1) according to the method described in [14, 15] while simulating the conditions of high-temperature oxidation of cyclohexane by *KuibyshevAzot*.

The approximately 1.5 wt % cyclohexyl hydroperoxide obtained in the oxidation products, which was concentrated by vacuum rectification at a temperature of 65–70°C and a residual pressure of 0.15–0.2 atm to 5 wt %, was used for subsequent research purposes.

Cyclohexene epoxidation with cyclohexyl hydroperoxide was carried out in a closed-flow installation (Fig. 2) made available at the Department of General and Physical Chemistry of Yaroslavl State Technical University. A mixture containing calculated amounts of fortified cyclohexane oxidate with a hydroperoxide content of 5 wt % was loaded into a glass reactor having a capacity of 10 cm^3 along with cyclohexene and the catalyst. Air was supplied at atmospheric pressure. The process was carried out at a constant temperature and continuous stirring [16].

Ammonium paramolybdate $(\text{NH}_4)_6\text{Mo}_7\text{O}_{24} \cdot 4\text{H}_2\text{O}$ dissolved in propylene glycol was used as a catalyst

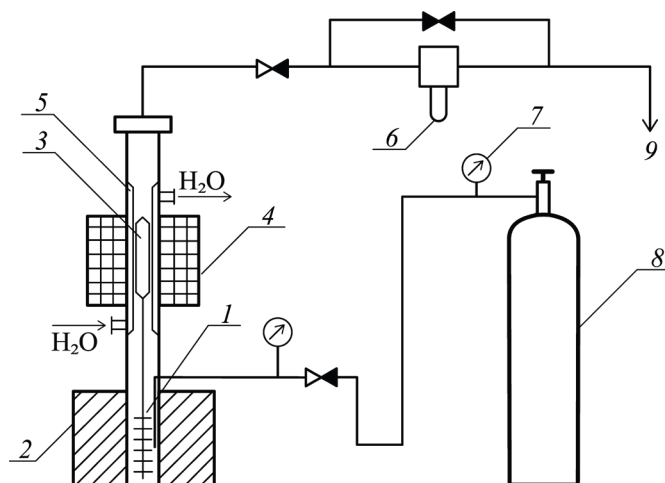


Fig. 1. Scheme of a setup for the oxidation of liquefied hydrocarbon gases [14, 15]: (1) autoclave; (2) electric furnace; (3) magnetic stirrer; (4) electromagnet; (5) fridge; (6) rheometer; (7) reducer; (8) compressed air cylinder; (9) air discharge; ►◄ adjusting valve.

for cyclohexene epoxidation with cyclohexyl hydroperoxide. The process was carried out according to the method described in [17] in an electrically-heated, round-bottomed, four-neck 150-mL flask equipped with a reflux condenser, a thermometer, a stirrer, and a bubbler for purging the reaction mixture with air.

RESULTS AND DISCUSSION

Although information concerning the regularities of olefins epoxidation with hydroperoxides is abundant, there is practically no data relating to the process of cyclohexene epoxidation with cyclohexyl hydroperoxide in the scientific and technical literature. However, the synthesis of cyclohexanol and cyclohexanone together with epoxycyclohexane by epoxidizing cyclohexene with cyclohexyl hydroperoxide is described at a conversion of the latter of 60–65% on a heterogeneous Ti/Si catalyst at 80°C [18, 19]. The limited number of scientific studies and publications on the above problem is primarily due to the difficulties of obtaining cyclohexane hydroperoxide, as well as its extremely low stability during storage and transportation.

The study of the patterns of cyclohexene epoxidation using cyclohexyl hydroperoxide was preceded by a study of the conditions for high-temperature oxidation of cyclohexane to cyclohexyl hydroperoxide, as well as its concentration and production in larger quantities. This problem was

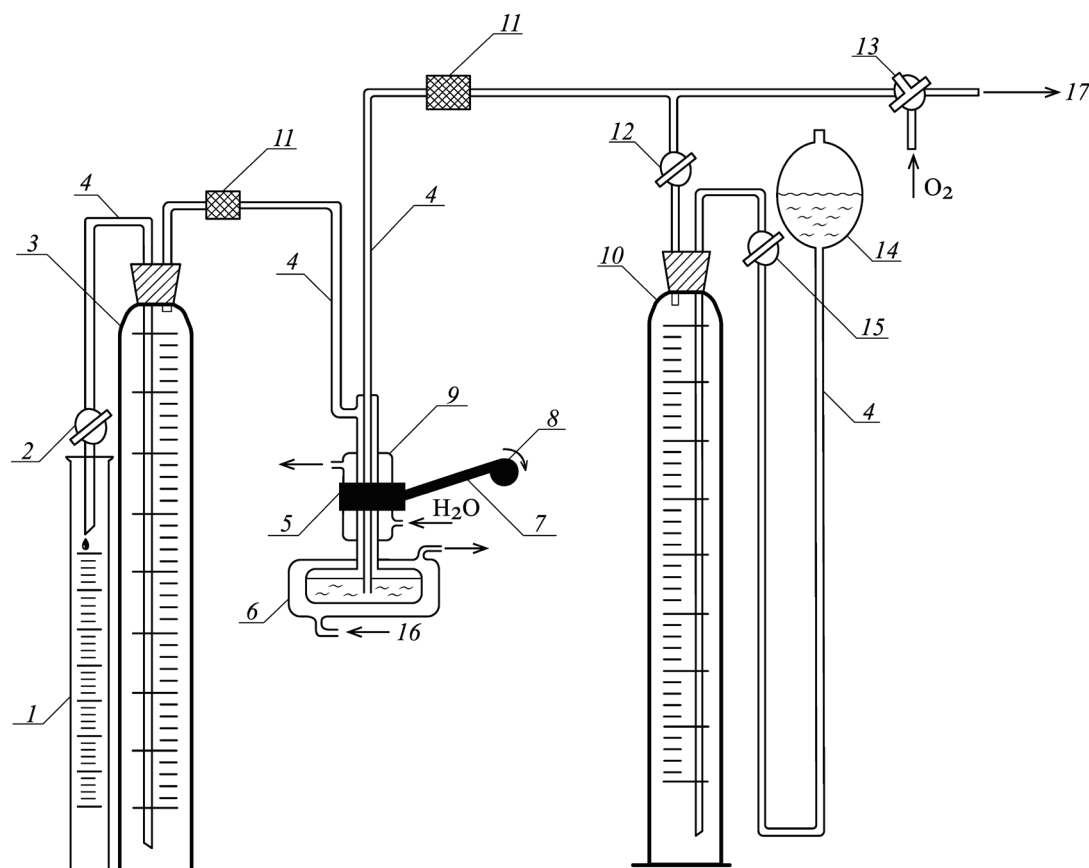


Fig. 2. Scheme of the setup for cyclohexene epoxidation with cyclohexyl hydroperoxide [16]:

(1) measuring cylinder; (2), (12), (15) valves; (3), (10) gas burettes; (4) connecting hose; (5) reactor holder; (6) reactor; (7) connecting rod; (8) electric motor pulley; (9) fridge; (11) calcium chloride tube; (13) three-way cock; (14) pressure bottle; (16) thermostat; (17) vacuum setup.

solved by carrying out liquid-phase oxidation of cyclohexane under conditions as close as possible to those used at *KuibyshevAzot*.

A study of the influence of temperature and reaction duration on cyclohexyl hydroperoxide formation (Table 1) showed that at a temperature of 160°C, an increase in the process duration from 20 to 40 min increases the content of cyclohexyl hydroperoxide slightly; in this case, the content of carboxylic acids formed along with the target products increases by a factor of six. A subsequent increase in temperature leads to a significant decrease in the process selectivity due to the formation of a large quantity of carboxylic acids.

Thus, the possibility of achieving a hydroperoxide content in the oxidate of 1.5 wt % with a minimum content of carboxylic acids at a temperature of 160°C, a pressure in the system of 25 atm and a reaction duration of 20 min is demonstrated. This is consistent with the indicators of the oxidation process at *KuibyshevAzot*. After increasing the cyclohexyl hydroperoxide content in the oxidate to 5 wt %

according to the method given in the Experimental section, the product was used for cyclohexene epoxidation. In [18], cyclohexene epoxidation was carried out using cyclohexyl hydroperoxide isolated from the products of cyclohexane catalytic oxidation using a NaOH solution.

In order to determine the most favorable conditions for carrying out the epoxidation reaction, the influence of the molar ratio of reagents, catalyst concentration, and temperature on the yield of target products and hydroperoxide conversion was studied. The results obtained are presented in Figs. 3 and 4 and in Tables 2 and 3.

One of the factors that significantly influences both the yield of target products and the rate of hydroperoxide conversion is the molar ratio of cyclohexyl hydroperoxide and cyclohexene (Fig. 1). Changing this ratio from 1:1 to 3:1 increases the yield of epoxycyclohexane with respect to reacted hydroperoxide from 30–35% to 75–80%. In this case, the selectivity of cyclohexanol and cyclohexanone formation increases to 99.5%.

Table 1. Influence of various parameters on cyclohexane oxidation. Pressure is 25 atm

Temperature, °C	Reaction time, min	Concentration, wt %	
		Cyclohexyl hydroperoxide	Carboxylic acids
160	20	1.5	0.06
	30	1.6	0.27
	40	1.7	0.36
170	20	1.5	0.14

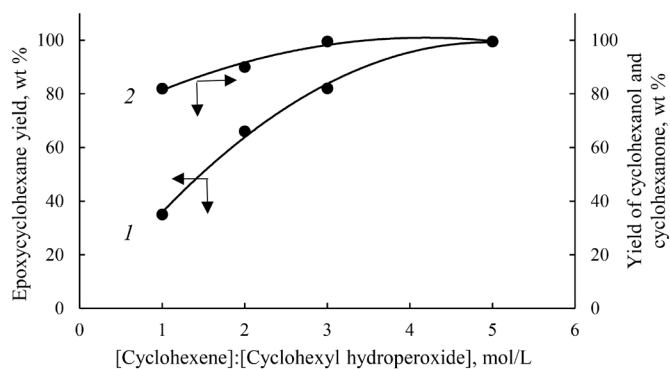


Fig. 3. Influence of the molar ratio of cyclohexyl hydroperoxide and cyclohexene on cyclohexene epoxidation with cyclohexyl hydroperoxide at a temperature of 90°C and a catalyst concentration of 0.00013 g/atom of Mo per 1 g of hydroperoxide: (1) yield of epoxycyclohexane; (2) yield of cyclohexanol and cyclohexanone.

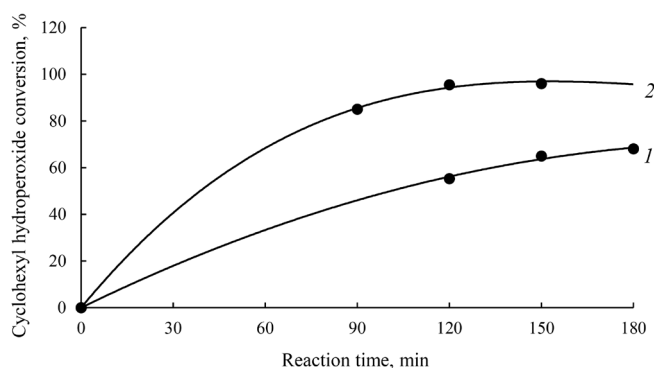


Fig. 4. Influence of temperature on cyclohexene epoxidation with cyclohexyl hydroperoxide. Cyclohexyl hydroperoxide/cyclohexene ratio is 1:3, the catalyst concentration is 0.0005 g/Mo atom per 1 g of hydroperoxide: (1) 80°C; (2) 90°C.

From analyzing the influence of temperature and cyclohexene epoxidation duration (Table 2) it was shown that complete conversion of cyclohexyl hydroperoxide cannot be achieved at 80°C even after 3 h of reaction. In addition, a low yield of epoxycyclohexane is observed. By increasing the temperature to 90°C, the process was significantly intensified due to the increased conversion of cyclohexyl hydroperoxide from 65% to 95%. Under these conditions, no boiling of the reaction mass was observed. Conversely, lowering the temperature to 70°C significantly reduces the reaction rate. Thus, the most favorable temperature is 90°C.

Reducing the catalyst concentration from 0.0005 to 0.00003 g/Mo atom per 1 g of hydroperoxide results in a decrease in the conversion of cyclohexyl hydroperoxide and in the yield of epoxycyclohexane (Table 3). Thus, a yield of epoxycyclohexane of about 82% is achieved with an ammonium paramolybdate content of 0.00013 g/Mo atom per 1 g of hydroperoxide. Further reduction of the catalyst concentration is impractical due to a decrease in the yield of epoxycyclohexane, while increasing catalyst concentration above 0.0005 g/Mo atom per 1 g of hydroperoxide is not economically feasible.

Based on the obtained experimental data, the following conditions can be recommended for cyclohexene epoxidation with cyclohexyl hydroperoxide: temperature is 90°C; reaction duration is 90 min; ammonium paramolybdate content is 0.00013 g/Mo atom per 1 g of hydroperoxide. Under these conditions, cyclohexyl hydroperoxide conversion is 85%, while the yield of epoxycyclohexane is about 82%, and the yield of cyclohexanol and cyclohexanone is 99.5%.

Table 2. Influence of various parameters on cyclohexene epoxidation with cyclohexyl hydroperoxide. Cyclohexyl hydroperoxide/cyclohexene ratio is 1:3. The catalyst concentration is 0.0005 g/Mo atom per 1 g hydroperoxide

Temperature, °C	Reaction time, min	Cyclohexyl hydroperoxide conversion, %	Yield per reacted cyclohexyl hydroperoxide, %		Cyclohexanol/cyclohexanone molar ratio
			Cyclohexanol + cyclohexanol	Epoxy cyclohexane	
80	120	55.3	96.0	35.0	4:1
	150	65.0	99.0	38.0	3:1
	180	68.0	99.2	45.0	5:1
90	60	33.0	98.0	75.0	4:1
	90	94.5	99.1	80.0	4:1
	120	95.5	99.3	78.0	4:1
	150	96.0	99.4	75.0	2:1

Table 3. Influence of catalyst concentration on cyclohexene epoxidation with cyclohexyl hydroperoxide. Cyclohexyl hydroperoxide/cyclohexene ratio is 1:3, temperature is 90°C, reaction time is 90 min

Catalyst concentration, g/Mo atom per 1 g of hydroperoxide	Cyclohexyl hydroperoxide conversion, %	Yield per reacted cyclohexyl hydroperoxide, %		Cyclohexanol/ cyclohexanone molar ratio
		Cyclohexanol + cyclohexanone	Epoxy cyclohexane	
0.00003	77.0	76.2	65.0	1:1
0.00013	85.0	99.5	82.1	4:1
0.00025	87.0	99.4	99.5	4:1
0.00050	95.0	94.5	99.1	4:1

CONCLUSIONS

The possibility of producing epoxycyclohexane together with cyclohexanol and cyclohexanone by epoxidizing cyclohexene with cyclohexyl hydroperoxide contained in the products of high-temperature, liquid-phase oxidation of cyclohexane as an alternative to the process of producing cyclohexanol and cyclohexanone by alkaline-catalytic decomposition of cyclohexyl hydroperoxide is experimentally substantiated.

Financial support

This study had no financial support from outside organizations.

Authors' contributions

E.A. Kurganova – research concept, design of the experiments, analysis of the results, writing the text of the manuscript;

A.S. Frolov – research concept, data processing, writing the text of the manuscript;

S.A. Kanaev – analysis of the results;

G.N. Koshelev – research concept, analysis of the results, writing the text of the manuscript;

A.A. Petukhov – research concept, analysis of the results;

G.V. Rybina – analysis of the results;

V.V. Plakhtinskii – analysis of the results, writing the text of the manuscript;

V.S. Kabanova – conducting the experiments, writing the text of the manuscript;

A.A. Smurova – conducting the experiments, writing the text of the manuscript.

The authors declare no conflicts of interest.

REFERENCES

1. Lebedev N.N. *Khimiya i tekhnologiya osnovnogo organicheskogo i neftekhimicheskogo sinteza* (Chemistry and Technology of Basic Organic and Petrochemical Synthesis). Moscow: Al'yanS; 2013. 588 p. (in Russ.). ISBN 978-5-91872-035-6
2. Lipes V.V., Geberger F.A., Khar'kova T.V., Shafran M.I., Uspenskii V.B., Pravdivyi I.N., Bukseev V.V., Stepenyuk L.S., Polyukhov I.D. *Method of Obtaining Cyclohexanone and Cyclohexanol*: USSR Pat. RU1641804. Publ. 15.04.1991 (in Russ.).
3. Furman M.S., Lipes V.V., Golyaeva N.A. Investigation of the process of liquid-phase high-temperature oxidation of cyclohexane. *Khimiya i tekhnologiya produktov organicheskogo sinteza = Chemistry and Technology of Organic Synthesis Products*. 1966;17(1):21–30 (in Russ.).
4. Furman M.S., Arrest-Yakubovich I.A., Lipes V.V. Thermal and alkaline decomposition of cyclohexane hydroperoxide in oxidants obtained by high-temperature oxidation of cyclohexane. *Khimiya i tekhnologiya produktov organicheskogo sinteza = Chemistry and Technology of Organic Synthesis Products*. 1974;27:46–56 (in Russ.).

СПИСОК ЛИТЕРАТУРЫ

1. Лебедев Н.Н. *Химия и технология основного органического и нефтехимического синтеза*. М.: АльянС; 2013. 588 с. ISBN 978-5-91872-035-6
2. Липес В.В., Гебергер Ф.А., Харьков Т.В., Шафран М.И., Успенский В.Б., Правдивый И.Н., Буксеев В.В., Степенюк Л.С., Полухович И.Д. *Способ получения циклогексанона и циклогексанола*: авторское свидетельство 1641804 СССР. Заявка № 4655478/04; заявл. 29.12.1988; опубл. 15.04.1991. Бюл. № 14.
3. Фурман М.С., Липес В.В., Гольяева Н.А. Исследование процесса жидкофазного высокотемпературного окисления циклогексана. *Химия и технология продуктов органического синтеза*. 1966;17(1):21–30.
4. Фурман М.С., Арест-Якубович И.А., Липес В.В. Термическое и щелочное разложение гидропероксида циклогексана в оксидатах, полученных высокотемпературным окислением циклогексана. *Химия и технология продуктов органического синтеза*. 1974;27:46–56.
5. Wittcoff H.A., Reuben B.G., Plotkin J.S. *Industrial Organic Chemicals*. Hoboken, New Jersey: John Wiley & Sons; 2004. 662 p.

5. Wittcoff H.A., Reuben B.G., Plotkin J.S. *Industrial Organic Chemicals*. Hoboken, New Jersey: John Wiley & Sons; 2004. 662 p.
6. Kotelnikova T.S., Voronina S.G., Puchkov S.V., Perkel A.L. Assessment of reactivity of cyclohexene oxide in relation to *tert*-butylperoxy radical. *Vestnik Kuzbasskogo gosudarstvennogo tekhnicheskogo universiteta = Bulletin of the Kuzbass State Technical University*. 2013;5(99):4–9 (in Russ.).
7. Yahiaouia A., Belbachir M., Soutif J.C., Fontaine L. Synthesis and structural analyses of poly (1, 2-cyclohexene oxide) over solid acid catalyst. *Mater. Lett.* 2005;59:759–767. <https://doi.org/10.1016/j.matlet.2004.11.017>
8. Seo T., Tsuji J. *Process for Producing Propylene Oxide*: Pat. US 6646139. Publ. 11.11.2003.
9. Fischer R., Weitz H.-M., Rieber N., Boehm H. *Process for the Preparation of Oxiranes*: Pat. EU 0129814. Publ.16.06.1984.
10. Accrombessi G.C., Geneste P., Olive J.-L., Pavia A.A. Mechanism of the liquid-phase catalytic hydrogenolysis on palladium/carbon of cyclohexene epoxides. *J. Org. Chem.* 1980;45(21):4139–4143. <https://doi.org/10.1021/jo01309a014>
11. Dahlhoff G., Barsnick U., Hölderich W.F. Use of MCM-22 as catalyst for the Beckmann rearrangement of cyclohexanone oxime to ϵ -caprolactam. *Appl. Catal. A: General*. 2001;210(1–2):83–95. [https://doi.org/10.1016/S0926-860X\(00\)00789-4](https://doi.org/10.1016/S0926-860X(00)00789-4)
12. Fasi A., Palinko I. Transformations of cyclohexene oxide over silica-supported Cu, Pd, and Rh catalysts in H_2/D_2 atmosphere. *J. Catal.* 1999;181(1):28–36. <https://doi.org/10.1006/jcat.1998.2284>
13. Antonovskii V.L., Buzlanova M.M. *Analiticheskaya khimiya organicheskikh peroksidnykh soedinenii (Analytical Chemistry of Organic Peroxidic Compounds)*. Moscow: Khimiya; 1978. 309 p. (in Russ.).
14. Frolov A.S., Kurganova E.A., Yarkina E.M., Lebedeva N.V., Koshel G.N., Kalenova A.S. Intensification of the cyclohexane liquid phase oxidation process. *Tonk. Khim. Tekhnol. = Fine Chem. Technol.* 2018;13(4):50–57 (in Russ.). <https://doi.org/10.32362/2410-6593-2018-13-4-50-57>
15. Kurganova E.A., Frolov A.S., Koshel G.N., Kabanova V.S. The reaction of cyclohexylbenzene oxidation in the presence of solvents. *Ot khimii k tekhnologii shag za shagom = From Chemistry Towards Technology Step-By-Step*. 2022;3(1):88–94 (in Russ.). https://doi.org/10.52957/27821900_2022_01_88
16. Frolov A.S., Kurganova E.A., Koshel' G.N., Nesterova T.N. Aerobic Oxidation of 2-isopropyl-1,4-dimethylbenzene to tertiary hydroperoxide. *Eur. J. Anal. Appl. Chem.* 2015;(1):16–22. <https://doi.org/10.20534/EJAAC-15-1-16-22>
17. Puchkova T.L., Nasrtdinova R.R., Pisareva M.L. The use of a glycol solution of molybdenum as a catalyst in the process of epoxidation of propylene with ethylbenzene hydroperoxide. *Vestnik tekhnologicheskogo universiteta = Herald of Technological University*. 2015;18(24):27–29 (in Russ.).
18. Hereijgers B.P.C., Parton R.F., Weckhuysen B.M. Cyclohexene Epoxidation with Cyclohexyl Hydroperoxide: A Catalytic Route to Largely Increase Oxygenate Yield from Cyclohexane Oxidation. *ACS Catal.* 2011;1(10):1183–1192. <https://doi.org/10.1021/cs200354c>
19. Hereijgers B.P.C., Parton R.F., Weckhuysen B.M. Mechanistic insights in the olefin epoxidation with cyclohexyl hydroperoxide. *Catal. Sci. Technol.* 2012;2(5):951–960. <https://doi.org/10.1039/C2CY00455K>
6. Котельникова Т.С., Воронина С.Г., Пучков С.В., Перкель А.Л. Оценка реакционной способности циклогексеноксида по отношению к *трет*-бутилпероксирадикалу. *Вестник Кузбасского государственного технического университета*. 2013;5(99):4–9.
7. Yahiaouia A., Belbachir M., Soutif J.C., Fontaine L. Synthesis and structural analyses of poly (1, 2-cyclohexene oxide) over solid acid catalyst. *Mater. Lett.* 2005;59:759–767. <https://doi.org/10.1016/j.matlet.2004.11.017>
8. Seo T., Tsuji J. *Process for Producing Propylene Oxide*: Pat. US 6646139. Publ. 11.11.2003.
9. Fischer R., Weitz H.-M., Rieber N., Boehm H. *Process for the Preparation of Oxiranes*: Pat. EU 0129814. Publ.16.06.1984.
10. Accrombessi G.C., Geneste P., Olive J.-L., Pavia A.A. Mechanism of the liquid-phase catalytic hydrogenolysis on palladium/carbon of cyclohexene epoxides. *J. Org. Chem.* 1980;45(21):4139–4143. <https://doi.org/10.1021/jo01309a014>
11. Dahlhoff G., Barsnick U., Hölderich W.F. Use of MCM-22 as catalyst for the Beckmann rearrangement of cyclohexanone oxime to ϵ -caprolactam. *Appl. Catal. A: General*. 2001;210(1–2):83–95. [https://doi.org/10.1016/S0926-860X\(00\)00789-4](https://doi.org/10.1016/S0926-860X(00)00789-4)
12. Fasi A., Palinko I. Transformations of cyclohexene oxide over silica-supported Cu, Pd, and Rh catalysts in H_2/D_2 atmosphere. *J. Catal.* 1999;181(1):28–36. <https://doi.org/10.1006/jcat.1998.2284>
13. Антоновский В.Л., Бузланова М.М. *Аналитическая химия органических пероксидных соединений*. М.: Химия; 1978. 309 с.
14. Фролов А.С., Курганова Е.А., Яркина Е.М., Лебедева Н.В., Кошель Г.Н., Каленова А.С. Интенсификация процесса жидкофазного окисления циклогексана. *Тонкие химические технологии*. 2018;13(4):50–57. <https://doi.org/10.32362/2410-6593-2018-13-4-50-57>
15. Курганова Е.А., Фролов А.С., Кошель Г.Н., Кabanova V.S. Изучение реакции окисления циклогексилбензола в присутствии растворителей. *От химии к технологии шаг за шагом*. 2022;3(1):21–27. https://doi.org/10.52957/27821900_2022_01_21
16. Frolov A.S., Kurganova E.A., Koshel' G.N., Nesterova T.N. Aerobic Oxidation of 2-isopropyl-1,4-dimethylbenzene to tertiary hydroperoxide. *Eur. J. Anal. Appl. Chem.* 2015;(1):16–22. <https://doi.org/10.20534/EJAAC-15-1-16-22>
17. Пучкова Т.Л., Насртдинова Р.Р., Писарева М.Л. Использование гликолевого раствора молибдена в качестве катализатора в процессе эпоксицирования пропилена гидропероксидом этилбензола. *Вестник технологического университета*. 2015;18(24):27–29.
18. Hereijgers B.P.C., Parton R.F., Weckhuysen B.M. Cyclohexene Epoxidation with Cyclohexyl Hydroperoxide: A Catalytic Route to Largely Increase Oxygenate Yield from Cyclohexane Oxidation. *ACS Catal.* 2011;1(10):1183–1192. <https://doi.org/10.1021/cs200354c>
19. Hereijgers B.P.C., Parton R.F., Weckhuysen B.M. Weckhuysen. Mechanistic insights in the olefin epoxidation with cyclohexyl hydroperoxide. *Catal. Sci. Technol.* 2012;2(5):951–960. <https://doi.org/10.1039/C2CY00455K>

About the authors:

Ekaterina A. Kurganova, Dr. Sci. (Chem.), Professor, Department of General and Physical Chemistry, Yaroslavl State Technical University (88, Moskovskii pr., Yaroslavl, 150023, Russia). E-mail: kurganova@ystu.ru. Scopus Author ID 24338325800, ResearcherID B-4021-2018, RSCI SPIN-code 2617-8020, <https://orcid.org/0000-0002-0087-1784>

Aleksandr S. Frolov, Cand. Sci. (Chem.), Associate Professor, Department of General and Physical Chemistry, Yaroslavl State Technical University (88, Moskovskii pr., Yaroslavl, 150023, Russia). E-mail: frolovas@ystu.ru. Scopus Author ID 56412435400, ResearcherID I-8533-2018, RSCI SPIN-code 4081-9087, <https://orcid.org/0000-0002-0491-7452>

Sergei A. Kanaev, Head of Caprolactam Production, KuibyshevAzot (6, Novozavodskaya ul., Togliatti, 445007, Russia). E-mail: KanaevSA@kuzot.ru. <https://orcid.org/0000-0003-4088-8617>

Georgiy N. Koshel, Dr. Sci. (Chem.), Professor, Department of General and Physical Chemistry, Yaroslavl State Technical University (88, Moskovskii pr., Yaroslavl, 150023, Russia). E-mail: koshelgn@ystu.ru. Scopus Author ID 6602886373, ResearcherID I-7782-2017, RSCI SPIN-code 1119-6642, <https://orcid.org/0000-0002-1020-4643>

Aleksandr A. Petukhov, Dr. Sci. (Eng.), Professor, Department of Synthetic Rubber Technology, Kazan National Research Technological University (68, K. Marksa ul., Kazan, 420015, Russia). E-mail: petukhov-aa@yandex.ru. RSCI SPIN-code 4948-6691, <https://orcid.org/0000-0001-5345-0863>

Galina V. Rybina, Cand. Sci. (Chem.), Associate Professor, Department of Chemical Technology of Organic Substances, Director of the Institute of Chemistry and Chemical Technology, Yaroslavl State Technical University (88, Moskovskii pr., Yaroslavl, 150023, Russia). E-mail: rybinagv@ystu.ru. Scopus Author ID 36765810200. RSCI SPIN-code 4163-9580, <https://orcid.org/0000-0002-5603-3464>

Vladimir V. Plakhtinskii, Dr. Sci. (Chem.), Professor, Department of Organic and Analytical Chemistry, Yaroslavl State Technical University (88, Moskovskii pr., Yaroslavl, 150023, Russia). E-mail: plakhtinskiyvv@ystu.ru. Scopus Author ID 6602528008, RSCI SPIN-code 3754-6178, <https://orcid.org/0000-0002-6560-0600>

Viktoriya S. Kabanova, Postgraduate Student, Department of General and Physical Chemistry, Yaroslavl State Technical University (88, Moskovskii pr., Yaroslavl, 150023, Russia). E-mail: viktoriya.kabanova.1999@mail.ru. Scopus Author ID 57749250400, RSCI SPIN-code 1221-0200, <https://orcid.org/0000-0001-6635-6315>

Alina A. Smurova, Master Student, Yaroslavl State Technical University (88, Moskovskii pr., Yaroslavl, 150023, Russia). E-mail: smurovaa@mail.ru. <https://orcid.org/0000-0002-5280-7573>

Об авторах:

Курганова Екатерина Анатольевна, д.х.н., доцент, профессор кафедры «Общая и физическая химия», ФГБОУ ВО «Ярославский государственный технический университет» (150023, Россия, Ярославль, Московский пр-т, д. 88). E-mail: kurganova@ystu.ru. Scopus Author ID 24338325800, ResearcherID B-4021-2018, SPIN-код РИНЦ 2617-8020, <https://orcid.org/0000-0002-0087-1784>

Фролов Александр Сергеевич, к.х.н., доцент кафедры «Общая и физическая химия», ФГБОУ ВО «Ярославский государственный технический университет» (150023, Россия, Ярославль, Московский пр-т, д. 88). E-mail: frolovas@ystu.ru. Scopus Author ID 56412435400, ResearcherID I-8533-2018, SPIN-код РИНЦ 4081-9087, <https://orcid.org/0000-0002-0491-7452>

Канаев Сергей Александрович, начальник производства капролактама, ПАО «КуйбышевАзот» (445007, г. Тольятти, ул. Новозаводская, д. 6). E-mail: KanaevSA@kuzot.ru. <https://orcid.org/0000-0003-4088-8617>

Кошель Георгий Николаевич, д.х.н., профессор, профессор кафедры «Общая и физическая химия», ФГБОУ ВО «Ярославский государственный технический университет» (150023, Россия, Ярославль, Московский пр-т, д. 88). E-mail: koshelgn@ystu.ru. Scopus Author ID 6602886373, ResearcherID I-7782-2017, SPIN-код РИНЦ 1119-6642, <https://orcid.org/0000-0002-1020-4643>

Петухов Александр Александрович, д.т.н., профессор, профессор кафедры «Технологии синтетического каучука», ФГБОУ ВО «Казанский национальный исследовательский технологический университет» (420015, Россия, Казань, ул. К. Маркса, д. 68). E-mail: petukhov-aa@yandex.ru. SPIN-код РИНЦ 4948-6691, <https://orcid.org/0000-0001-5345-0863>

Рыбина Галина Викторовна, к.х.н., доцент, доцент кафедры «Химическая технология органических веществ», директор Института химии и химической технологии, ФГБОУ ВО «Ярославский государственный технический университет» (150023, Россия, Ярославль, Московский пр-т, д. 88). E-mail: rybinagv@ystu.ru. Scopus Author ID 36765810200, SPIN-код РИНЦ 4163-9580, <https://orcid.org/0000-0002-5603-3464>

Плахтинский Владимир Владимирович, д.х.н., профессор, профессор кафедры «Общая и аналитическая химия», ФГБОУ ВО «Ярославский государственный технический университет» (150023, Россия, Ярославль, Московский пр-т, д. 88). E-mail: plakhtinskiyvv@ystu.ru. Scopus Author ID 6602528008, SPIN-код РИНЦ 3754-6178, <https://orcid.org/0000-0002-6560-0600>

Кабанова Виктория Сергеевна, аспирант кафедры «Общая и физическая химия», ФГБОУ ВО «Ярославский государственный технический университет» (150023, Россия, Ярославль, Московский пр-т, д. 88). E-mail: viktoriya.kabanova.1999@mail.ru. Scopus Author ID 57749250400, SPIN-код РИНЦ 1221-0200, <https://orcid.org/0000-0001-6635-6315>

Смурова Алина Александровна, магистрант, ФГБОУ ВО «Ярославский государственный технический университет» (150023, Россия, Ярославль, Московский пр-кт, д. 88). E-mail: smurovaaa@mail.ru. <https://orcid.org/0000-0002-5280-7573>

The article was submitted: February 27, 2023; approved after reviewing: March 29, 2023; accepted for publication: November 08, 2023.

*Translated from Russian into English by M. Povorin
Edited for English language and spelling by Thomas A. Beavitt*

CHEMISTRY AND TECHNOLOGY OF ORGANIC SUBSTANCES

ХИМИЯ И ТЕХНОЛОГИЯ ОРГАНИЧЕСКИХ ВЕЩЕСТВ

ISSN 2686-7575 (Online)

<https://doi.org/10.32362/2410-6593-2023-18-6-517-533>



UDC 548.03+53.092+539.26+535.375.54

RESEARCH ARTICLE

Effect of adding technologically processed antibodies to interferon-gamma into a parent solution on the structural features of triglycine sulfate crystals grown from this solution

German O. Stepanov¹, Natalia N. Rodionova^{1,✉}, Roman R. Konstantinov¹, Kirill A. Subbotin^{2,3}

¹*Materia Medica Holding, Moscow, 129172 Russia*

²*Prokhorov General Physics Institute of the Russian Academy of Sciences, Moscow, 119991 Russia*

³*Mendeleev University of Chemical Technology of Russia, Moscow, 125047 Russia*

✉ *Corresponding author, e-mail: rodionovann@materiamedica.ru*

Abstract

Objectives. *Ferroelectric triglycine sulfate (TGS) belongs to a group of crystals whose properties are sensitive even to minor changes in growth conditions. The mechanism of spontaneous polarization in TGS is associated with the adjustment of protons which participate in the formation of hydrogen bonds. Therefore, the state of the parent solution plays an important role in the crystal formation. The study aims to investigate the structural features of TGS crystals grown using aqueous alcoholic solutions of technologically processed antibodies to interferon-gamma, in comparison with those of the crystals grown using the control solutions (technologically processed phosphate-buffered saline and intact aqueous alcoholic solution).*

Methods. X-ray diffraction assay and Raman spectroscopy.

Results. The effect of solutions of the technologically processed antibodies to interferon-gamma added to a parent solution on the growth of TGS single crystals is established. This effect manifests in the changing in occupancy of the proton sublattice of the crystal grown from the parent solution containing technologically processed antibodies to interferon-gamma, as compared with the crystals grown from the control solutions. In the case of the crystal grown from the solution containing technologically processed antibodies to interferon-gamma, this change in the occupancy of the proton lattice is expressed in an increase in the length of N2–C3 bonds.

Conclusions. Adding the technologically processed antibodies in the parent solution before the crystal growth can affect the structure of TGS crystals.

Keywords: technologically processed antibodies, triglycine sulfate, single crystal, X-ray diffraction assay, Raman spectroscopy

For citation: Stepanov G.O., Rodionova N.N., Konstantinov R.R., Subbotin K.A. Effect of adding technologically processed antibodies to interferon-gamma into a parent solution on the structural features of triglycine sulfate crystals grown from this solution. *Tonk. Khim. Tekhnol. = Fine Chem. Technol.* 2023;18(6):517–533. <https://doi.org/10.32362/2410-6593-2023-18-6-517-533>

НАУЧНАЯ СТАТЬЯ

Влияние добавления в маточный раствор технологически отработанных антител к интерферону-гамма на структурные особенности выращиваемых из этого раствора кристаллов триглицинсульфата

Г.О. Степанов¹, Н.Н. Родионова^{1,✉}, Р.Р. Константинов¹, К.А. Субботин^{2,3}

¹НПФ «МАТЕРИА МЕДИКА ХОЛДИНГ», Москва, 129172 Россия

²Институт общей физики им. А.М. Прохорова РАН, Москва, 119991 Россия

³Российский химико-технологический университет им. Д.И. Менделеева, Москва, 125047 Россия

✉ Автор для переписки, e-mail: rodionovann@materiamedica.ru

Аннотация

Цели. Сегнетоэлектрик триглицинсульфат (ТГС) относится к группе кристаллов, свойства которых чувствительны даже к незначительным изменениям условий получения. Механизм возникновения спонтанной поляризации в ТГС связан с упорядочением протонов, участвующих в образовании водородных связей, поэтому при формировании кристалла важна роль состояния маточного водного раствора. Цель работы — изучить структурные особенности кристаллов ТГС, выращенных с применением водно-спиртового раствора технологически обработанных антител

к интерферону-гамма, по сравнению с таковыми у кристаллов, выращенных с применением контрольных растворов (технологически-обработанного раствора фосфатно-солевого буфера и интактного водно-спиртового раствора).

Методы. Рентгеноструктурный анализ и спектроскопия комбинационного рассеяния света.

Результаты. Показано влияние растворов технологически обработанных антител к интерферону-гамма, применявшихся при изготовлении маточных растворов, использованных при выращивании кристаллов ТГС, на структурные особенности этих кристаллов. Данное влияние выражается в изменении заселенностей протонной подрешетки кристаллов, выращенных из раствора, содержащего технологически обработанные антитела к интерферону-гамма, по сравнению с кристаллами, выращенными из контрольных растворов, и проявляется в увеличении длины связей N2–C3.

Выводы. Добавление технологически обработанных антител к маточному раствору, используемому для выращивания кристаллов, способно оказывать влияние на структуру кристаллов ТГС.

Ключевые слова: технологически обработанные антитела, триглицинсульфат, кристалл, рентгеноструктурный анализ, спектроскопия комбинационного рассеяния света

Для цитирования: Степанов Г.О., Родионова Н.Н., Константинов Р.Р., Субботин К.А. Влияние добавления в маточный раствор технологически обработанных антител к интерферону-гамма на структурные особенности выращиваемых из этого раствора кристаллов триглицинсульфата. *Тонкие химические технологии*. 2023;18(6):517–533. <https://doi.org/10.32362/2410-6593-2023-18-6-517-533>

INTRODUCTION

Triglycine sulfate (TGS) is a well-known ferroelectric which finds wide application in electronics and other fields. The properties of ferroelectrics are sensitive to even slight variations in synthesis conditions [1]. TGS consists of three glycine molecules and one sulfate anion. Glycine, due to its amphoteric nature, presents positively charged glycinium cations $\text{NH}_3^+\text{CH}_2\text{COOH}$ in acidic solutions, negatively charged anions $\text{NH}_2\text{CH}_2\text{COO}^-$ in alkaline solutions, and bipolar zwitterions $\text{NH}_3^+\text{CH}_2\text{COO}^-$ in a neutral medium. Thus, two glycinium cations chemically bonded to sulfate ions and one zwitter ion are present in the structure of TGS. Carboxyl groups, amino groups, and sulfate ions are connected to each other in the crystal by a complex network of hydrogen bonds [2] (Fig. 1).

Since the mechanism of spontaneous polarization in TGS is related to the ordering of protons involved in the formation of hydrogen bonds [3],

the role of the state of aqueous or aqueous alcoholic solution (AAS) of TGS during crystal growth from this solution cannot be overestimated. In particular, it has been previously shown that the amount of water and its structural localization in the crystal at low and high temperatures differ. TGS crystals grown at room temperature (20°C) contain about 9 wt % of water, whereas when growing the crystal at temperatures below 0°C, the water content reaches almost 19 wt %. Most of the water is located in microinclusions rather than in the form of solid solution [1, 4–5].

The technological processing (TP) of solutions of various substances includes multiple consecutive dilutions accompanied by intensive vibration treatment. It can lead to changes in various physicochemical properties of TP substances. A large number of dilution steps leads to a theoretical reduction of the concentration of the initial substance in the solution of at least 10^{24} (i.e., the resulting solution may contain only single molecules of the dissolved

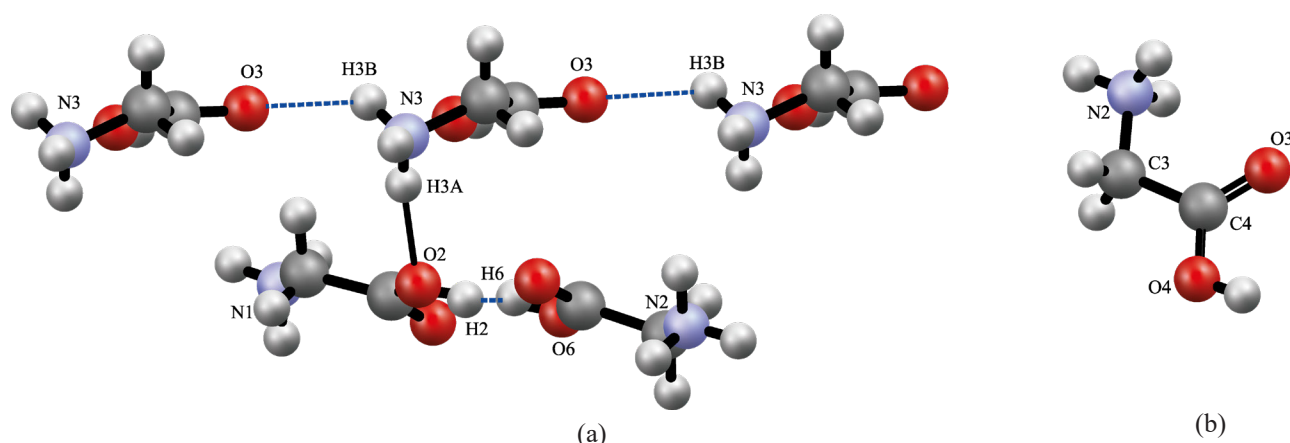


Fig. 1. Glycine groups and intermolecular hydrogen bonds (represented by lines-dots) in the TGS molecule (a) and a schematic representation of the glycine cation (b).

Structurally equivalent atoms are indicated by the same numbers.

Figures are created in Mercury soft (Cambridge Crystallographic Data Center, United Kingdom).

substance or not contain them at all). Despite this, such a solution differs in its physicochemical characteristics from the characteristics of the solvent: water or AAS [7–13]. A change in the nature of hydrogen bonds between water molecules in the substance, which has undergone this treatment, is also shown in comparison to usual water [13–20].

It was shown at the example of TP-antibodies (TP-Abs) to interferon-gamma (IFN- γ), that their biological effects are based on the modifying action of TP-Abs on its target [6, 21]. This is attained through the influence on the hydrate shells surrounding the protein in aqueous solution [22]. Thus, since TP affects the solution properties by changing the hydrogen bonds, which in turn are involved in the occurrence of spontaneous polarization in TGS, it can be assumed that the TP solution will also affect the structure of the crystal grown in such an aqueous solution, whose new properties may be fundamental for the realization of the effect.

The aim of this work is to study the structural features of TGS crystals grown using AAS of TP-Abs to IFN- γ in comparison with those of crystals grown using the technologically treated phosphate-buffered saline (PBS) or intact AAS. The study was carried out by X-ray diffraction (XRD) assay and Raman spectroscopy.

MATERIALS AND METHODS

Solvents for crystal preparation

In the process of crystal growth, the following types of aqueous alcoholic solvents for preparations of the parent solutions were used:

1) AAS of Abs to IFN- γ subjected to the process of gradual reduction of their initial concentration—TP-Abs to IFN- γ . The technique of obtaining of the TP-Abs to IFN- γ is as follows: the preparation of Abs to IFN- γ solution (2.5 mg/mL) was mixed with aqueous solution of ethyl alcohol (36 vol %) in a ratio of 1:100 with intensive vibration treatment to obtain the first centesimal dilution. All the subsequent dilutions contained one part of the previous solution and 99 parts of AAS, and intensive vibration treatment was applied at each subsequent dilution stage. Finally, the sample obtained was a mixture of centesimal dilutions: 12th, 30th, and 50th. More detailed description of the TP-Abs to IFN- γ preparation technique can be found in [7].

Based on the overall dilution ratio, the theoretical concentration of Ab in the final solution should not exceed $2.5 \cdot 10^{-24}$ mg/mL. However, according to physicochemical studies, for samples made with use of the high dilution preparation technique, this estimate may be incorrect due to the non-linear decrease in the concentration of the dissolved substance. In fact, it was shown that even at dilutions lower than 10^{24} -fold, the dissolved substance molecules can be retained due to the flotation effect [23, 24]. Abs to IFN- γ were produced in accordance with the current European Union Good Manufacturing Practice (GMP) requirements for starting materials¹ by *AB Biotechnology* (Edinburgh, United Kingdom).

¹ Europe U. Directive 2004/27/EC of the European Parliament and of the Council of March 31, 2004 Amending Directive 2001/83/EC on the Community Code Relating to Medicinal Products for Human Use. Official Journal of the European Union. L2004;136:34–57. URL: <https://eur-lex.europa.eu/legal-content/EN/TXT/PDF/?uri=CELEX:32004L0027>. Accessed November 01, 2023.

2) Placebo control solution in AAS was prepared using a similar dilution procedure applied to the PBS solution prepared from PBS tablet (*Sigma-Aldrich*, USA), pH = 7.2.

3) Intact control solution was an AAS, not subjected to any additional treatment.

All the solutions were prepared using water obtained with the Milli-Q purification system (*Millipore*, Darmstadt, Germany) and checked for possible impurities by fluorescence spectroscopy and specific conductivity measurements. The sample manufacturer is GMP certified, in order to ensure strict adherence to sample preparation protocols. All samples were prepared under clean conditions (purity class D) in a laminar flow hood using sterile automatic pipettes with sterile tips. All the samples were prepared on the same day by the same staff member and under the same conditions. The preparation protocol took into account any contamination of vials from other glassware, solvent batches or the atmosphere. This allowed compensation for the possible effects of variations in atmospheric pressure and temperature.

TGS crystal growth

Crystalline samples of TGS were grown from solutions using the above solvents by the method of gradual temperature reduction. The growth experiments were carried out in two stages. In the first stage, seed crystals (up to 3 mm in size) were prepared by spontaneous crystallization in a laboratory glass with the natural temperature reduction. Further, in order to obtain larger crystalline samples using the seed crystals, a controlled reduction in the temperature of the parent solution was carried out in a special laboratory programmable crystallization unit (crystallizer). The description of this crystallizer can be found in [25].

Preparation of the seed crystals

At the beginning, parent solutions were prepared in the crystallizer using the above solvents containing TP-Abs to IFN- γ , TP-PBS, and AAS with a concentration of 42 wt % TGS. Such solutions had a saturation temperature of about 40–45°C, determined by preheating the solution to temperatures slightly higher than the saturation temperature. Such overheating was performed, in order to prevent spontaneous crystallization of the solution during its pouring into the crystallizer [25].

For the preparation of the parent solutions, we used TGS of pure grade (*Shostka Chemical Reagents Plant*, Ukraine), which underwent additional purification. Additional purification consisted in fractional recrystallization in two stages. At the first stage, a saturated hot solution (prepared using

tridistilled water) was fabricated and then filtered from the precipitate on a Schott filter No. 3. This step was followed by spontaneous mass crystallization overnight with stirring. In the next step, the crystalline precipitate obtained was again dissolved in tridistilled water and the above procedure of the filtration and mass crystallization was repeated. Three parent solutions of 350 mL each were prepared.

A 50-mL aliquot was taken from each parent solution at a temperature higher than the saturation temperature and transferred to a separate laboratory glass. Here it was spontaneously crystallized for 8 h at a natural temperature reduction to room temperature (20°C) without stirring. After the aliquot cooled down, the remained solution was decanted from the formed seed crystals.

Preparation of crystals for research

Seed crystals were placed in the parent solution prepared in the crystallizer at the above-mentioned saturation temperature. Then the crystallizer was sealed. After 72 h of holding the parent solution with the inoculum crystal at saturation temperature, stirring was initiated at the temperature decrease. The temperature reduction was carried out for 14 days according to a special schedule (the temperature reduction rate was gradually increased from about 0.1°C/day in the 1st day to 4°C/day in the 14th day of cooling, similar to [26]). After that, the crystallizer was opened, the parent solution was decanted from the crystals. Then the crystals were removed from the crystallizer, blotted on filter paper and air-dried.

The grown crystals had a pronounced natural cut. After they had been obtained, the crystal samples were stored in plastic tubes at room temperature. From the parent solution with TP-Abs to IFN- γ , 4 large SST crystals (with a size in one direction of more than 5 mm) were grown. From the parent solution with TP-PBS, 5 large SST crystals (more than 5 mm) and 5 small crystals (less than 5 mm) were grown. From the parent solution with AAS, about 20 small crystals (less than 3 mm) were grown.

Preparation of crystals for XRD

For each type of solvent three crystal samples were investigated by XRD. The preparation of samples for XRD was carried out by splintering from the main crystal a fragment with the size not less than $0.1 \times 0.1 \times 0.1$ mm³. The visually perfect transparent crystal fragment selected with the help of an optical microscope was attached to a glass thread with the help of vacuum grease (Fig. 2).



Fig. 2. Photos of TGS crystals pasted on a glass thread for conducting XRD.

In order to determine the quality of the sample, a preliminary express scan was performed using the built-in function included in the CrysAlisPro XRD experiment control software package (*Rigaku*, USA)².

XRD

A Xcalibur, Sapphire 3, Gemini single crystal diffractometer (*Rigaku*, Japan), MoK_α radiation ($\lambda = 0.71073 \text{ \AA}$) was used for XRD studies. In the

experiment, ω -scanning with a step of 1° was used. The exposure was 15 s per step. The angular position of the CCD detector (54.25°) was chosen to record the reflections with the best resolution of $\sin\theta/\lambda \approx 0.5 \text{ \AA}^{-1}$.

The processing of diffractograms (peak search, determination of unit cell parameters, integration of reflections intensities) was carried out in automatic mode in the CrysAlisPro program (*Rigaku*, USA). The solution and refinement of the atomic structure of crystals was performed in the Shelx program complex using the ShelxLe graphical shell (*Shelx*, Germany)³.

² <https://www.rigaku.com/products/crystallography/crystalis>. Accessed November 01, 2023.

³ <https://www.shelxle.org/shelx/eingabe.php>. Accessed November 01, 2023.

Methodology for the determination of hydrogen atoms

Under normal conditions, TGS crystals are in the ferroelectric phase (Curie point (T_c) is 49°C). This ensures that the crystal is partitioned into domains possessing spontaneous polarization. Without additional measures (e.g., imposition of an external electric field), which are not available for the instrument configuration used, the XRD results of such material may contain artifacts related to twinning. Therefore, the position of only certain hydrogen atoms in the structure was determined from electron density difference synthesis. The missing hydrogen atoms were then added on the basis of geometric calculations of characteristic valence angles in organic compounds. However, in the final solution of each structure, all hydrogen atoms were localized and refined according to the so-called riding model to avoid fluctuations. The N–H, O–H, and C–H bond lengths, as well as valence angles and thermal parameters, were fixed. The exact coordinates are refined parameters and are calculated according to the standard scheme. The above approach is generally accepted and enabled us to avoid problems with the occurrence of distortions which contradict the fundamental crystallochemical approaches (e.g., unrealistically short or unrealistically long bonds between atoms) [3].

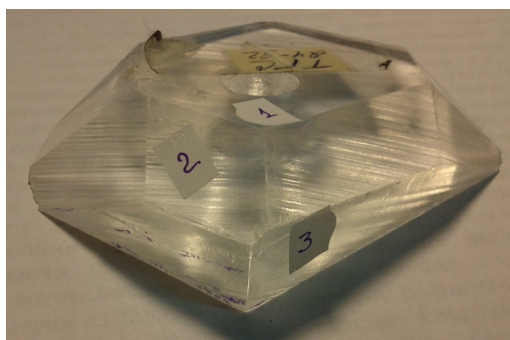
Raman spectroscopy

The Raman spectra of crystals were measured using an Integra Spectra micro-Raman spectrometer

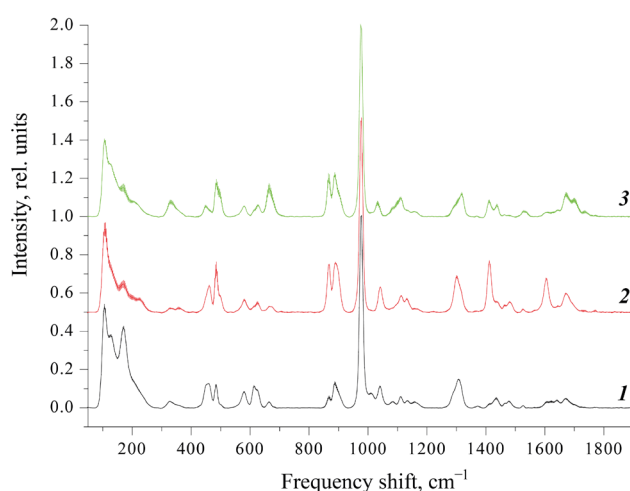
(NT-MDT, Zelenograd, Russia). The crystal was placed on a cover glass and positioned on the slide of an inverted microscope, in order that the trial laser beam (MSL-III-532 50 mW laser, Changchun New Industries Optoelectronics Technology Co., China) fell on the selected facets. Measurement parameters: excitation light wavelength 532 nm, power on the sample approximately 5 mW, grating 600, objective lens 5×, recording time of one spectrum 60 s.

Four crystals grown from a parent solution containing TP-Abs to IFN- γ and two crystals grown from a parent solution containing TP-PBS were analyzed. Three natural facets of each crystal were analyzed. Three spectra were measured from each facet while moving the crystal slightly across the slide.

In addition, the facet spectra of a reference TGS crystal (Fig. 3a), previously grown using the technique described in [26], were measured. The TGS reference crystal under consideration belongs to the monoclinic syngony with the 2/m point group. This point group is characterized by open simple shapes: pinocoids and rhombic prisms. The measured spectra of different faces of the reference crystal are shown in Fig. 3b. The crystal faces were conventionally labeled as type 1, 2, or 3 depending on the shape of the spectrum. Based on the data of [26] with the description of the basic equilibrium faceting of the TGS crystal, we can refer 1, 2, and 3 type faces to the following simple forms. By shape and location, the facet of type 1 (as well as by the trace from the



(a)



(b)

Fig. 3. Standard crystal of TGS (a) and the RAMAN spectra from the characteristic facets of this crystal (b).

The numbers indicate the facets from which the corresponding spectra were recorded.

All Raman spectra are presented here and further as average value \pm error of the average.

columnar seed holder) belongs to the pinocoid facet belonging to the $\{001\}$ family. The face of type 2 belongs to the family of faces of the rhombic prism $\{-111\}$. The facet of type 3 (neighboring between facets a and b with indices (100) and (010), respectively) belongs to the faces of the rhombic prism $\{110\}$.

The faces of the crystals investigated (grown from the parent solution containing TP-Abs to IFN- γ or TP-PBS) were correlated with the faces of the reference TGS crystal on the basis of the correspondence of Raman spectra. For this purpose, the ratio of spectral bands in the regions of 860–930, 1060–1140, 1360–1440, and 1560–1700 cm^{-1} was visually evaluated. Comparison of the investigated crystals of TGS was carried out on the basis of the spectra of those faces which correspond to the spectra of the face of type 2 (family of faces of rhombic prism $\{-111\}$) of the standard crystal of TGS.

When processing the measured spectra, we subtracted the background value obtained by fitting the baseline with a polynomial function coinciding with the points of the spectrum minimum. Then the spectra obtained were normalized by the intensity of the band with frequency $\nu = 975 \text{ cm}^{-1}$ (the most intense band of the spectrum due to vibrations of the SO_4 group). After that, we determined the intensity of peaks with $\nu = 1671 \text{ cm}^{-1}$ and 1604 cm^{-1} .

The intensities of maxima on the spectra obtained from one face of one crystal were averaged. The mean value and the error of the mean at each point characterizing the statistical scatter of the data were given.

Statistical analysis

Analysis and visualization of the data obtained were performed using the R statistical computing environment version 4.0.2 (*R Foundation for Statistical Computing*, Vienna, Austria).

Descriptive statistics were calculated based on the results of Raman spectroscopy, while comparison of groups was performed using Student's t -test. Distribution normality was evaluated by the Shapiro–Wilk test, while homogeneity of dispersions was evaluated by the Bartlett test. XRD data were compared using the parametric Tukey's criterion.

Differences between the analyzed groups were considered statistically significant with an error probability $p < 0.05$ (i.e., the probability of obtaining such or stronger differences, provided that there were no differences between the compared groups, was less than 5%).

RESULTS AND DISCUSSION

XRD

According to XRD data, all crystals possessed symmetry corresponding to the space group $P2_1$ of the monoclinic syngony, i.e., they did not contain an inversion center. In all experiments, the value of the signal-to-noise ratio $(\Delta/\sigma)_{\text{max}}/(\Delta/\sigma)_{\text{av}}$ was close or strictly equal to zero. This indicates that these models meet the real minimum of the least squares method, i.e., the model of atomic-molecular composition of crystals had been chosen correctly. The high quality of the crystal and the correspondence of the found model to the experimental data are evidenced by the following values:

- The maximum value of the scattering angles θ exceeds 36° , indicating a good intensity of reflection by crystals at far scattering angles. It also corresponds to the high number of measured reflection intensities (more than 12000).
- The minimum and maximum residual electron density in most experiments does not exceed the absolute value of $0.5 \text{ e}/\text{\AA}^3$, corresponding to a high degree of fit of the model to the experimental data.
- All calculated R-factors (inconsistency factors) are quite small, also corresponding to a high degree of model fit to the experimental data.

The structure of TGS is complex and represents a grid of $\text{NH}_2\text{CH}_2\text{COOH}$ glycine molecules and SO_4 tetrahedrons linked by $\text{O}-\text{H}\cdots\text{O}$ and $\text{N}-\text{H}\cdots\text{O}$ hydrogen bonds (Fig. 1). The lengths of valence bonds (Table 1), as well as valence angles (Table 2), were calculated from the XRD data for the grown TGS samples.

The statistical analysis of the obtained results revealed statistically significant differences in the values of N2–C3 bond length between the samples of TGS grown from solutions containing TP-Abs to IFN- γ and TP-PBS (Fig. 4).

This parameter corresponds to the distance between the amino group $-\text{NH}_2$ and the methylene bridge $-\text{CH}_2-$ of the glycine molecule. The nearest environment of the $-\text{NH}_2$ functional group, which is not connected with it by a rigid covalent bond, is represented by two SO_4^{2-} anions and a similar grouping of the neighboring glycine molecule. Since these groupings of atoms include electronegative elements (O, N) and electropositive hydrogen, all the conditions for the formation of hydrogen bonds between these groupings are met. The observed difference in the lengths of N2–C3 bonds can be explained by differences in the proton occupancy of the positions of hydrogen bonds, in which the N2 atoms participate.

Table 1. Lengths of interatomic bonds in TGS crystals grown from various parent solutions, Å (measurement errors are given in parentheses)

Bond	TP-Abs to IFN- γ			TP-PBS			AAS		
	1	2	3	1	2	3	1	2	3
C1–N1	1.466(4)	1.466(3)	1.465(3)	1.465(3)	1.476(7)	1.470(3)	1.467(3)	1.472(4)	1.467(3)
C1–C2	1.503(4)	1.507(3)	1.504(3)	1.504(3)	1.512(8)	1.505(3)	1.500(3)	1.500(4)	1.505(3)
S1–O9	1.4647(13)	1.4664(9)	1.4654(10)	1.4652(10)	1.464(2)	1.4651(9)	1.4602(10)	1.4665(11)	1.4668(10)
S1–O8	1.466(2)	1.4674(15)	1.4668(18)	1.4681(16)	1.468(3)	1.4670(15)	1.4637(15)	1.4683(19)	1.4690(17)
S1–O10	1.4765(19)	1.4794(14)	1.4800(17)	1.4773(16)	1.477(3)	1.4777(15)	1.4732(14)	1.4775(18)	1.4788(17)
C3–C4	1.512(4)	1.514(3)	1.513(3)	1.511(3)	1.500(8)	1.514(3)	1.510(3)	1.518(4)	1.513(3)
N3–C5	1.466(3)	1.470(2)	1.470(3)	1.470(3)	1.473(6)	1.470(3)	1.465(3)	1.470(3)	1.470(3)
C6–O5	1.201(3)	1.205(2)	1.201(2)	1.202(2)	1.202(5)	1.201(2)	1.197(2)	1.205(2)	1.206(2)
C6–O6	1.303(2)	1.3026(18)	1.304(2)	1.304(2)	1.298(4)	1.302(2)	1.3013(19)	1.303(2)	1.302(2)
C6–C5	1.511(3)	1.5102(19)	1.512(2)	1.511(2)	1.509(4)	1.515(2)	1.508(2)	1.512(2)	1.514(2)
S1–O7	1.4833(13)	1.4847(9)	1.4838(11)	1.4832(10)	1.484(2)	1.4840(10)	1.4799(10)	1.4852(11)	1.4864(11)
O1–C2	1.230(4)	1.229(3)	1.231(3)	1.232(3)	1.218(7)	1.229(3)	1.229(3)	1.234(3)	1.229(3)
O2–C2	1.284(4)	1.287(2)	1.285(3)	1.286(3)	1.280(6)	1.286(3)	1.282(3)	1.285(3)	1.285(3)
N2–C3	1.470(4)	1.468(3)	1.467(3)	1.466(3)	1.460(7)	1.461(3)	1.461(3)	1.463(4)	1.467(3)
O3–C4	1.209(4)	1.216(3)	1.216(3)	1.212(3)	1.223(7)	1.216(3)	1.209(3)	1.212(3)	1.216(3)

Table 2. Values of valence bond angles in TGS crystals grown from various parent solutions, degrees (measurement errors are given in parentheses)

Angle	TP-Abs to IFN- γ			TP-PBS			AAS		
	1	2	3	1	2	3	1	2	3
N1–C1–C2	111.4(3)	111.42(17)	111.6(2)	111.5(2)	110.9(5)	111.31(18)	111.25(18)	111.3(2)	111.5(2)
O9–S1–O8	111.01(15)	111.28(11)	111.15(12)	111.12(12)	111.0(3)	111.13(11)	111.27(11)	111.10(13)	111.12(12)
O9–S1–O10	110.22(15)	110.06(11)	110.21(13)	110.27(12)	110.5(3)	110.30(11)	110.19(11)	110.29(13)	110.18(12)
O8–S1–O10	109.72(8)	109.78(6)	109.70(7)	109.65(7)	109.68(12)	109.72(6)	109.59(6)	109.74(7)	109.81(7)
O9–S1–O7	110.26(8)	110.24(6)	110.27(7)	110.29(7)	110.27(12)	110.25(6)	110.26(6)	110.21(7)	110.29(6)
O8–S1–O7	108.11(14)	108.02(10)	108.07(12)	108.00(11)	107.8(2)	107.99(10)	108.09(10)	108.11(13)	108.00(12)
O10–S1–O7	107.43(14)	107.35(10)	107.34(12)	107.41(12)	107.5(3)	107.36(11)	107.35(10)	107.30(13)	107.35(12)

Table 2. Continued

Bond	TP-Abs to IFN- γ			TP-PBS			AAS		
	1	2	3	1	2	3	1	2	3
O1–C2–O2	126.2(3)	126.12(19)	126.2(2)	126.1(2)	127.1(6)	126.2(2)	126.1(2)	125.7(3)	126.2(2)
O1–C2–C1	120.4(2)	120.49(17)	120.5(2)	120.52(19)	120.6(4)	120.68(18)	120.62(17)	120.8(2)	120.5(2)
O2–C2–C1	113.4(3)	113.40(19)	113.3(2)	113.3(2)	112.3(5)	113.1(2)	113.2(2)	113.5(2)	113.3(2)
N2–C3–C4	110.8(3)	110.79(16)	111.0(2)	110.8(2)	111.7(5)	111.01(18)	110.81(18)	111.1(2)	111.0(2)
O5–C6–O6	125.2(2)	125.10(14)	125.04(17)	125.09(16)	125.3(3)	125.19(15)	124.99(15)	124.99(17)	125.07(16)
O5–C6–C5	121.6(2)	121.59(14)	121.71(17)	121.76(16)	121.2(3)	121.64(16)	121.72(15)	121.62(17)	121.51(16)
O6–C6–C5	113.24(17)	113.30(12)	113.25(15)	113.14(14)	113.4(3)	113.17(13)	113.28(13)	113.39(15)	113.43(14)
N3–C5–C6	112.17(18)	111.84(13)	111.92(15)	111.97(14)	111.8(3)	111.80(14)	111.87(13)	111.88(16)	111.85(15)
O3–C4–O4	126.2(3)	126.5(2)	126.2(2)	126.1(2)	125.0(6)	126.2(2)	126.3(2)	126.6(3)	126.2(2)
O3–C4–C3	122.2(3)	121.81(17)	121.8(2)	122.1(2)	122.1(5)	121.77(19)	121.98(18)	121.7(2)	121.9(2)
O4–C4–C3	111.5(3)	111.71(19)	111.9(2)	111.8(2)	112.8(5)	112.0(2)	111.7(2)	111.6(3)	111.9(2)

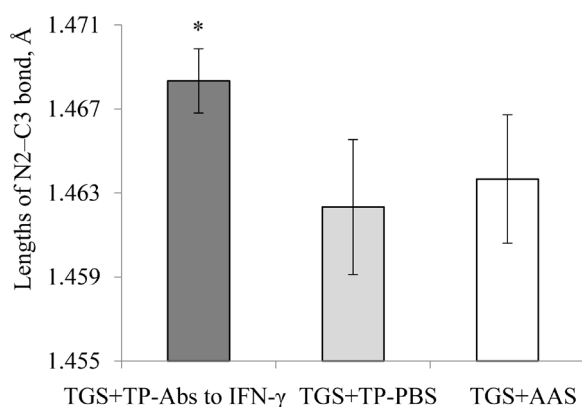


Fig. 4. Average value of the N2–C3 valence bond lengths for TGS crystals grown from a solution containing TP-Abs to IFN- γ , as well as from control solutions (Mean \pm Standard deviation (M \pm Sd)).

* $p < 0.05$ relative to the intensity for TGS crystals from a solution containing the TP-PBS.

Raman spectroscopy

The measured results of the Raman spectra of crystals obtained from solutions containing TP-Abs to IFN- γ and TP-PBS are presented in Table 3. The Raman spectra for each type of crystals are shown in Fig. 5. The spectra presented in Fig. 5a

correspond to the shape (namely, the ratio of spectral bands in the regions 860–930, 1060–1140, 1360–1440, and 1560–1700 cm^{-1}) of the spectrum of the face of the reference TGS crystal, conventionally labeled **2** (Fig. 3b). The intensity of the peak at 1671 cm^{-1} differs in crystals of different types (Fig. 5b). Therefore, we further compared the intensities of this maximum using statistical methods.

Statistical analysis using the Mann–Whitney criterion showed that band intensity at 1671 cm^{-1} for the samples obtained in the presence of TP-Abs to IFN- γ was statistically significantly higher than the intensity of the band of the same name for the samples grown in the presence of TP-PBS ($p < 0.05$) (Fig. 5c). The vibrational mode at 1671 cm^{-1} in the Raman spectra of TGS crystals corresponds to the valence vibrations of the C=O group (stretching-compression vibrations) [27]. These groups of atoms are involved in hydrogen bonding of individual glycine molecules into chains. Glycine group G3 is known to be ordered into chains by means of N3–H3B...O3 bonds, and glycine groups G1 and G2 form dimers by means of O2–H2...H4–O4 bonds [28]. More active binding of glycine molecules, with a degree of hydrogen bond occupancy by protons close to unity at a given position, leads to decreased intensity of valence

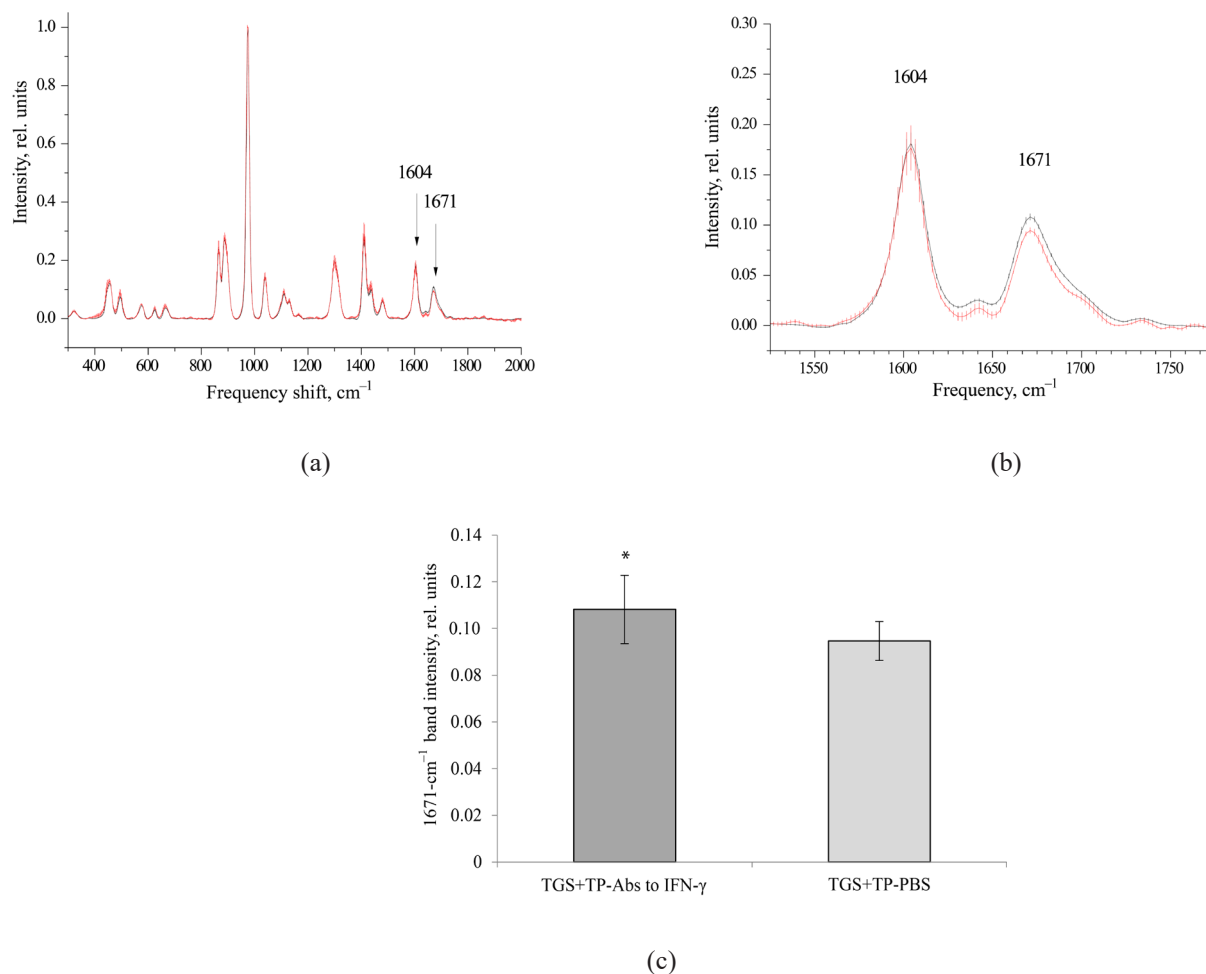


Fig. 5. (a) RAMAN spectra obtained from the type 2 facet of crystals grown in the presence of TP-Abs to IFN- γ (black line) and TP-PBS (red line). (b) Spectral region on a larger scale. (c) Intensity of the Raman band with $\nu = 1671 \text{ cm}^{-1}$ for TGS crystals grown from a solution containing TP-Abs to IFN- γ ($M \pm Sd$); * $p < 0.05$ relative to the intensity for TGS crystals from a solution containing the TP-PBS.

vibrations of the C=O double bond. It also leads to a decrease in the intensity of the corresponding vibrational mode of the Raman spectrum. Accordingly, with a decrease in the degree of occupancy of hydrogen bond positions in glycine dimers and chains, an increase in the intensity of the vibrational mode at 1671 cm^{-1} is observed. Thus, this parameter allows us to indirectly make a comparison between groups of samples of TGS crystals by the degree of occupancy of hydrogen bond positions. In this case it is probable that differences in the intensity of vibrations and polarizability can be caused by a small change in the microenvironment of these bonds in the glycine molecule. The stabilization of the zwitter-ion conformer most likely occurs with the participation of one water molecule [29].

Thus, the results of crystal studies by Raman spectroscopy show that a smaller number of hydrogen bonds is formed in the sample of TGS crystal obtained in the presence of TP-Abs to IFN- γ .

According to the XRD data, we can observe a change in the length of the N2–C3 bond within one molecule. TGS crystals are known to manifest a proton hopping mechanism of proton transfer along the OH–O hydrogen bonding network [30]. The differences in the degree of proton occupancy of hydrogen bond positions can account for the observed difference in the lengths of N2–C3 bonds. In the crystal grown in the presence of TP-Abs to IFN- γ , this bond appears to be longer than in crystals grown from control solutions (TP-PBS and AAS). This implies a decrease in the number of hydrogen bonds. This conclusion is supported by the results obtained in the studies by Raman spectroscopy.

Summarizing the data obtained, we can conclude that both methods show that a smaller number of hydrogen bonds is formed in the sample of TGS crystal when obtained in the presence of TP-Abs to IFN- γ , when compared to crystals grown from control solutions (TP-PBS and AAS). The action

Table 3. Intensity of characteristic bands at 1671 and 1604 cm⁻¹

Band intensity at 1671 cm ⁻¹		Band intensity at 1604 cm ⁻¹	
TGS crystals obtained from a solution containing TP-Abs to IFN- γ	TGS crystals obtained from a solution containing TP-PBS	TGS crystals obtained from a solution containing TP-Abs to IFN- γ	TGS crystals obtained from a solution containing TP-PBS
0.11095	0.08676	0.17695	0.10601
0.12549	0.08759	0.22240	0.09830
0.10790	0.09273	0.17639	0.10012
0.11084	0.10294	0.14632	0.20799
0.07034	0.11127	0.08469	0.24110
0.11334	0.09324	0.13901	0.22482
0.10890	0.08996	0.13426	0.21202
0.13704	0.09287	0.28414	0.22250
0.12293	–	0.25905	–
0.12321	–	0.25545	–
0.12234	–	0.22994	–
0.12176	–	0.22812	–
0.11706	–	0.22272	–
0.09194	–	0.17393	–
0.10321	–	0.11153	–
0.09831	–	0.18336	–
0.09902	–	0.17805	–
0.10156	–	0.17666	–
0.09457	–	0.17712	–
0.10626	–	0.14743	–
0.09664	–	0.14155	–
0.09604	–	0.13451	–

of TP-Abs to IFN- γ , not directed on its target, is probably due to the influence on the growth of TGS of the aqueous solution which acquired new properties when compared to control solutions in the process

of technological processing. This corresponds to the previously obtained data on the realization of the effect of technologically processed proteins through the influence on the hydrate shells of the target molecule [22].

CONCLUSIONS

Summarizing the experimental results, we can conclude that the main effect of TP-Abs solution used to grow the TGS crystals on the properties of these crystals consists in changing the properties of the proton sub-lattice of the crystal. This is a structural component of the crystal, which is the most sensitive to the effects of external factors. The significant importance of water in the electrical properties of crystals has been shown earlier. Therefore, it will be of further interest to study not only the structure but also the properties of crystals grown from AAS subjected to various types of technological processing.

Acknowledgments

The work was financially supported by *Materia Medica Holding, Moscow, Russia*.

Authors' contributions

G.O. Stepanov – data analysis, conceptualization, writing the text of the initial draft;

N.N. Rodionova – data analysis, conceptualization, writing the text of the initial draft;

R.R. Konstantinov – data analysis, editing the article;

K.A. Subbotin – counseling, editing the article.

Conflict of interest

The authors declared the following potential conflicts of interest in connection with the authorship and/or publication of this article: G.O. Stepanov, N.N. Rodionova, and R.R. Konstantinov are employees of *Materia Medica Holding*. *Materia Medica Holding* decided to publish the work and covered the costs associated with the publication of the article, paid for the experimental work, participated in the writing of the manuscript.

REFERENCES

1. Yacenko O.B., Chudotvortsev I.G., Stekhanova G.D., Milovidova S.D., Rogazinskaya O.V. Density and contents of water in triglycinesulfate crystals. *Vestnik Voronezhskogo gosudarstvennogo universiteta. Seriya: Khimiya. Biologiya. Farmatsiya = Proceedings of Voronezh State University. Series: Chemistry. Biology. Pharmacy*. 2006;(2):117–121 (in Russ.).
2. Epifanov G.I. *Fizika tverdogo tela (Solid State Physics)*. Moscow: Vysshaya shkola; 1977. 288 p. (in Russ.).
3. Lines M., Glass A. *Segnetoelektriki i rodstvennye im materialy (Ferroelectrics and Related Materials)*. Transl. from Engl. Moscow: Mir; 1981. 736 p. (in Russ.).
- [Lines M.E., Glass A.M. *Principles and Application of Ferroelectrics and Related Materials*. Oxford: Clarendon Press; 1977. 680 p.]
4. Stekhanova Zh.D., Yatsenko O.B., Milovidova S.D., Sidorkin A.S., Rogazinskaya O.V., Yur'ev A.N. Dielectric properties of crystals triglycine sulfate, grown from aqueous solutions at the temperatures below 0°C. *Vestnik Voronezhskogo gosudarstvennogo universiteta. Seriya: Khimiya. Biologiya. Farmatsiya = Proceedings of Voronezh State University. Series: Chemistry. Biology. Pharmacy*. 2004;(2):46–49 (in Russ.).
5. Stekhanova Z.D., Yatsenko O.B., Milovidova S.D., et al. Properties of Triglycine Sulfate Crystals Grown from Aqueous Solutions. *Russ. J. Appl. Chem*. 2005;78(1):42–49. <https://doi.org/10.1007/s11167-005-0228-9>

СПИСОК ЛИТЕРАТУРЫ

1. Яценко О.Б., Чудотворцев И.Г., Стеханова Ж.Д., Миловидова С.Д., Рогазинская О.В. Плотность и содержание воды в кристаллах триглицинсульфата. *Вестник ВГУ. Серия: Химия. Биология. Фармация*. 2006;(2):117–121.
2. Епифанов Г.И. *Физика твердого тела*. М.: Высшая школа; 1977. 288 с.
3. Лайнс М., Гласс А. *Сегнетоэлектрики и родственные им материалы*: пер. с англ. М.: Мир; 1981. 736 с.
4. Стеханова Ж.Д., Яценко О.Б., Миловидова С.Д., Сидоркин А.С., Рогазинская О.В., Юрьев А.Н. Диэлектрические свойства кристаллов триглицинсульфата, выращенных из водных растворов при температурах ниже 0°C. *Вестник ВГУ. Серия: Химия. Биология. Фармация*. 2004;(2):46–49.
5. Стеханова Ж.Д., Яценко О.Б., Миловидова С.Д., Сидоркин А.С., Рогазинская О.В. Свойства кристаллов триглицинсульфата, выращенных из водных растворов. *Журн. прикладной химии*. 2005;78(1):45–51.
6. Epstein O. The spatial homeostasis hypothesis. *Symmetry*. 2018;10(4):103. <https://doi.org/10.3390/sym10040103>
7. Рыжкина И.С., Муртазина Л.И., Киселева Ю.В., Коновалов А.И. Самоорганизация и физико-химические свойства водных растворов антител к интерферону-гамма в сверхвысоком разведении. *Доклады Академии наук*. 2015;462(2):185–189. <https://doi.org/10.7868/S0869565215140170>

[Original Russian Text: Stekhanova Z.D., Yatsenko O.B., Milovidova S.D., Sidorkin A.S., Rogazinskaya O.V. Properties of Triglycine Sulfate Crystals Grown from Aqueous Solutions. *Zhurnal Prikladnoi Khimii*. 2005;78(1):45–51 (in Russ.).]

6. Epstein O. The spatial homeostasis hypothesis. *Symmetry*. 2018;10(4):103. <https://doi.org/10.3390/sym10040103>

7. Ryzhkina I.S., Murtazina L.I., Kiseleva Ju.V., et al. Self-organization and physicochemical properties of aqueous solutions of the antibodies to interferon gamma at ultrahigh dilution. *Dokl. Phys. Chem.* 2015;462(1):110–114. <https://doi.org/10.1134/S0012501615050048>

[Original Russian Text: Ryzhkina I.S., Murtazina L.I., Kiseleva Ju.V., Konovalov A.I. Self-organization and physicochemical properties of aqueous solutions of the antibodies to interferon gamma at ultrahigh dilution. *Doklady Akademii Nauk*. 2015;462(2):185–189 (in Russ.). <https://doi.org/10.7868/S0869565215140170>]

8. Ryzhkina I., Murtazina L., Gainutdinov K., Konovalov A. Diluted aqueous dispersed systems of 4-aminopyridine: The relationship of self-organization, physicochemical properties, and influence on the electrical characteristics of neurons. *Front. Chem.* 2021;9:623860. <https://doi.org/10.3389/fchem.2021.623860>

9. Konovalov A.I., Mal'tseva E.L., Ryzhkina I.S., et al. Formation of nanoassociates is a factor determining physicochemical and biological properties of highly diluted aqueous solutions. *Dokl. Phys. Chem.* 2014;456(2):86–89. <https://doi.org/10.1134/S0012501614060050>

[Original Russian Text: Konovalov A.I., Ryzhkina I.S., Murtazina L.I., Kiseleva Y.V., Mal'tseva E.L., Kasparov V.V., Pal'mina N.P. Formation of nanoassociates is a factor determining physicochemical and biological properties of highly diluted aqueous solutions. *Doklady Akademii Nauk*. 2014;456(5):561–564 (in Russ.). <https://doi.org/10.7868/S0869565214170174>]

10. Lobyshev V.I. Biological activity of solutions of substances at low and ultra low concentrations. *Biophysics*. 2022;67(4):523–533. <https://doi.org/10.1134/S0006350922040145>

[Original Russian Text: Lobyshev V.I. Biological activity of solutions of substances at low and ultra low concentrations. *Biofizika*. 2022;67(4):658–670 (in Russ.). <https://doi.org/10.31857/S0006302922040044>]

11. Lobyshev V.I. Dielectric characteristics of highly diluted aqueous diclofenac solutions in the frequency range of 20 Hz to 10 MHz. *Phys. Wave Phen.* 2019;27(2):119–127. <https://doi.org/10.3103/S1541308X19020067>

12. Lobyshev V.I. Evolution of high-frequency conductivity of pure water samples subjected to mechanical action: effect of a hypomagnetic field. *Phys. Wave Phen.* 2021;29(2):98–101. <https://doi.org/10.3103/S1541308X21020084>

13. Yablonskaya O., Buravleva E., Novikov K., Voeikov V. Peculiarities of the physicochemical properties of hydrated C60 fullerene solutions in a wide range of dilutions. *Front. Phys.* 2021;9:627265. <https://doi.org/10.3389/fphy.2021.627265>

14. Belov V.V., Belyaeva I.A., Shmatov G.P., et al. IR spectroscopy of thin water layers and the mechanism of action α -tocopherol in ultra low concentrations. *Dokl. Phys. Chem.* 2011;439(1):123–126. <https://doi.org/10.1134/S0012501611070013>

[Original Russian Text: Belov V.V., Belyaeva I.A., Shmatov G.P., Zubareva G.M., Pal'mina N.P. IR spectroscopy of thin water layers and the mechanism of action α -tocopherol in ultra low concentrations. *Doklady Akademii Nauk*. 2011;439(1):68–71 (in Russ.).]

8. Ryzhkina I., Murtazina L., Gainutdinov K., Konovalov A. Diluted aqueous dispersed systems of 4-aminopyridine: The relationship of self-organization, physicochemical properties, and influence on the electrical characteristics of neurons. *Front. Chem.* 2021;9:623860. <https://doi.org/10.3389/fchem.2021.623860>

9. Коновалов А.И., Мальцева Е.Л., Рыжкина И.С., Муртазина Л.И., Киселева Ю.В., Каспаров В.В., Пальмина Н.П. Образование наноассоциатов – фактор, определяющий физико-химические и биологические свойства высоко-разбавленных водных растворов. *Доклады Академии наук*. 2014;456(5):561–564. <https://doi.org/10.7868/S0869565214170174>

10. Лобышев В.И. Биологическая активность малых и сверхмалых концентраций. *Биофизика*. 2022;67(4):658–670. <https://doi.org/10.31857/S0006302922040044>

11. Lobyshev V.I. Dielectric characteristics of highly diluted aqueous diclofenac solutions in the frequency range of 20 Hz to 10 MHz. *Phys. Wave Phen.* 2019;27(2):119–127. <https://doi.org/10.3103/S1541308X19020067>

12. Lobyshev V.I. Evolution of high-frequency conductivity of pure water samples subjected to mechanical action: effect of a hypomagnetic field. *Phys. Wave Phen.* 2021;29(2):98–101. <https://doi.org/10.3103/S1541308X21020084>

13. Yablonskaya O., Buravleva E., Novikov K., Voeikov V. Peculiarities of the physicochemical properties of hydrated C60 fullerene solutions in a wide range of dilutions. *Front. Phys.* 2021;9:627265. <https://doi.org/10.3389/fphy.2021.627265>

14. Белов В.В., Беляева И.А., Шматов Г.П., Зубарева Г.М., Пальмина Н.П. ИК-спектроскопия тонких слоев воды и механизм действия α -токоферола в малых дозах. *Доклады Академии наук*. 2011;439(1):68–71.

15. Бревик И., Шаповалов А.В. Эффекты низкой концентрации в водных растворах в рамках фрактального подхода. *Известия высших учебных заведений. Физика*. 2022;65(2):3–13. <https://doi.org/10.17223/00213411/65/2/3>

16. Shishkina A.V., Ksenofontov A.A., Penkov N.V., Vener M.V. Diclofenac ion hydration: experimental and theoretical search for anion pairs. *Molecules*. 2022;27(10):3350. <https://doi.org/10.3390/molecules27103350>

17. Slatinskaya O.V., Pyrkov Yu.N., Filatova S.A., Guryev D.A., Penkov N.V. Study of the effect of europium acetate on the intermolecular properties of water. *Front. Phys.* 2021;9:641110. <https://doi.org/10.3389/fphy.2021.641110>

18. Penkov N.V. Peculiarities of the perturbation of water structure by ions with various hydration in concentrated solutions of CaCl₂, CsCl, KBr, and KI. *Phys. Wave Phen.* 2019;27(2):128–134. <https://doi.org/10.3103/S1541308X19020079>

19. Penkov N., Fesenko E. Development of terahertz time-domain spectroscopy for properties analysis of highly diluted antibodies. *Appl. Sci.* 2020;10(21):7736. <https://doi.org/10.3390/app10217736>

20. Penkov N. Antibodies processed using high dilution technology distantly change structural properties of IFN γ aqueous solution. *Pharmaceutics*. 2021;13(11):1864. <https://doi.org/10.3390/pharmaceutics13111864>

21. Tarasov S.A., Gorbunov E.A., Don E.S., Emelyanova A.G., Kovalchuk A.L., Yanamala N., Schleker A.S.S., Klein-Seetharaman J., Groenestein R., Tafani J-P., van der Meide P., Epstein O.I. Insights into the mechanism of action of highly diluted biologics. *J. Immunol.* 2020;205(5):1345–1354. <https://doi.org/10.4049/jimmunol.2000098>

22. Woods K.N. Modeling of protein hydration dynamics is supported by THz spectroscopy of highly diluted solutions. *Front. Chem.* 2023;11:1131935. <https://doi.org/10.3389/fchem.2023.1131935>

15. Brevik I., Shapovalov A.V. Effects of low concentration in aqueous solutions within the fractal approach. *Russ. Phys. J.* 2022;65(2):197–207 (in Russ.). <https://doi.org/10.1007/s11182-022-02623-3>
[Original Russian Text: Brevik I., Shapovalov A.V. Effects of low concentration in aqueous solutions within the fractal approach. *Izvestiya Vysshikh Uchebnykh Zavedenii. Fizika.* 2022;65(2):3–13 (in Russ.). <https://doi.org/10.17223/00213411/65/2/3>]
16. Shishkina A.V., Ksenofontov A.A., Penkov N.V., Vener M.V. Diclofenac ion hydration: experimental and theoretical search for anion pairs. *Molecules.* 2022;27(10):3350. <https://doi.org/10.3390/molecules27103350>
17. Slatinskaya O.V., Pyrkov Yu.N., Filatova S.A., Guryev D.A., Penkov N.V. Study of the effect of europium acetate on the intermolecular properties of water. *Front. Phys.* 2021;9:641110. <https://doi.org/10.3389/fphy.2021.641110>
18. Penkov N.V. Peculiarities of the perturbation of water structure by ions with various hydration in concentrated solutions of CaCl_2 , CsCl , KBr , and KI . *Phys. Wave Phen.* 2019;27(2):128–134. <https://doi.org/10.3103/S1541308X19020079>
19. Penkov N., Fesenko E. Development of terahertz time-domain spectroscopy for properties analysis of highly diluted antibodies. *Appl. Sci.* 2020;10(21):7736. <https://doi.org/10.3390/app10217736>
20. Penkov N. Antibodies processed using high dilution technology distantly change structural properties of IFN γ aqueous solution. *Pharmaceutics.* 2021;13(11):1864. <https://doi.org/10.3390/pharmaceutics13111864>
21. Tarasov S.A., Gorbunov E.A., Don E.S., Emelyanova A.G., Kovalchuk A.L., Yanamala N., Schleker A.S.S., Klein-Seetharaman J., Groenestein R., Tafani J-P., van der Meide P., Epstein O.I. Insights into the mechanism of action of highly diluted biologics. *J. Immunol.* 2020;205(5):1345–1354. <https://doi.org/10.4049/jimmunol.2000098>
22. Woods K.N. Modeling of protein hydration dynamics is supported by THz spectroscopy of highly diluted solutions. *Front. Chem.* 2023;11:1131935. <https://doi.org/10.3389/fchem.2023.1131935>
23. Bunkin N.F., Shkirin A.V., Ninham B.W., Chirikov S.N., Chaikov L.L., Penkov N.V., Kozlov V.A., Gudkov S.V. Shaking-induced aggregation and flotation in immunoglobulin dispersions: differences between water and water-ethanol mixtures. *ACS Omega.* 2020;5(24):14689–14701. <https://doi.org/10.1021/acsomega.0c01444>
24. Chikramane P.S., Kalita D., Suresh A.K., Kane S.G., Bellare J.R. Why extreme dilutions reach non-zero asymptotes: a nanoparticulate hypothesis based on froth flotation. *Langmuir.* 2012;28(45):15864–15875. <https://doi.org/10.1021/la303477s>
25. Vainshtein B.K. *Sovremennaya kristallografiya: v 4 t. T. 3. Obrazovanie kristallov (Modern Crystallography: in 4 v. Vol. 3. Formation of Crystals).* Moscow: Nauka; 1980. 408 p. (in Russ.).
26. Koldobskaya M.F., Gavrilova I.V. Growing large faceted TGS crystals in laboratory conditions. In: *Rost kristallov (Crystal Growth).* Moscow: AN USSR; 1961. V. 3. P. 278–282 (in Russ.).
27. Malekfar R., Daraei A. Raman scattering and electrical properties of TGS:PCo (9%) crystal as ambient temperature IR detector. *Acta Physica Polonica A.* 2008;114(4):859–867. <http://doi.org/10.12693/APhysPolA.114.859>
28. Zheludev I.S. *Physics of Crystalline Dielectrics.* V. 1. *Crystallography and Spontaneous Polarization.* New York: Springer; 1971. 346 p. <https://doi.org/10.1007/978-1-4684-8076-4>
29. Крауклис И.В., Тулуб А.В., Головин А.В., Челибанов В.П. Спектры комбинационного рассеяния света глицина и их моделирование в дискретно-континуальной модели сольватной оболочки воды. *Оптика и спектроскопия.* 2020;128(10):1488–1491. <https://doi.org/10.21883/OS.2020.10.50019.161-20>
30. Гаврилова Н.Д., Малышкина И.А. Влияние изменений в структуре сетки водородных связей воды на электрофизические свойства систем «матрица-вода» при ступенчатом нагреве. *Вестник Московского университета. Серия 3. Физика. Астрономия.* 2018;(6):74–80. URL: <http://vmu.phys.msu.ru/file/2018/6/18-6-074.pdf>

29. Krauklis I.V., Tulub A.V., Golovin A.V., *et al.* Raman spectra of glycine and their modeling in terms of the discrete–continuum model of their water solvation shell. *Opt. Spectrosc.* 2020;128(10):1598–1601. <https://doi.org/10.1134/S0030400X20100161>

[Original Russian Text: Krauklis I.V., Tulub A.V., Golovin A.V., Chelibanov V.P. Raman spectra of glycine and their modeling in terms of the discrete–continuum model of their water solvation shell. *Optika i Spektroskopiya.* 2020;128(10):1488–1491 (in Russ.). <https://doi.org/10.21883/OS.2020.10.50019.161-20>]

30. Gavrilova N.D., Malyshkina I. A. The influence of changes in the structure of hydrogen bonds of water on the electrophysical properties of matrix-water systems in stepwise heating. *Moscow Univ. Phys.* 2018;73(6):651–658. <https://doi.org/10.3103/S0027134918060127>

[Original Russian Text: Gavrilova N.D., Malyshkina I. A. The influence of changes in the structure of hydrogen bonds of water on the electrophysical properties of matrix-water systems in stepwise heating. *Vestnik Moskovskogo Universiteta. Seriya 3. Fizika. Astronomiya.* 2018;(6):74–80 (in Russ.). URL: <http://vmu.phys.msu.ru/file/2018/6/18-6-074.pdf>]

About the authors:

German O. Stepanov, Cand. Sci. (Biol.), Senior Research, Materia Medica Holding, (47-1, Trifonovskaya ul., Moscow, 129272, Russia). E-mail: stepanovgo@materiamedica.ru. Scopus Author ID 15046034100, <https://orcid.org/0000-0002-8576-9745>

Natalia N. Rodionova, Cand. Sci. (Biol.), Head of Physicochemical Research, Materia Medica Holding, (47-1, Trifonovskaya ul., Moscow, 129272, Russia). E-mail: rodionovann@materiamedica.ru. <https://orcid.org/0009-0001-7138-9063>

Roman R. Konstantinov, Researcher, Materia Medica Holding, (47-1, Trifonovskaya ul., Moscow, 129272, Russia). E-mail: konstantinovrr@materiamedica.ru. <https://orcid.org/0009-0000-6692-2583>

Kirill A. Subbotin, Cand. Sci. (Eng.), Head of the Department of Laser Crystals and Solid-State Lasers, Prokhorov General Physics Institute, Russian Academy of Sciences (38, Vavilova ul., Moscow, 119991, Russia); Associate Professor, Department of Chemistry and Technology of Crystals, Mendeleev University of Chemical Technology of Russia (9, Miusskaya pl., Moscow, 125047, Russia). E-mail: soubbot1970@gmail.com. Scopus Author ID 6701562918, RSCI SPIN-code 7976-1488, <https://orcid.org/0000-0001-9590-7403>

Об авторах:

Степанов Герман Олегович, к.б.н., ведущий научный сотрудник, ООО «НПФ «Материя Медика Холдинг» (129272, Россия, Москва, ул. Трифоно́вская, д. 47, стр. 1). E-mail: stepanovgo@materiamedica.ru. Scopus Author ID 15046034100, <https://orcid.org/0000-0002-8576-9745>

Родионова Наталья Николаевна, к.б.н., руководитель физико-химических исследований, ООО «НПФ «Материя Медика Холдинг» (129272, Россия, Москва, ул. Трифоно́вская, д. 47, стр. 1). E-mail: rodionovann@materiamedica.ru. <https://orcid.org/0009-0001-7138-9063>

Константинов Роман Романович, научный сотрудник, ООО «НПФ «Материа Медика Холдинг» (129272, Россия, Москва, ул. Трифоновская, д. 47, стр. 1). E-mail: konstantinovrr@materiamedica.ru. <https://orcid.org/0009-0000-6692-2583>

Субботин Кирилл Анатольевич, к.т.н., заведующий отделом лазерных кристаллов и твердотельных лазеров, ФГБУН ФИЦ «Институт общей физики им. А.М. Прохорова Российской академии наук» (119991, Россия, Москва, ул. Вавилова, д. 38); доцент кафедры химии и технологии кристаллов, ФГБОУ ВО «Российский химико-технологический университет им. Д.И. Менделеева» (125047, Россия, Москва, Миусская пл. д. 9). E-mail: soubbot1970@gmail.com. Scopus Author ID 6701562918, SPIN-код РИНЦ 7976-1488, <https://orcid.org/0000-0001-9590-7403>

The article was submitted: October 06, 2023; approved after reviewing: November 03, 2023; accepted for publication: November 24, 2023.

Translated from Russian into English by H. Moshkov

Edited for English language and spelling by Dr. David Mossop

**SYNTHESIS AND PROCESSING OF POLYMERS
AND POLYMERIC COMPOSITES**

**СИНТЕЗ И ПЕРЕРАБОТКА ПОЛИМЕРОВ
И КОМПОЗИТОВ НА ИХ ОСНОВЕ**

ISSN 2686-7575 (Online)

<https://doi.org/10.32362/2410-6593-2023-18-3-534-548>



UDC 541.64:536.4

RESEARCH ARTICLE

**Swelling of rubbers of different chemical natures
in supercritical carbon dioxide**

**Sakhaya T. Mikhailova^{1,✉}, Sergey V. Reznichenko¹, Evgeniy A. Krasnikov²,
Pavel Yu. Tsygankov², Natalia V. Menshutina², Igor D. Simonov-Emel'yanov¹**

¹MIREA – Russian Technological University (M.V. Lomonosov Institute of Fine Chemical Technologies),
Moscow, 119571 Russia

²Mendeleev University of Chemical Technology of Russia, Moscow, 125480 Russia

✉Corresponding author, e-mail: mst2904@mail.ru

Abstract

Objectives. To investigate the swelling of the main types of rubbers used in the rubber industry in carbon dioxide in a supercritical state (SC-CO₂), in order to assess the possibility of obtaining elastomeric materials with porous structures using fluid technology, based on them.

Methods. The process of swelling of rubbers in SC-CO₂ and subsequent foaming was carried out according to a specially developed technique using the original installation. This is a high-pressure apparatus with transparent windows, allowing for the use of an optical technique to directly measure the geometric dimensions of samples during swelling and foaming using a digital video camera. The study of the porous structure of foamed rubbers was carried out using scanning electron microscopy.

Results. The study established experimental curves of the swelling kinetics in SC-CO₂ of isoprene, butadiene, styrene butadiene, ethylene propylene, chloroprene, ethylene acrylate, siloxane, and organofluorine rubbers. The influence of temperature and pressure on the rate and equilibrium degree of swelling was studied. The diffusion coefficients of SC-CO₂ in rubbers of various chemical natures were also determined.

Conclusions. It was shown that the equilibrium swelling degree of rubbers in SC-CO₂ depends on the chemical nature of rubbers. It does not correlate with the value of their solubility parameters, changes directly proportional to the diffusion coefficient and increases with increasing temperature and pressure. It was found that irrespective of the degree of swelling in SC-CO₂, all the rubbers studied are intensively foamed at a sharp pressure drop. The size of the pores formed is tens of microns: significantly smaller than the size of pores formed when chemical pore formers are used.

Keywords: supercritical fluid technology, rubber, porosity, carbon dioxide, swelling

For citation: Mikhailova S.T., Reznichenko S.V., Krasnikov E.A., Tsygankov P.Yu., Menshutina N.V., Simonov-Emel'yanov I.D. Swelling of rubbers of different chemical natures in supercritical carbon dioxide. *Tonk. Khim. Tekhnol. = Fine Chem. Technol.* 2023;18(6):534–548. <https://doi.org/10.32362/2410-6593-2023-18-6-534-548>

НАУЧНАЯ СТАТЬЯ

Исследование набухания каучуков различной химической природы в сверхкритическом диоксиде углерода

С.Т. Михайлова^{1,✉}, С.В. Резниченко¹, Е.А. Красников², П.Ю. Цыганков², Н.В. Меньшутина², И.Д. Симонов-Емельянов¹

¹МИРЭА – Российский технологический университет (Институт тонких химических технологий им. М.В. Ломоносова), Москва, 119571 Россия

²Российский химико-технологический университет им. Д.И. Менделеева, Москва, 125480 Россия

✉ Автор для переписки, e-mail: mst2904@mail.ru

Аннотация

Цели. Исследование набухания основных типов каучуков, применяющихся в резиновой промышленности, в диоксиде углерода, находящемся в сверхкритическом состоянии (СК-CO₂), для оценки возможности получения на их основе эластомерных материалов с пористыми структурами с использованием флюидной технологии.

Методы. Процесс набухания каучуков в СК-CO₂ и последующее их вспенивание проводили по специально разработанной методике на оригинальной установке, представляющей собой аппарат высокого давления с прозрачными окнами, позволяющими использовать оптическую методику непосредственного измерения геометрических размеров образцов в процессе набухания и вспенивания с помощью цифровой видеокамеры. Исследование пористой структуры вспененных каучуков проводили с помощью сканирующей электронной микроскопии.

Результаты. Получены экспериментальные кривые кинетики набухания в СК-СО₂ изопренового, бутадиенового, бутадиен-стирольного, этиленпропиленового, хлорпренового, этилен-акрилатного, силоксанового и фторорганического каучуков. Исследовано влияние температуры и давления на скорость и равновесную степень набухания. Определены коэффициенты диффузии СК-СО₂ в каучуках различной химической природы.

Выводы. Показано, что степень равновесного набухания каучуков в СК-СО₂ зависит от химической природы каучуков, не коррелирует с величиной их параметров растворимости, изменяется прямо пропорционально коэффициенту диффузии и увеличивается с ростом температуры и давления. Установлено, что независимо от степени набухания в СК-СО₂ все исследованные каучуки интенсивно вспениваются при резком сбросе давления. Размер образующихся пор составляет десятки микрон, что существенно меньше размера пор, образующихся при использовании химических порообразователей.

Ключевые слова: сверхкритическая флюидная технология, каучук, пористость, диоксид углерода, набухание

Для цитирования: Михайлова С.Т., Резниченко С.В., Красников Е.А., Цыганков П.Ю., Меньшутин Н.В., Симонов-Емельянов И.Д. Исследование набухания каучуков различной химической природы в сверхкритическом диоксиде углерода. *Тонкие химические технологии*. 2023;18(6):534–548. <https://doi.org/10.32362/2410-6593-2023-18-6-534-548>

INTRODUCTION

Porous (foamed) elastomeric materials are widely used in many fields of engineering due to their unique heat-insulating, sound-insulating and deformation properties. The presence of a porous structure in elastomeric materials allows their density to be significantly reduced and the material intensity of products to be reduced.

At the present time, chemical pore formers are mainly used, in order to obtain porous elastomeric materials. The gaseous decomposition products lead to foaming of rubber mixtures, and the subsequent vulcanization stage defines the formed porous structure. Russian industry uses oxydibenzene sulfonylhydrazide and azodicarbonamide as foaming agents: with a decomposition temperature of 160 and 190°C, respectively. The disadvantages of porous materials production technologies using chemical pore formers are the presence of toxic chemical products in the porous structures of elastomeric materials. They are

hazardous to humans and the environment, and possess quite large and poorly regulated pore sizes. It has a strong influence on the mechanical properties of elastomeric materials. In addition, the high decomposition temperatures of foaming agents, at which the vulcanization process may start prematurely, and their high chemical activity do not allow the use of these pore-forming agents for obtaining porous rubbers from rubber compounds of a number of formulations.

One of the promising areas for obtaining porous polymeric materials is the use of fluid technology. This has been successfully developed in recent years for the production, modification, and processing of polymers [1].

The method of porous polymeric materials production using fluids consists in the swelling of polymeric material in a substance in a supercritical (SC) state at elevated pressure. The subsequent sharp pressure release can lead to the transition of this substance into a gaseous state and pore formation in the polymeric material [2].

Substances in the SC state have intermediate properties between those of liquids and gases. Thus, unlike gases, they can dissolve many organic and inorganic substances; unlike ordinary liquids, SC liquids can shrink when pressure increases and change their dissolving ability with changes in pressure and temperature [3–6].

Carbon dioxide in the SC state (SC-CO₂) appears to be the most suitable for elastomeric porous materials [7, 8]. The solubility parameter of SC-CO₂ can vary from 2.7 to 15.0 MJ/m³ with temperature and pressure changes [9], i.e., it is a solvent for polymers of different chemical natures. Carbon dioxide can change to the SC state at a relatively low temperature and low pressure (minimum temperature ~31°C, minimum pressure ~7.38 MPa). In addition, carbon dioxide is a non-toxic, non-flammable and relatively inexpensive substance which exists under normal conditions in gaseous form, facilitating its removal after the completion of the foaming process.

In the literature, only a small number of publications contain systematic studies of pore formation processes in elastomers (mainly in elastomers based on polyorganosiloxanes) using SC-CO₂ [10–15].

The aim of this work is to investigate the swelling processes in the SC-CO₂ medium of the main types of rubbers used in the rubber industry, in order to evaluate the possibility of obtaining elastomeric materials with porous structures on their basis.

EXPERIMENTAL

Types, trademarks, and some characteristics of the studied rubbers are given in Table 1.

The research samples were prepared according to the scheme shown in Fig. 1. The rubbers were homogenized for several minutes using mixing rollers with the 1:1.25 friction ratio. Then they were removed in the form of ~3-mm thick plates.

Table 1. General characteristics of the investigated rubbers

No.	Rubber type, brand, manufacturer, and country of origin	ρ , g/cm ³	δ , MJ/m ³	Monomer formula	T_g , °C	Mooney viscosity ML (1+4) 100°C
1	Natural, NR STR, Natural Art & Technology Co., Thailand	0.92	16.8	(C ₅ H ₈) _n	–72	80–95
2	Polyisoprene, SKI-3, SIBUR, Russia	0.91	16.9	(C ₅ H ₈) _n	–70	75–85
3	Butadiene nitrile, BNKS-40 AN, SIBUR, Russia	0.96	18.8	[–(CH ₂ –CH=CH–H ₂) _n –(–CH(CN)–)] _m	–20	100–120
4	Styrene-butadiene, DSSK-1810F, Voronezhskintezkauchuk, Russia	0.97	17.4	[–(CH ₂ –CH=CH–CH ₂) _m –CH(C ₆ H ₅)–CH ₂)] _n	–90	77–82
5	Ethylene-propylene, SKEPT-50, Ufaorgsintez, Russia	0.85	15.5	[–CH ₂ CH ₂ –] _n –[–CH(CH ₃)CH ₂ –] _m	–58	55–60
6	Siloxane, SKTV-1, S.V. Lebedev Institute of Synthetic Rubber, Russia	1.23	7.0–9.0	(R–O) _n –(R'–SiO–) _m	–120	–
7	Fluorocarbon rubber, SKF-26, HaloPolymer, Russia	1.83	19.0 ¹	[–CF ₂ –CH ₂ –CF ₂ –CF–(CF ₃)–] _n	–15	80–105

¹ Boksha M.Y. *Solvent as a prescription factor for managing the process of processing and combining polymers*: Cand. Sci. Thesis (Eng.). Moscow: 2010. 24 p.

Table 1. Continued

No.	Rubber type, brand, manufacturer, and country of origin	ρ , g/cm ³	δ , MJ/m ³	Monomer formula	T_G , °C	Mooney viscosity ML (1+4) 100 °C
8	Chloroprene rubber, Baypren® 611, Arlanxeo Holding B.V., The Netherlands	1.23	19.2	$(-H_2C-CCl=CH-CH_2-)_n$	-40	35–48
9	Ethylene acrylate rubber, Vamac® Ultra LT, DuPont de Nemours, USA	0.98	–	$[-CH_2CH_2-]_n[-CH_2-CH(COOCH_3)-]_m[-CH_2CHR]_k$	-30	11

Note: ρ is the rubber density, g/cm³; δ is the rubber solubility parameter, MJ/m³ [16–18]; T_G is the glass transition temperature, °C.

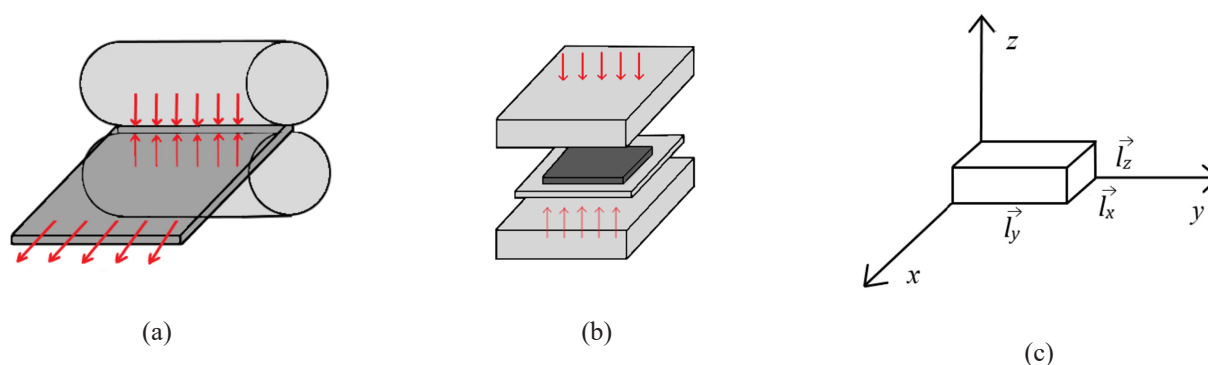


Fig. 1. Scheme of sample preparation for swelling in SC-CO₂: (a) rolling; (b) pressing; (c) three-dimensional coordinates of the sample after pressing.

Calibrated 2-mm thick plates taken from them were molded in a hydraulic press at a temperature of 100°C. Samples were cut from the plates thus obtained in the form of a parallelepiped with dimensions of ~5 mm in length, and ~3 mm in width. The direction of compression on the z -axis and the direction of spreading on the x - and y -axes were defined in the samples.

The study of the processes of rubber swelling in SC-CO₂ and their subsequent foaming was carried out by means of a specially developed optical technique of direct measurement of the linear dimensions of samples in three coordinates. This uses an original setup as shown in Fig. 2.

The high-pressure apparatus was made in the form of a steel cylinder with a volume of 0.25 L, equipped with observation windows made of borosilicate glass.

In order to record the changes in the sample sizes occurring during the experiments, a digital

video camera was placed in front of one of the windows. An electric lamp was installed opposite the other window to illuminate the samples. At the beginning of each experiment, the high-pressure apparatus was dried with compressed air and purged with high-purity (99.99%) carbon dioxide. The test samples were placed in the high-pressure apparatus, heated to a given temperature on a special stand. After that, carbon dioxide was fed into the apparatus which at a given pressure and temperature passed into the SC state. Using a video camera, changes in the linear dimensions of the samples in length l_x , width l_y , and height l_z during their swelling in SC-CO₂ were recorded. The accuracy of measuring the geometric dimensions of the samples was ~5%.

By measuring the linear dimensions of the samples during the swelling process, the volume values of the swelling samples were calculated and kinetic curves of swelling were plotted.

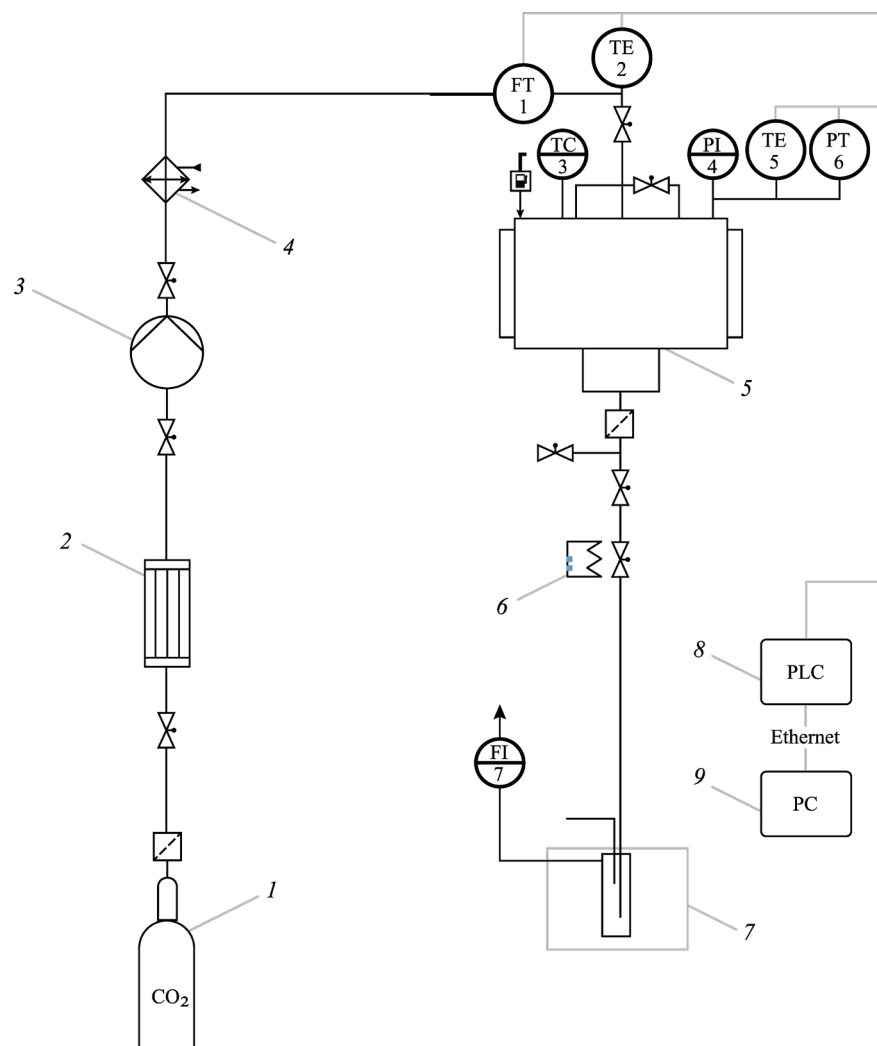


Fig. 2. Principle scheme of the installation for swelling processes in SC- CO_2 :

(1) carbon dioxide cylinder (60 bar); (2) condenser; (3) pump; (4) heat exchanger; (5) 250 mL high-pressure apparatus; (6) heating element; (7) solvent collector with cooling jacket; (8) programmable logic controller (PLC); (9) personal computer (PC). PI4 — pressure gauge; TC3 — temperature controller; FT5 — Coriolis flowmeter; TE2 and TE5 — thermoelectric converters; PT6 — pressure transducer; FI7 — rotameter.

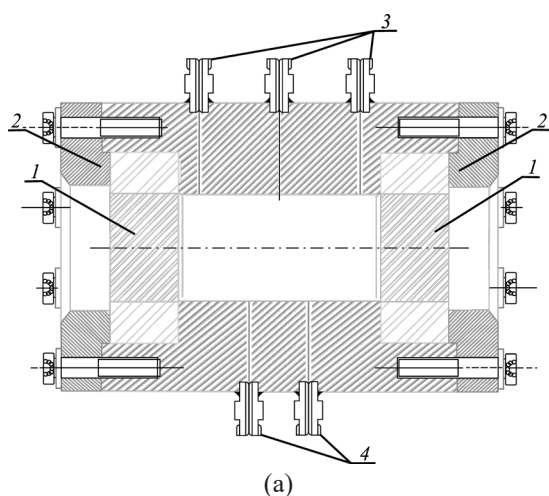


Fig. 3. (a) Sketch of the high pressure apparatus: (1) inspection windows; (2) pressure flange; (3) inlet connections; (4) outlet connections. (b) External view of the apparatus from the side of the inspection window.

The swelling degree S of samples in SC-CO₂ was calculated using Eq. (1):

$$S = \frac{V_1 - V_0}{V_0} \times 100\%, \quad (1)$$

where V_1 is the volume of the swollen sample, V_0 is the volume of the initial rubber sample.

The change in the size Δl of the samples in the process of swelling was determined using Eq. (2):

$$\Delta l = \frac{l_1 - l_0}{l_0} \times 100\%, \quad (2)$$

where l_1 is the size of the swollen sample, mm; l_0 is the size of the initial rubber sample, mm.

After completion of the process of swelling the samples up to the equilibrium state, foaming was carried out. The pressure in the apparatus was sharply released, and the sizes of foamed samples were recorded. The study of the porous structure of foamed rubbers was carried out using scanning electron microscopy on an EVO 10 electron microscope (Zeiss, Germany).

RESULTS AND DISCUSSION

The measurements of the dimensions of rubber samples in the process of their swelling showed that swelling of samples along the x , y , and z axes occurs unevenly (Fig. 4). There is a significant increase in the dimensions of samples along the z axis corresponding to the direction of compression

of samples during pressing. There is also a small change in the dimensions of samples along the x and y axes corresponding to the direction of deformation of samples during spreading. The reason for this phenomenon may be the processes of orientation of rubber macromolecules in the process of its spreading along the x and y axes during rolling and pressing of samples [19]. Indeed, as the experiments (Fig. 5a) have shown, if the pressed samples are not removed immediately from the press after molding, but left in the press at elevated temperature (100°C), which accelerates the transition of oriented rubber macromolecules to the equilibrium non-oriented state, the difference in the swelling degrees of the samples along the three axes gradually decreases and disappears. Similar regularities are observed when toluene is used as a solvent instead of SC-CO₂. The degree of swelling of rubber in this solvent is higher and the orientation effects disappear faster (Fig. 5b).

As shown by preliminary experiments, the presence of oriented macromolecules in rubber samples lowers the value of equilibrium volume swelling of rubbers. Therefore, in order to investigate the swelling kinetics, we used samples aged in the press after molding for at least 3 h at temperatures of 90–180°C to remove the orientation effects.

Figures 6 and 7 show typical kinetic curves of swelling of different rubbers in SC-CO₂. Their character indicates limited swelling of all types of rubbers, when after reaching a certain limit swelling stops. The swollen samples retain their shape and a clear interface with the supercritical medium.

As is known, the maximum equilibrium degree of swelling of polymers is determined by its nature as well as the nature of the solvent or affinity between them. In practical terms, the degree is judged by the proximity of their solubility parameters.

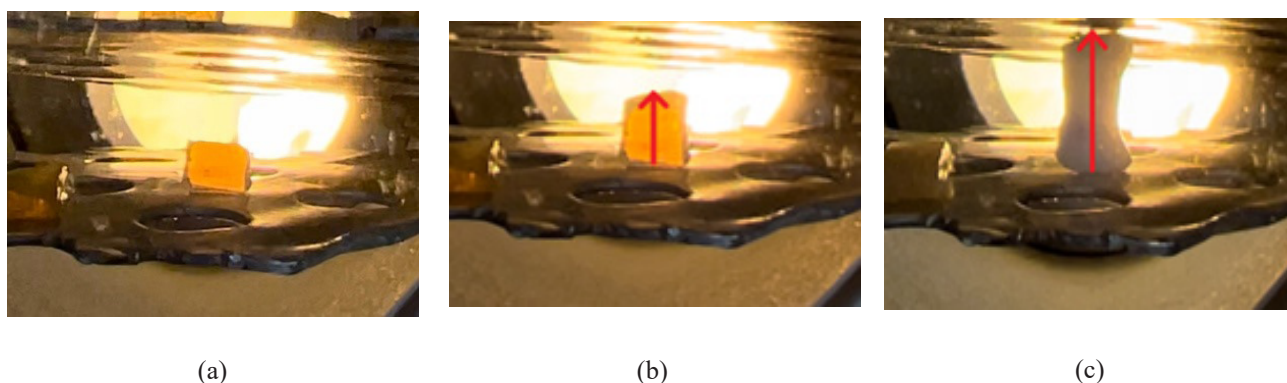


Fig. 4. Swelling of SCTV-1 rubber in SC-CO₂ at 50°C and 15 MPa:
(a) original sample, (b) 1 min swelling, (c) 10 min swelling.

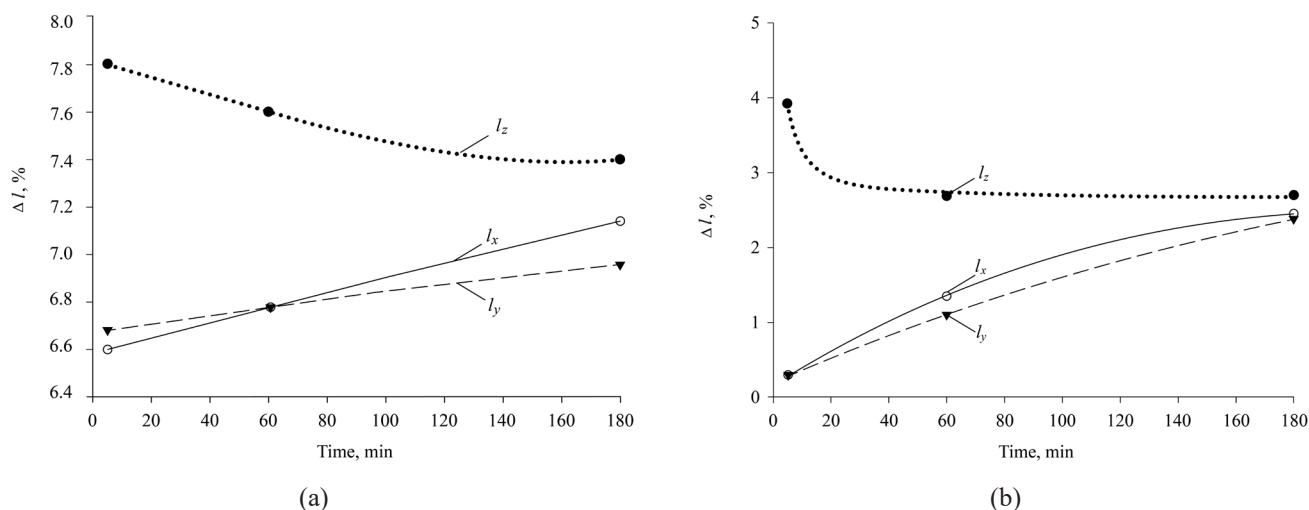


Fig. 5. Variation of linear dimensions of SCF-26 fluorocarbon rubber samples in the state of equilibrium swelling in SC-CO₂ (a) and in toluene (b) as a function of the time of holding the samples at 100°C before swelling.

Indeed, as can be seen from Fig. 6, the maximum degree of swelling (about 100%) is characteristic of siloxane rubber which has the closest value of the solubility parameter to the solubility parameter of SC-CO₂ (Table 1). Butadiene-styrene, butadiene-nitrile, ethylene-propylene rubbers, which along with siloxane rubber belong to the first group of rubbers, also swell by tens of percentages. The time to reach maximum swelling for these rubbers is 40–60 min.

A significantly lower degree of swelling (less than 10%) is observed for the second group of rubbers, including synthetic and natural polyisoprene, chloroprene and fluorocarbon rubber (Fig. 7).

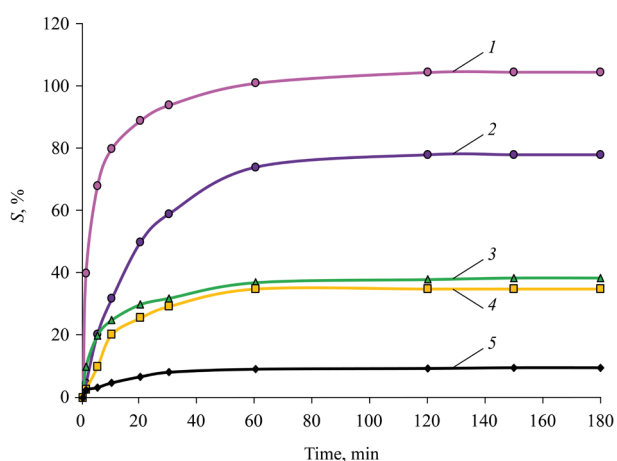


Fig. 6. Kinetic curves of rubber swelling in SC-CO₂ at 50°C and 15 MPa pressure: siloxane (1), butadiene-nitrile (2), butadiene-styrene (3), ethylene-propylene (4), and ethylene-acrylate (5) rubbers.

In comparison to other rubbers, they have solubility parameters which differ more from the solubility parameters of SC-CO₂. These rubbers are also characterized by faster (within 10–20 min) achievement of the degree of equilibrium swelling. However, monotonic dependence of the ultimate degree of swelling on the solubility parameters of rubbers is not observed.

Butadiene-nitrile and butadiene-styrene rubbers with solubility parameters almost equal to the solubility parameters of polyisoprenes and fluorocarbon rubber have a significantly higher degree of swelling and take more time to reach equilibrium swelling (40–60 min), when compared

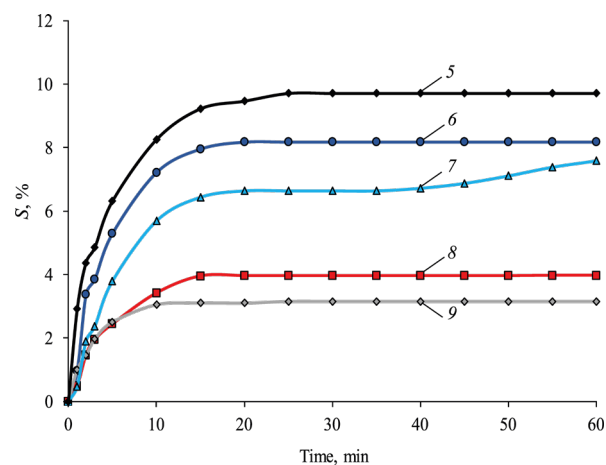


Fig. 7. Kinetic curves of rubber swelling in SC-CO₂ at 50°C and 15 MPa pressure: ethylene acrylate (5), fluorocarbon (6), chloroprene (7), polyisoprene (8), and natural (9) rubbers.

to the second group of rubbers. Polychloroprene differs more in its solubility parameter from SC-CO₂ and swells more when compared to polyisoprenes. A possible reason for this is the specific interactions of SC-CO₂ with rubbers of different chemical nature.

Figure 8 shows the influence of pressure on the swelling kinetics of SCF-26 rubber in SC-CO₂. It can be seen that with increasing pressure from 5.0 to 20.0 MPa, the value of equilibrium swelling of samples in the medium of SC-CO₂ increases.

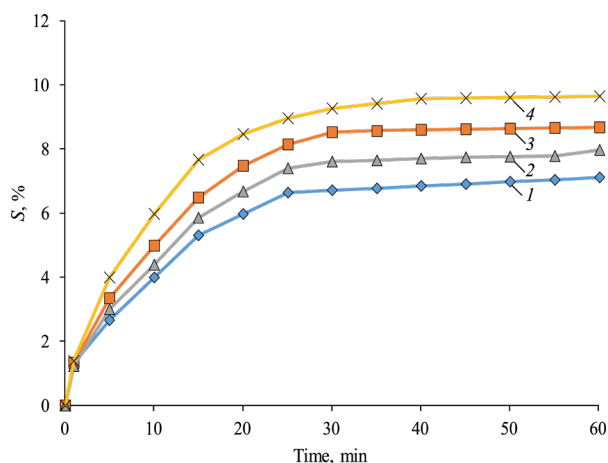


Fig. 8. Time dependence of swelling degree of SCF-26 rubber in SC-CO₂ at 50°C and pressures of 5 (1), 10 (2), 15 (3), and 20 MPa (4).

Similar dependencies of the equilibrium swelling value on pressure can be observed for all types of rubbers (Fig. 9).

As seen in Fig. 10, an increase in the equilibrium swelling also leads to an increase in the swelling temperature.

Thus, by varying the pressure and temperature, it is possible to change the equilibrium degree of swelling of rubbers in SC-CO₂.

The swelling of polysiloxanes in SC-CO₂ is known [8] to occur by diffusion mechanism, and the siloxane rubber/SC-CO₂ system obeys Fick's second law (3):

$$\frac{dc}{dt} = D \frac{d^2c}{dx^2}, \quad (3)$$

where c is the concentration of CO₂ in the polymer, D is the diffusion factor, cm²/s.

In order to understand the main regularities of swelling of the studied rubbers in the SC-CO₂ medium and to calculate the diffusion coefficients of SC-CO₂ in rubbers, it was first of all necessary

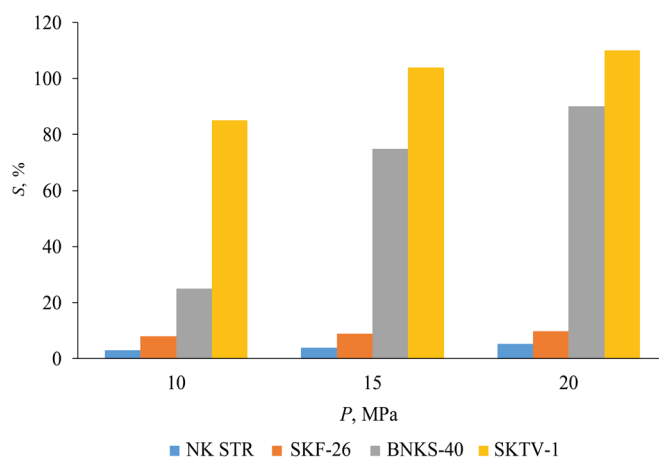


Fig. 9. Effect of pressure P on the equilibrium swelling of different rubbers at 50°C.

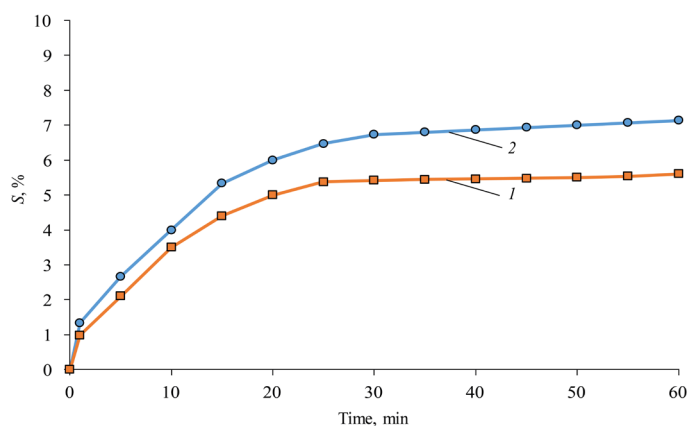


Fig. 10. Time dependence of the swelling degree of SCF-26 in SC-CO₂ at temperatures of 40 (1) and 50°C (2).

to establish whether the rubber/SC-CO₂ systems under study obey this law, despite the above-mentioned possible specific interactions between them.

The equation describing Fick's second law is known to have a number of solutions depending on the boundary conditions [20]. If the sample sorbing SC-CO₂ has the shape of a plate with thickness l , then under the boundary conditions $0 < x < l$ and $0 < c < c_{\text{eq}}$ (equilibrium concentration), the solution of the equation has the form (4):

$$\frac{M_t}{M_\infty} = \frac{4}{l} \left(\frac{Dt}{\pi} \right)^{\frac{1}{2}}, \quad (4)$$

where M_t is the amount of adsorbed substance over time t , M_∞ is the equilibrium amount of the adsorbed substance.

Assuming [8], the degree of swelling is equal to:

$$\frac{M_t}{M_\infty} = \frac{V_t - V_0}{V_\infty - V_0}, \quad (5)$$

where V_0 is the initial sample volume; V_t is the volume of swollen sample over time t ; V_∞ is the equilibrium volume of the swollen sample.

Equation (5) can be written in the following form (6):

$$\frac{V_t - V_0}{V_\infty - V_0} = f\left(t^{\frac{1}{2}}\right). \quad (6)$$

For systems obeying Fick's law, the dependence $\frac{V_t - V_0}{V_\infty - V_0}$ from $t^{1/2}$ should have the form of a straight line, the tangent of the angle of which allows calculating the value of D [21].

The root mean square dependence $\frac{V_t - V_0}{V_\infty - V_0}$ of swelling time in SC-CO₂ medium for different rubbers is shown in Fig. 11.

The data in Fig. 11 indicates that Fick's second law is observed for all types of rubbers and SC-CO₂.

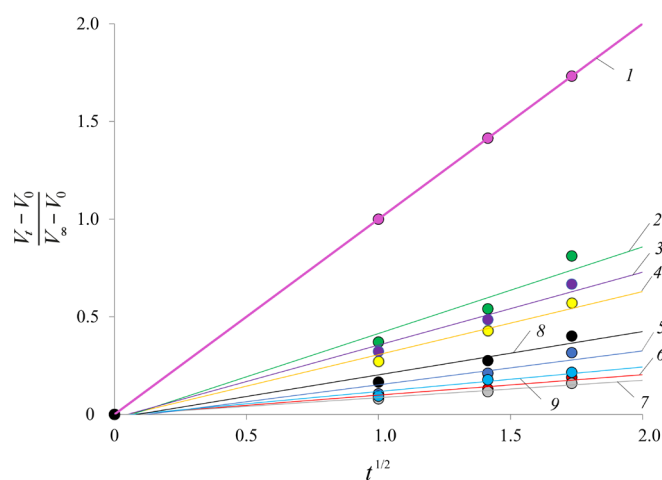


Fig. 11. Dependence $\frac{V_t - V_0}{V_\infty - V_0}$ on the square root of the swelling time of samples of different rubbers: siloxane (1), butadiene-styrene (2), butadiene-nitrile (3), ethylene-propylene (4), fluorocarbon (5), natural (6), isoprene (7), chloroprene (8), ethylene-acrylate (9).

Table 2 shows the values of diffusion coefficients of SC-CO₂ in different rubbers calculated from the tangent of the angle of slope of the straight lines presented in Fig. 11.

Figure 12 shows that the diffusion coefficients depend linearly on the values of the equilibrium degree of swelling of rubbers.

Thus, the swelling ability of rubbers grows in direct proportion to the diffusion coefficient of SC-CO₂ in them. The experimental data for all types of rubbers fits into one straight line. Therefore, it is not the solubility parameter of rubber but the diffusion coefficient of SC-CO₂ into it which may serve as a more accurate characteristic of the affinity degree of SC-CO₂ and rubber.

The rubber samples which reached equilibrium swelling were subjected to foaming. It was found that all rubbers swollen to equilibrium state foamed intensively, regardless of their degree of equilibrium swelling, varying from a few to 100%.

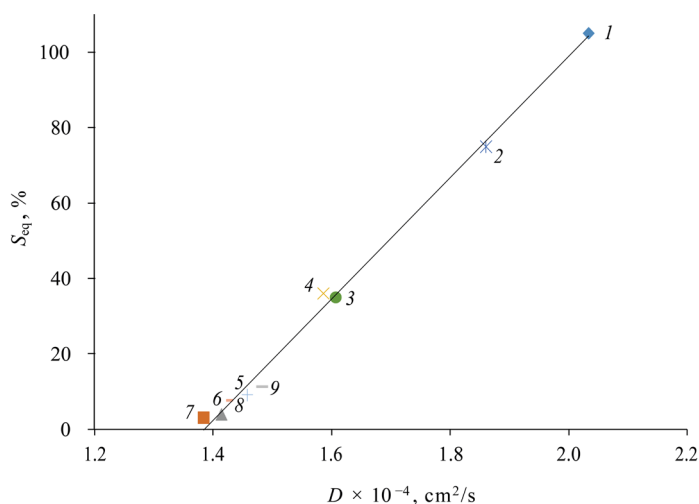


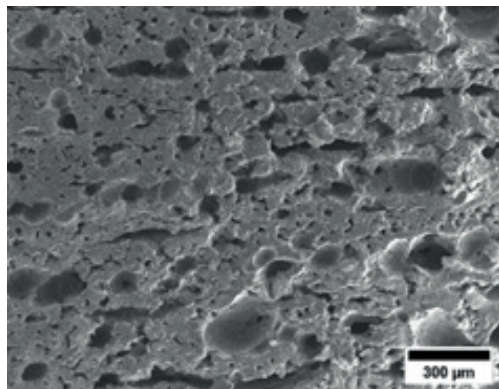
Fig. 12. Dependence of the equilibrium degree of swelling of rubbers S_{eq} on the diffusion coefficient D of SC-CO₂ in them. (1) Siloxane, (2) butadiene-styrene, (3) butadiene-nitrile, (4) ethylene-propylene, (5) fluorocarbon, (6) natural, (7) polyisoprene, (8) chloroprene, (9) ethylene acrylate rubbers.

The typical porous structure of foamed rubber samples obtained using SC-CO₂ is shown in Fig. 13 using a sample from SCF-26 rubber as an example. For comparison, the porous structure of this rubber obtained using a chemical pore former (azodicarbonamide) used as a pore former in the rubber industry is also shown here.

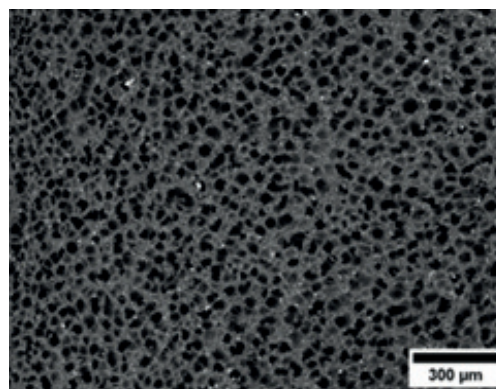
The high uniformity of the porous structure of the obtained materials and significantly smaller pore sizes of tens of microns, when compared

Table 2. SC-CO₂ diffusion coefficient in rubbers of different chemical nature

Rubber brand	Diffusion coefficient $D \times 10^{-4}$, cm ² /s
NR STR	1.40
SKI-3	1.38
BNKS-40 AN	1.83
DSSK1810F	1.61
SKEPT-50	1.58
SKTV-1	2.12
SKF-26	1.45
Baypren® 611	1.41
Vamac® Ultra LT	1.48



(a)



(b)

Fig. 13. Electron micrographs of the structure of SCF-26 foamed rubber samples obtained using chemical foaming agent (a) and SC-CO₂ (b).

to the pore sizes of hundreds of microns for samples obtained with chemical pore formers, indicate the undoubted advantages of fluid technology in obtaining finely porous elastomeric materials.

The influence of technological parameters of foaming of various rubbers in SC-CO₂ and formulations of rubber mixtures on the structure of the resulting porous elastomeric materials will be investigated in a subsequent report, being prepared for publication by the authors of this article.

CONCLUSIONS

1. An optical technique has been developed for studying the process of rubber swelling in supercritical carbon dioxide using the original setup, consisting in the direct measurement of geometric dimensions of swelling samples using a digital video camera. The experimental study of swelling in SC-CO₂ of the main types of rubbers used in the manufacture of rubber products was carried out using the developed methodology.

2. The diffusion coefficients of SC-CO₂ in rubbers of different chemical nature were calculated for the first time using mathematical modeling and swelling data.

3. It has been shown that the dependence of the equilibrium swelling degree of rubbers in SC-CO₂ on their solubility parameters is non-monotonic. This is probably related to the specific interaction of SC-CO₂ with some types of rubbers. The equilibrium swelling degree of rubbers in SC-CO₂ increases in direct proportion to its diffusion coefficient and increases with rising pressure and temperature.

4. It has been established that intensive foaming occurs when rubber swells in SC-CO₂ by only a few percent at a sharp pressure drop. The size of the pores formed in rubbers is tens of microns, significantly smaller than the pore size formed when using chemical pore formers and is an undeniable advantage of the fluid technology of porous elastomeric materials production in comparison with the traditional one. With the help of this technology, all the main types of rubbers studied here and used in the rubber industry can be used for production of porous rubbers.

Authors' contributions

S.T. Mikhailova – carrying out the experiment, analyzing, collecting, and processing the material, writing the article;

S.V. Reznichenko – formulating research aims and objectives, analyzing, processing results, writing the text of the article;

E.A. Krasnikov – carrying out the experiment;

P.Yu. Tsygankov – scientific and technical support, editing the text of the article;

N.V. Menshutina – scientific advising, editing the text of the article;

I.D. Simonov-Emel'yanov – scientific advising, editing the text of the article.

The authors declare no conflicts of interest.

REFERENCES

1. Arzhakova O.V., Arzhakov M.S., Badamshina E.R., Bryuzgina E.B., Bryuzgin E.V., et al. Polymer for the future. *Russ. Chem. Rev.* 2022;91(12):RCR5062. <https://doi.org/10.57634/RCR5062>
2. Sarver J.A., Kiran E. Foaming of polymers with carbon dioxide – The year-in-review – 2019. *J. Supercritical Fluids*. 2021;173:105166. <https://doi.org/10.1016/j.supflu.2021.105166>
3. Bruno T.J., Ely J.F. *Supercritical Fluid Technology: Reviews in Modern Theory and Applications*. Taylor & Francis Group; 2017. 606 p. ISBN 978-11-385-07-005
4. McHugh M.A., Krukonis V.J. *Supercritical Fluid Extraction: Principles and Practice*. Stoneham: Butterworth Publishers; 1986. 507 p.
5. Razgonova M.P., Zakharenko A.M., Sergievich A.A. *Sverkhkriticheskie fliyuidy: teoriya, etapy stanovleniya, sovremennoe primeneniye: uchebnoye posobie (Supercritical Fluids: Theory, Stages of Formation, Modern Application: textbook)*. St. Petersburg: Lan; 2019. 192 p. (in Russ). ISBN 978-5-8114-3915-7

СПИСОК ЛИТЕРАТУРЫ

1. Аржакова О.В., Аржаков М.С., Бадамшина Э.Р., Брюзгина Е.Б., Брюзгин Е.В. и др. Полимеры будущего. *Успехи химии*. 2022;91(12):RCR5062. <https://doi.org/10.57634/RCR5062>
2. Sarver J.A., Kiran E. Foaming of polymers with carbon dioxide – The year-in-review – 2019. *J. Supercritical Fluids*. 2021;173:105166(27). <https://doi.org/10.1016/j.supflu.2021.105166>
3. Bruno T.J., Ely J.F. *Supercritical Fluid Technology: Reviews in Modern Theory and Applications*. Taylor & Francis Group; 2017. 606 p. ISBN 978-11-385-07-005
4. McHugh M.A., Krukonis V.J. *Supercritical Fluid Extraction: Principles and Practice*. Stoneham: Butterworth Publishers; 1986. 507 p.
5. Разгонова М.П., Захаренко А.М., Сергиевич А.А. *Сверхкритические флюиды: теория, этапы становления, современное применение: учебное пособие*. СПб: Лань; 2019. 192 с. ISBN 978-5-8114-3915-7

6. Johnston K.J., Penninger J.M.L. *Supercritical Fluid Science and Technology*. Washington: American Chemical Society; 1989. 547 p.
7. Dubous J., Grau E, Tassaing T., Dumon M. On the CO₂ sorption and swelling of elastomers by supercritical CO₂ as studied by *in situ* high pressure FTIR microscopy. *J. Supercritical Fluids*. 2018;131:150–156. <https://doi.org/10.1016/j.supflu.2017.09.003>
8. Royer J.R., DeSimone J.M., Khan S.A. Carbon Dioxide-Induced Swelling of Poly(dimethylsiloxane). *Macromolecules*. 1999;32(26):8965–8973. <https://doi.org/10.1021/ma9904518>
9. Yizhak M. Solubility Parameter of Carbon Dioxide – An Enigma. *ACS Omega*. 2018;3(1):524–528. <https://doi.org/10.1021/acsomega.7b01665>
10. Hong I.-K., Lee S. Microcellular foaming of silicone rubber with supercritical carbon dioxide. *Korean J. Chem. Eng.* 2014;31(1):166–171. <https://doi.org/10.1007/s11814-013-0188-3>
11. Xiang B., Jia Y., Lei Y., Zhang F., He J., Liu T., Luo S. Mechanical properties of microcellular and nanocellular silicone rubber foams obtained by supercritical carbon dioxide. *Polymer J.* 2019;51(6):559–568. <https://doi.org/10.1038/s41428-019-0175-6>
12. Xiang B., Deng Z., Zhang F., Wen N., Lei Y., Liu T., Luo S. Microcellular silicone rubber foams: the influence of reinforcing agent on cellular morphology and nucleation. *Polym. Eng. Sci.* 2019;59(1):5–14. <https://doi.org/10.1002/pen.24857>
13. Tang W., Liao X., Zhang Y., Li J., Wang G., Li. G. Mechanical–microstructure relationship and cellular failure mechanism of silicone rubber foam by the cell microstructure designed in supercritical CO₂. *J. Phys. Chem. C*. 2019;123(44):26947–26956. <https://doi.org/10.1021/acs.jpcc.9b06992>
14. Tessanan W., Phinyochee, P., Daneil P., Gibaud A. Microcellular natural rubber using supercritical CO₂ technology. *J. Supercritical Fluids*. 2019;149:70–78. <https://doi.org/10.1016/j.supflu.2019.03.022>
15. Song Y., Dattatray A., Yu Z., Zhang X., Du A., Wang H., Zhang Z.X. Lightweight and flexible silicone rubber foam with dopamine grafted multi-walled carbon nanotubes and silver nanoparticles using supercritical foaming technology: Its preparation and electromagnetic interference shielding performance. *Eur. Polym. J.* 2021;161(5):110839. <https://doi.org/10.1016/j.eurpolymj.2021.110839>
16. Kerber M.L. Sheryshev M.A., Bukanov A.M., Vol'fson S.I., Gorbunova I.Yu., Kandyrin L.B., Sirota A.G. *Tekhnologiya pererabotki polimerov. Fizicheskie i khimicheskie protsessy (Polymer Processing Technology. Physical and Chemical Processes)*. Moscow: Yurait; 2017. 316 p. (in Russ.). ISBN 978-5-534-04915-2
17. Koltsov N.I., Ushmarin N.F., Issakova S.A., Vinogorova S.S., Chernova N.A., Verkhunov S.M., Petrova N.N. Investigation of the influence of plasticizers PEF-1 and trichloroethyl phosphate on the technological, physical and mechanical properties and frost resistance of rubbers based on nitrile butadiene rubbers. *Vestnik Kazanskogo tekhnologicheskogo universiteta = Bulletin of the Kazan Technological University*. 2012;15(2):41–44 (in Russ.).
18. Shvarts A.G., Dinzbarg B.N. *Sovmeshchenie kauchukov s plastikami i sinteticheskimi smolami (Combination of Rubbers with Plastics and Synthetic Resins)*. Moscow: Khimiya; 1972. 224 p. (in Russ.).
6. Johnston K.J., Penninger J.M.L. *Supercritical Fluid Science and Technology*. Washington: American Chemical Society; 1989. 547 p.
7. Dubous J., Grau E, Tassaing T., Dumon M. On the CO₂ sorption and swelling of elastomers by supercritical CO₂ as studied by *in situ* high pressure FTIR microscopy. *J. Supercritical Fluids*. 2018;131:150–156. <https://doi.org/10.1016/j.supflu.2017.09.003>
8. Royer J.R., DeSimone J.M., Khan S.A. Carbon Dioxide-Induced Swelling of Poly(dimethylsiloxane). *Macromolecules*. 1999;32(26):8965–8973. <https://doi.org/10.1021/ma9904518>
9. Yizhak M. Solubility Parameter of Carbon Dioxide – An Enigma. *ACS Omega*. 2018;3(1):524–528. <https://doi.org/10.1021/acsomega.7b01665>
10. Hong I.-K., Lee S. Microcellular foaming of silicone rubber with supercritical carbon dioxide. *Korean J. Chem. Eng.* 2014;31(1):166–171. <https://doi.org/10.1007/s11814-013-0188-3>
11. Xiang B., Jia Y., Lei Y., Zhang F., He J., Liu T., Luo S. Mechanical properties of microcellular and nanocellular silicone rubber foams obtained by supercritical carbon dioxide. *Polymer J.* 2019;51(6):559–568. <https://doi.org/10.1038/s41428-019-0175-6>
12. Xiang B., Deng Z., Zhang F., Wen N., Lei Y., Liu T., Luo S. Microcellular silicone rubber foams: the influence of reinforcing agent on cellular morphology and nucleation. *Polym. Eng. Sci.* 2019;59(1):5–14. <https://doi.org/10.1002/pen.24857>
13. Tang W., Liao X., Zhang Y., Li J., Wang G., Li. G. Mechanical–microstructure relationship and cellular failure mechanism of silicone rubber foam by the cell microstructure designed in supercritical CO₂. *J. Phys. Chem. C*. 2019;123(44):26947–26956. <https://doi.org/10.1021/acs.jpcc.9b06992>
14. Tessanan W., Phinyochee, P., Daneil P., Gibaud A. Microcellular natural rubber using supercritical CO₂ technology. *J. Supercritical Fluids*. 2019;149:70–78. <https://doi.org/10.1016/j.supflu.2019.03.022>
15. Song Y., Dattatray A., Yu Z., Zhang X., Du A., Wang H., Zhang Z.X. Lightweight and flexible silicone rubber foam with dopamine grafted multi-walled carbon nanotubes and silver nanoparticles using supercritical foaming technology: Its preparation and electromagnetic interference shielding performance. *Eur. Polym. J.* 2021;161(5):110839. <https://doi.org/10.1016/j.eurpolymj.2021.110839>
16. Кербер М.Л. Шерышев М.А., Буканов А.М., Вольфсон С.И., Горбунова И.Ю., Кандырин Л.Б., Сирота А.Г. *Технология переработки полимеров. Физические и химические процессы*. М.: Юрайт; 2017. 316 с. ISBN 978-5-534-04915-2
17. Кольцов Н.И., Ушмарин Н.Ф., Исакова С.А., Виногорова С.С., Чернова Н.А., Верхунов С.М., Петрова Н.Н. Исследование влияния пластификаторов ПЭФ-1 и трихлорэтилфосфата на технологические, физико-механические свойства и морозостойкость резин на основе бутадиен-нитрильных каучуков. *Вестник Казанского технологического университета*. 2012;15(2):41–44.
18. Шварц А.Г., Динзбург Б.Н. *Совмещение каучуков с пластиками и синтетическими смолами*. М.: Химия; 1972. 224 с.
19. Власов С.В., Марков А.В. *Ориентационные явления в процессах переработки полимерных материалов*. М.: МИТХТ; 2014. 138 с. ISBN 978-5-904742-29-4

19. Vlasov S.V., Markov A.V. *Orientatsionnye yavleniya v protsessakh pererabotki polimernykh materialov (Orientation Phenomena in the Processes of Polymeric Materials Recycling)*. Moscow: MITHT; 2014. 138 p. (in Russ.). ISBN 978-5-904742-29-4

20. Tager A.A. *Fizikokhimiya polimerov (Physicochemistry of Polymers)*. Moscow: Khimiya; 1978. 544 p. (in Russ.).

20. Тареп А.А. *Физикохимия полимеров*. М.: Химия; 1978. 544 с.

About the authors:

Sakhaya T. Mikhailova, Postgraduate Student, Department of Chemistry and Technology of Plastics and Polymer Composites Processing, M.V. Lomonosov Institute of Fine Chemical Technologies, MIREA – Russian Technological University (1-5, Malaya Pirogovskaya ul., Moscow, 119435, Russia). E-mail: mst2904@mail.ru. <https://orcid.org/0009-0000-9988-3058>

Sergey V. Reznichenko, Dr. Sci. (Eng.), Professor, Department of Chemistry and Technology of Plastics and Polymer Composites Processing, M.V. Lomonosov Institute of Fine Chemical Technologies, Director of the Research Center “Innovative Polymer Materials and Products,” MIREA – Russian Technological University (1-5, Malaya Pirogovskaya ul., Moscow, 119435, Russia). E-mail: svrezn@gmail.com. RSCI SPIN-code 9257-1554, <https://orcid.org/0009-0009-5903-6861>

Evgeniy A. Krasnikov, Postgraduate Student, Department of Chemical and Pharmaceutical Engineering, Mendeleev University of Chemical Technology of Russia (20-1, Geroev Panfilovtsev ul., Moscow, 125480, Russia). E-mail: evgenykrasnikov01@gmail.com. <https://orcid.org/0009-0007-6510-9495>

Pavel Yu. Tsygankov, Cand. Sci. (Eng.), Researcher, Department of Chemical and Pharmaceutical Engineering, Mendeleev University of Chemical Technology of Russia (20-1, Geroev Panfilovtsev ul., Moscow, 125480, Russia). E-mail: tsygangov.p.i@muctr.ru. Scopus Author ID 57195294645, RSCI SPIN-code 6928-6980, <https://orcid.org/0000-0003-2630-3838>

Natalia V. Menshutina, Dr. Sci. (Eng.), Professor, Head of the Department of Chemical and Pharmaceutical Engineering, Mendeleev University of Chemical Technology of Russia (20-1, Geroev Panfilovtsev ul., Moscow, 125480, Russia). E-mail: chemcom@muctr.ru. Scopus Author ID 6602274789, ResearcherID G-2802-2014, RSCI SPIN-code 6317-0757, <https://orcid.org/0000-0001-7806-1426>

Igor D. Simonov-Emel'yanov, Dr. Sci. (Eng.), Professor, Head of the Department of Chemistry and Technology of Plastics and Polymer Composites Processing, M.V. Lomonosov Institute of Fine Chemical Technologies, MIREA – Russian Technological University (1-5, Malaya Pirogovskaya ul., Moscow, 119435, Russia). E-mail: igor.simonov1412@gmail.com. Scopus Author ID 6603181099, RSCI SPIN-code 7313-3844, <https://orcid.org/0000-0002-6611-5746>

Об авторах:

Михайлова Сахая Трофимовна, аспирант, кафедры химии и технологии переработки пластмасс и полимерных композитов, Институт тонких химических технологий им. М.В. Ломоносова, ФГБОУ ВО «МИРЭА – Российский технологический университет» (119435, Россия, Москва, ул. Малая Пироговская, д. 1, стр. 5). E-mail: mst2904@mail.ru. <https://orcid.org/0009-0000-9988-3058>

Резниченко Сергей Владимирович, д.т.н., профессор кафедры химии и технологии переработки пластмасс и полимерных композитов, Институт тонких химических технологий им. М.В. Ломоносова, директор НИЦ «Инновационные полимерные материалы и изделия», ФГБОУ ВО «МИРЭА – Российский технологический университет» (119435, Россия, Москва, ул. Малая Пироговская, д. 1, стр. 5). E-mail: svrezn@gmail.com. SPIN-код РИНЦ 9257-1554, <https://orcid.org/0009-0009-5903-6861>

Красников Евгений Алексеевич, аспирант, кафедры химического и фармацевтического инжиниринга, ФГБОУ ВО «Российский химико-технологический университет им. Д.И. Менделеева» (125480, Россия, Москва, ул. Героев Панфиловцев, д. 20, к. 1). E-mail: evgenykrasnikov01@gmail.com. <https://orcid.org/0009-0007-6510-9495>

Цыганков Павел Юрьевич, к.т.н., научный сотрудник, кафедра химического и фармацевтического инжиниринга, ФГБОУ ВО «Российский химико-технологический университет им. Д.И. Менделеева» (125480, Россия, Москва, ул. Героев Панфиловцев, д. 20, к. 1). E-mail: tsygankov.p.i@muctr.ru. Scopus Author ID 57195294645, SPIN-код РИНЦ 6928-6980, <https://orcid.org/0000-0003-2630-3838>

Меньшутина Наталья Васильевна, д.т.н., профессор, заведующий кафедрой химического и фармацевтического инжиниринга ФГБОУ ВО «Российский химико-технологический университет им. Д.И. Менделеева» (125480, Россия, Москва, ул. Героев Панфиловцев, д. 20, к. 1). E-mail: chemcom@muctr.ru. Scopus Author ID 6602274789, ResearcherID G-2802-2014, SPIN-код РИНЦ 6317-0757, <https://orcid.org/0000-0001-7806-1426>

Симонов-Емельянов Игорь Дмитриевич, д.т.н., профессор, заведующий кафедрой химии и технологии переработки пластмасс и полимерных композитов, Институт тонких химических технологий им. М.В. Ломоносова, ФГБОУ ВО «МИРЭА – Российский технологический университет» (119435, Россия, Москва, ул. Малая Пироговская, д. 1, стр. 5). E-mail: igor.simonov1412@gmail.com. Scopus Author ID 6603181099, SPIN-код РИНЦ 7313-3844, <https://orcid.org/0000-0002-6611-5746>

The article was submitted: April 19, 2023; approved after reviewing: August 29, 2023; accepted for publication: November 17, 2023.

Translated from Russian into English by H. Moshkov

Edited for English language and spelling by Dr. David Mossop

SYNTHESIS AND PROCESSING OF POLYMERS
AND POLYMERIC COMPOSITES

СИНТЕЗ И ПЕРЕРАБОТКА ПОЛИМЕРОВ
И КОМПОЗИТОВ НА ИХ ОСНОВЕ

ISSN 2686-7575 (Online)

<https://doi.org/10.32362/2410-6593-2023-18-6-549-558>



UDC 661.717.5

RESEARCH ARTICLE

High-performance slow-curing polyurea compositions

Sergei V. Romanov¹, Olga A. Botvinova¹, Evgenii A. Timakov²,
Dariya A. Rashchupkina², Yuri T. Panov^{2,✉}

¹ Elast PU Production Company, Vladimir, 600026 Russia

² Alexander and Nikolay Stoletovs Vladimir State University, Vladimir, 600014 Russia

✉ Corresponding author, e-mail: tpp_vlgu@mail.ru

Abstract

Objectives. To improve the technology for obtaining polymer spray coatings based on polycarbodiimides (polyureas) by studying changes in the process and operational parameters due to the introduction of aspartic acid derivatives (AADs) into the composition.

Methods. The process of the production of sprayed and contact polyureas involves a number of difficulties, not least in terms of the cost of the components and high-pressure equipment. For this reason, mathematical modeling was used to optimize experimental design. The curing time of the composition was measured under conditions simulated to be close to actual. After thermostating and mixing Components A and B in predetermined ratios, the gelation time was measured to represent the curing time of the composition. The hardness of the material was determined by the Shore method according to GOST 24621-91. Tensile strength and relative elongation were determined according to a standard method (GOST 30436-96).

Results. The effect of three AADs on the properties of the finished polyurea was studied. It was found that the introduction of two of them (AAD-1 and AAD-2) into polyurea in an amount of up to 40 wt % produces slow-curing (>250 s) polyureas capable of manual application. The finished products have physical properties on par with machine-poured materials (breaking strength >73 MPa; tensile strength >23 MPa; elongation >500%). Compiled regression equations were used to construct graphs of equal levels showing the possible areas of directed modification of the studied compositions.

Conclusions. AAD can be used as a modifying component for polyurea systems to obtain slow-curing polyureas with high performance properties, which can be purposefully controlled by mathematical modeling. The resulting products have commercial value due to their combination of valuable physical and mechanical properties.

Keywords: polyurea, curing time, polymer coatings, physical and mechanical properties, mathematical modeling

For citation: Romanov S.V., Botvinova O.A., Timakov E.A., Rashchupkina D.A., Panov Yu.T. High-performance slow-curing polyurea compositions. *Tonk. Khim. Tekhnol.* = *Fine Chem. Technol.* 2023;18(6):549–558. <https://doi.org/10.32362/2410-6593-2023-18-6-549-558>

НАУЧНАЯ СТАТЬЯ

Медленные полимочевинные композиции с высокими эксплуатационными свойствами

С.В. Романов¹, О.А. Ботвинова¹, Е.А. Тимаков², Д.А. Ращупкина²,
Ю.Т. Панов^{2,✉}

¹Производственная компания «Эласт-ПУ», Владимир, 600026 Россия

²Владимирский государственный университет им. Александра Григорьевича и Николая Григорьевича Столетовых, Владимир, 600014 Россия

✉ Автор для переписки, e-mail: tpp_vlgu@mail.ru

Аннотация

Цели. Совершенствование технологии получения полимерных напыляемых покрытий на основе поликарбодиимидов (полимочевин), путем изучения закономерностей изменения технологических и эксплуатационных свойств при введении в состав композиции производных аспарагиновой кислоты (ПАК).

Методы. Процесс производства напыляемых и контактных полимочевин сопряжен с рядом трудностей, главной из которых является стоимость используемых компонентов и работа с высокопроизводительным оборудованием высокого давления, поэтому авторами было предложено использовать метод математического моделирования для оценки оптимального плана проведения эксперимента. Измерение времени жизни композиции проводили в условиях, приближенных к реальным условиям нанесения. Компоненты А и Б термостатировали, смешивали в заданных соотношениях. Затем измеряли время гелеобразования, которое считали временем жизни композиции. Твердость материала определяли по методу Шора по ГОСТ 24621-91. Прочность и относительное удлинение при растяжении определяли по стандартной методике (ГОСТ 30436-96).

Результаты. Исследовано влияние трех ПАК на свойства готовой полимочевины и показано, что введение в состав полимочевины двух из них (ПАК1 и ПАК2) в количестве до 40 мас. % дает возможность получить полимочевины со временем жизни >250 с, что позволяет перевести их в разряд «медленных», то есть способных наноситься вручную. Готовые продукты обладают физическими свойствами, аналогичными материалам, полученным методом машинной заливки (прочностью на разрыв >73 МПа, прочностью при растяжении >23 МПа и относительным удлинением >500%). Составлены уравнения регрессии, на основании которых построены графики равных уровней, показывающие возможные области направленной модификации исследуемых композиций.

Выводы. Применение ПАК в качестве модифицирующего компонента для полимочевинных систем позволяет получить «медленные» полимочевины с высокими эксплуатационными свойствами, которые можно целенаправленно регулировать, используя метод математического моделирования. Помимо прочего, полученные продукты несут в себе коммерческую ценность, так как обладают совокупностью нужных физико-механических свойств.

Ключевые слова: полимочевина, время жизни, полимерные покрытия, физико-механические свойства, математическое моделирование

Для цитирования: Романов С.В., Ботвинова О.А., Тимаков Е.А., Рашупкина Д.А., Панов Ю.Т. Медленные полимочевинные композиции с высокими эксплуатационными свойствами. *Тонкие химические технологии*. 2023;18(6):549–558. <https://doi.org/10.32362/2410-6593-2023-18-6-549-558>

INTRODUCTION

In order to compete in the production of high-performance finished coatings used as construction and finishing materials, it is necessary to combine operational simplicity with process rapidity. Polyurea coatings are widely used as electrical insulating, lining, and anti-corrosion materials. However, such coatings require the use of expensive high-pressure equipment operated by highly qualified personnel. While these difficulties do not present a major hurdle when applying coatings to large surfaces, they quickly become insurmountable if it is necessary to apply coatings to small surfaces, e.g., during repair work. For this reason, there is a demand for compositions having a curing time of more than 5 min, which can be manually mixed and applied. Preliminary experiments showed that the known methods of reducing the reaction rate (increasing the curing time of the system) can be used only with the simultaneous reduction in the performance properties of the finished coatings [1].

The use of aspartic acid derivatives (AADs) as the amine component for polyurea coatings has recently been proposed [2–4]. Thus, the present work set out to study the possibility of obtaining slow-curing high-performance AAD-based polyurea elastomers.

EXPERIMENTAL

Many studies have shown the potential of AADs as modifiers for the synthesis of polymers used to improve the physical and mechanical properties of finished products. Currently, a large number of AADs are produced on an industrial scale. This work used AADs synthesized by the interaction of unsaturated bisimides with aliphatic and aromatic diamines. Figure 1 and Table 1 present the AADs used in this work along with their general formula and reactivity.

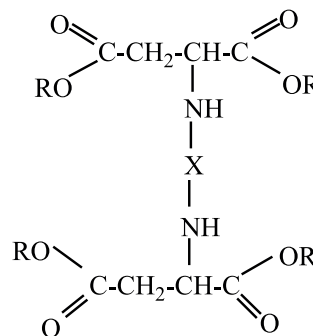


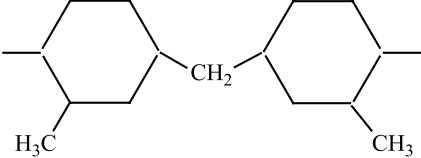
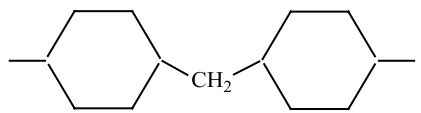
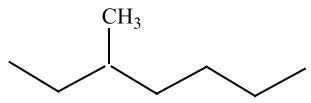
Fig. 1. General formula of an aspartic acid derivative (AAD).

As shown in Fig. 2, AADs react with isocyanates to form polyurea, which does not contain hydroxyl-containing components [3]:

The main components of the polyurethane–polyurea system are hydroxyl- and amine-containing substances

(e.g., polyols and polyetheramines), which are collectively called component A of the system. Component B of the system comprises substances belonging to the class of isocyanates, which are responsible for the reaction of urethane formation.

Table 1. Structure of the main chain of AADs and their reactivity

Notation	Structure of main chain (X in Fig. 1)	Gelation time, h
AAD 1	Methylenebis(2-methylcyclohexane-4,1-diyl) 	8
AAD 2	Methylenedicyclohexane-4,1-diyl 	1
AAD 3	2-Methylpentane-1,5-diyl 	0.1

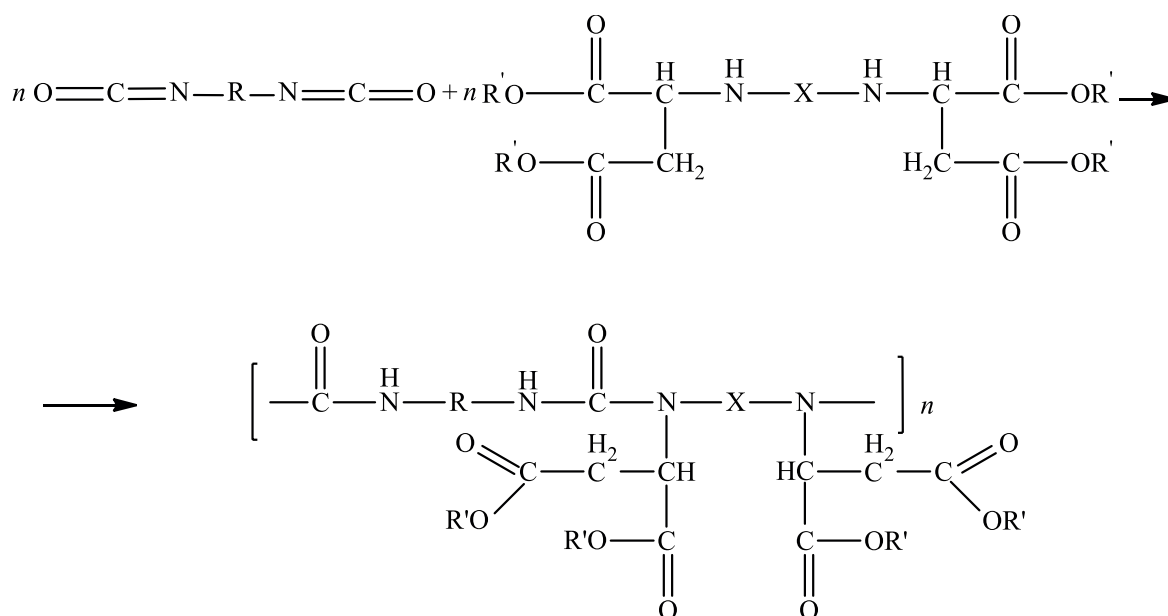


Fig. 2. Reaction to produce polyurea from AADs [3].

In the experiment, AADs were added to component A of the system in different ratios, provided that the index of the system would be in the range of 1.1–1.2.

The curing time of the composition was measured under conditions similar to the actual application conditions. Components A and B were thermostated and mixed in specified ratios. Then, the gelation time was measured, which represented the curing time of the composition. The hardness of the material was determined using the Shore method according to GOST 24621-91¹ with a TVR-A durometer (*VOSTOK-7*, Russia). Strength and relative tensile elongation were determined according to a standard method (GOST 11262-2017²) with an RKM 2.1 tensile testing machine (*Etalon-profit*, Russia). Table 2 presents the curing time and main performance properties of polyureas based on various AADs.

Table 2 shows that the addition of AAD-1 and AAD-2 makes the compositions capable of being applied manually. Moreover, the coatings based on AAD-2 are comparable to classical polyurea in hardness, and the coatings based on AAD-1 are superior to classical ones in elasticity. The addition of AADs in an amount of more than 40 wt % is unjustified since, in this case, the curing time exceeds several times the values convenient for work with them. Because of this, the performance characteristics of the finished

coating are reduced, and the cost of the composition increases. In order to improve the properties of polyurea coatings, it was proposed to combine the two types of AADs.

Since studying the effect of the initial components in a polyurea composition is known to involve complex factors and expensive equipment operating at high pressure for long experimental times [5], it is most convenient to use mathematical modeling when taking such factors into account. While there are many methods of mathematical analysis for processing experimental data, the active experiment approach is useful for obtaining accurate data due to the possibility of processing several input factors simultaneously [6]. The active experiment approach was used in the present work to reduce the number of necessary experiments and visually represent the results of the analysis for further design of the synthesis of products that meet the specified requirements. Processing of experimental data to obtain a mathematical model was carried out the methods of classical regression and correlation analyses [7, 8].

The regression analysis method can be used if the following conditions are met [6, 8]:

- 1) the observation results are independent, normally distributed random variables;
- 2) the input variables are measured with a small error in comparison with the error in determining random variables and are nonrandom;

Table 2. Properties of coatings based on polyurea in the presence of various AAD

Notation	AAD content, wt %	Curing time, s	Shore A hardness, units	Tensile strength, MPa	Relative extension, %
AAD 1	20	850	65	18.5	580
	40	3600	58	15.0	615
AAD 2	20	250	75	23.4	531
	40	300	73	26.1	505
AAD 3	20	25	85	25.8	520
	40	50	92	26.5	390
Without AAD	0	10	78	22.1	550

¹ GOST 24621-91. State Standard of the USSR. Plastics and ebonite. Determination of indentation hardness by means of a durometer (Shore hardness). Moscow: Izdatelstvo standartov; 1992. URL: <https://progost.com/gost/001.083.080/gost-24621-91/>. Accessed November 08, 2023.

² GOST 11262-2017. Interstate Standard. Plastics. Tensile test method. Moscow: Standartinform; 2018. URL: <https://docs.cntd.ru/document/1200158280>. Accessed November 08, 2023.

3) the estimates of the variances of input parameters obtained under the same conditions are homogeneous.

To find analytical dependencies between the main performance characteristics (abrasion, tensile strength, relative elongation) and the contents of components of the composition, the experimental data were processed by the least squares method.

In the work, the mathematical description was made using a complete square polynomial

$$Y = b_0 + b_1 \cdot x_1 + b_2 \cdot x_2 + b_3 \cdot x_1 \cdot x_2 + b_4 \cdot x_1^2 + b_5 \cdot x_2^2,$$

where b_0, b_1, b_2, b_3, b_4 , and b_5 are regression coefficients; x_1 and x_2 are dimensionless input variables calculated by the equation

$$x_j = \frac{X_j - X_{0j}}{h_j},$$

where x_j is the dimensionless j th input variable; X_j is the dimensional j th input variable; h_j is the variation range of the j th input variable, which is calculated by the equation

$$h_j = \frac{X_j^{\max} - X_j^{\min}}{2};$$

X_{0j} is the average value of the dimensional j th input variable, which is calculated by the equation:

$$X_{0j} = \frac{X_j^{\max} + X_j^{\min}}{2},$$

where X_j^{\max} and X_j^{\min} are the maximum and minimum values of the dimensional j th input variable, respectively.

In the work, a two-factor experiment was carried out: X_1 is the content of AAD-1 and X_2 is the content of free NCO groups, %. Table 3 presents the values of these factors for all levels of variation.

RESULTS AND DISCUSSION

The optimal design of experiment was developed using the MATLAB software (*MathWorks*, USA)³. Table 4 presents the extended design matrix and the experimental values of the properties of the composition.

To characterize these dependencies, a MATLAB program was developed, whose input data set comprises:

1) extended experimental design matrix, the dimension of which is determined by the number of input variables and the order of the regression equation (Table 4);

2) experimental values of output variables in accordance with the design matrix, which is written into the program in the form of a column vector;

3) ranges for each input variable.

The input data block comprises:

1) calculated values of the regression coefficients of the required equation;

2) table of comparison of experimental and calculated data using the obtained regression equation;

3) variance of the relative mean of the output variable;

Table 3. Input data for calculating the regression equation

Input variables Levels of variation	Input factors			
	AAD 1 content in component A		Fraction of NCO-groups, %	
	X_1 , wt %	x_1 , dimensionless units	X_2 , %	x_2 , dimensionless units
Upper level	100	+1	15	+1
Lower level	0	−1	10	−1
Zero level	50	0	12.5	0
Variation step, h	50	—	2.5	—

³ MATLAB. <https://www.mathworks.com/>. MathWorks, USA. Accessed November 08, 2023.

Table 4. Extended planning matrix in coded variables and property values

No. of experiment	x_0	x_1	x_2	$x_1 \times x_2$	x_2^2	x_1^2	Curing time, s	Tensile strength, MPa	Elongation at break, %
1	1	-1	1	-1	1	1	8	22	550
2	1	-1	-1	1	1	1	16	13	1050
3	1	-1	0	0	1	0	14	15	850
4	1	1	1	1	1	1	150	20	580
5	1	1	-1	-1	1	1	280	17	700
6	1	1	0	0	1	0	240	19	650
7	1	0	1	0	0	1	90	19	620
8	1	0	-1	0	0	1	260	16	720
9	1	0	0	0	0	0	210	17	680

4) residual variance;

5) Fisher's exact test;

6) graphic material, including the response surface obtained from the found regression equation and the isoline map.

The regression coefficients were calculated using the developed MATLAB program. The obtained regression equations are the following:

– for curing time,

$$Y1 = 200.44 + 105.33x_1 - 51.33x_2 + 30.5x_1x_2 + 68.67x_1^2 + 20.67x_2^2;$$

– for tensile strength,

$$Y2 = 16.78 + 1.0x_1 + 2.5x_2 + 1.5x_1x_2 + 0.33x_1^2 + 0.83x_2^2;$$

– for relative elongation at break,

$$Y3 = 688.89 - 86.67x_1 + 120x_2 + 95x_1x_2 + 56.67x_1^2 - 23.33x_2^2.$$

The adequacy of the equations was assessed using the Fisher's exact test. The adequacy estimate

F_p was assessed with respect to the mean $S_{\bar{y}}^2$ of the output variable and the residual variance S_{res}^2 :

$$F_p = \frac{S_{\bar{y}}^2}{S_{\text{res}}^2},$$

where the residual variance was found by the equation

$$S_{\text{res}}^2 = \frac{\sum_{i=1}^N (y_i - \bar{y}_i)^2}{N - K}.$$

The variance of the mean of the output variable was calculated by the formula

$$S_{\bar{y}}^2 = \frac{\sum_{i=1}^N (y_i - \bar{y})^2}{N - 1},$$

where N is the total number of experiments, K is the number of significant coefficients in the regression equation, and \bar{y} are the means.

The calculated values of the Fisher's exact test are the following: strength is 191.1; relative elongation is 54.55; curing time is 32.15. The tabulated value

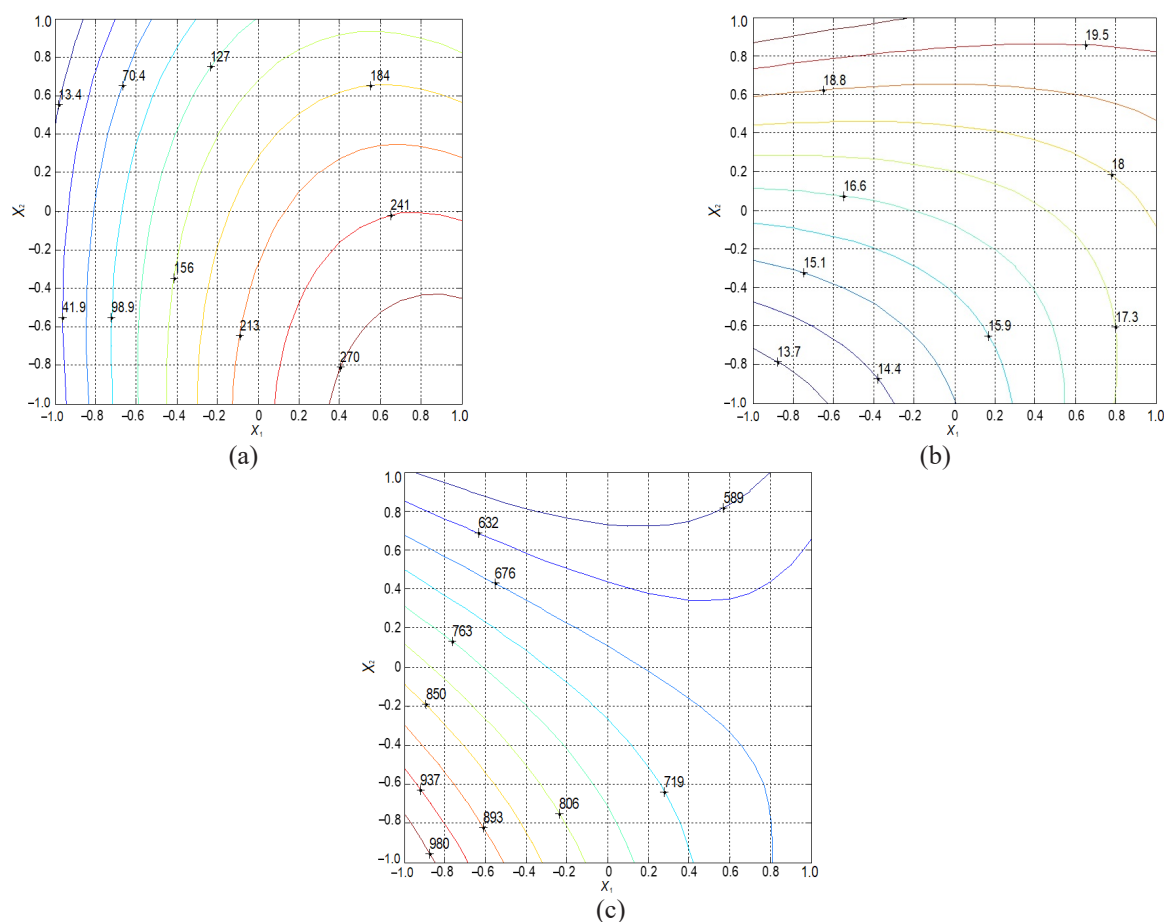


Fig. 3. Isoline maps of the main performance characteristics of polyurea coatings based on a mixture of AAD-1 and AAD-2: (a) for curing time, (b) for tensile strength, and (c) for relative elongation.

of Fisher's exact test under the corresponding conditions is 8.8 [7]. As can be seen, the calculated values of the Fisher's exact test exceed the tabulated value; consequently, the equations adequately describe the process.

Figure 3 presents the isoline map of the constructed regression functions for the selected factors.

The isoline maps depicted in Fig. 3 demonstrate the possibility of optimizing the process under study. The wide variation in the studied properties allows the composition developers to vary the performance parameters of the finished product depending on customer requirements. Importantly, throughout the studied range of properties, coatings of satisfactory quality were obtained.

CONCLUSIONS

This study showed that the use of AADs can increase the curing time to the 5 min required by the consumer. By introducing two of them (AAD-1 and AAD-2) in an amount of up to 40 wt %,

it is possible to obtain polyurea compositions with a curing time >250 s, a breaking strength >73 MPa, tensile strength >23 MPa, and a relative elongation >500%.

According to the two-factor experimental design, regression equations were compiled for each of the studied properties. The adequacy of the equations was determined by the Fisher's exact test. Isoline maps constructed on the basis of the equations are used to form to model polyurea compositions over a wide range of performance properties in accordance with customer requirements.

Authors' contributions

S.V. Romanov – research idea, resource provision;

O.A. Botvinova – conducting research, analysis of the results;

E.A. Timakov – writing the text of the article, analysis of the results;

D.A. Rashchupkina – writing the text of the article;

Yu.T. Panov – supervision, scientific editing.

The authors declare no conflicts of interest.

REFERENCES

1. Romanov S.I., Botvinova O.A., Timakov E.A., Chizhova L.A., Panov Yu.T. Development of a polyurea-based composition with an extended life span. *Tonk. Khim. Technol. = Fine Chem. Technol.* 2021;16(2):176–183 (Russ., Eng.). <https://doi.org/10.32362/2410-6593-2021-16-2-176-183>
2. Arzhakov M.S., Yakovlev P.P., Yarysheva A.Y., et al. Mechanical Properties of Insulation Coatings Based on Modified Polyurea. *Dokl. Phys. Chem.* 2021;497(1):25–27. <https://doi.org/10.1134/S0012501621030015>
[Original Russian Text: Arzhakov M.S., Yakovlev P.P., Yarysheva A.Yu., Lopatkin A.I., Yaroslavov A.A. Mechanical Properties of Insulation Coatings Based on Modified Polyurea. *Doklady Rossiiskoi akademii nauk. Khimiya, nauki o materialakh.* 2021;497(1):29–32 (in Russ.). <https://doi.org/10.31857/S2686953521020035>]
3. Botvinova O.A., Panov Y.T., Romanov S.V. Producing Bicomponent Sealants Based on Polyaspartate Urea Resins. *Polym. Sci. Ser. D.* 2020;13:407–413. <https://doi.org/10.1134/S1995421220040048>
4. Posey M.L., Hillman K.M., Klein H.P. New Secondary Amine Chain Extenders for Aliphatic Polyurea Materials. *Materials Science.* 2003. Corpus ID: 92430089
5. Akindoyo J., Beg M., Ghazali S., Islam M., Jeyaratnam N., Yuvaraj A.R. Polyurethane types, synthesis and applications-a Review. *RSC Adv.* 2016;6(115):114453–114482. <https://doi.org/10.1039/C6RA14525F>
6. Zilg C., Mulhaupt R. Morphology and toughness/stiffness balance of nanocomposites based upon anhydride-cured epoxy resins and layered silicates. *Macromol. Chem. Phys.* 1999;200(3):661–670. [https://doi.org/10.1002/\(SICI\)1521-3935\(19990301\)200:3<661::AID-MACP661>3.0.CO;2-4](https://doi.org/10.1002/(SICI)1521-3935(19990301)200:3<661::AID-MACP661>3.0.CO;2-4)
7. Umnov A.E. *Metody matematicheskogo modelirovaniya (Methods of mathematical modeling)*. Moscow: MFTI; 295 p. (in Russ.).
8. Zakgeim A.Yu. *Vvedenie v modelirovanie protsessov khimicheskoi inzhenerii. Seriya "Khimicheskaya kibernetika" (Introduction to chemical engineering process modeling. Series "Chemical cybernetics")*. Moscow: Khimiya; 1982. 288 p. (in Russ.).
9. Akhnazarova S.L., Kafarov V.V. *Metody optimizatsii eksperimenta v khimicheskoi tekhnologii: uchebnik dlya khimiko-tekhnologicheskikh spetsial'nostei vuzov (Methods of experiment optimization in chemical technology: a textbook for chemical engineering specialties of universities)*. Moscow: Vysshaya shkola; 1985. 327 p. (in Russ.).

About the authors:

Sergei V. Romanov, Cand. Sci. (Eng.), Director of the Elast PU Production Company (21a, Gastello ul., Vladimir, 600026, Russia). E-mail: romanov-elastpu@mail.ru. Scopus Author ID 55809569400, RSCI SPIN-code 9952-4171, <https://orcid.org/0000-0002-5152-4678>

Olga A. Botvinova, Cand. Sci. (Eng.), Head of Research Laboratory, Elast PU Production Company (21a, Gastello ul., Vladimir, 600026, Russia). E-mail: ermolaeva_olya@inbox.ru. Scopus Author ID 56907022800, RSCI SPIN-code 3933-6884, <https://orcid.org/0000-0003-0217-8446>

Evgenii A. Timakov, Senior Lecturer, Chemical Technologies Department, Alexander and Nikolay Stoletovs Vladimir State University (87, Gor'kogo ul., Vladimir, 600026, Russia). E-mail: okakie@yandex.ru. Scopus Author ID 57219018403, RSCI SPIN-code 3178-1477, <https://orcid.org/0000-0003-3312-0810>

СПИСОК ЛИТЕРАТУРЫ

1. Романов С.И., Ботвинова О.А., Тимаков Е.А., Чижова Л.А., Панов Ю.Т. Разработка композиции на основе полимочевины с увеличенным сроком службы. *Тонкие химические технологии.* 2021;16(2):176–183. <https://doi.org/10.32362/2410-6593-2021-16-2-176-183>
2. Аржаков М.С., Яковлев П.П., Ярышева А.Ю., Лопаткин А.И., Ярославов А.А. Механические свойства изоляционных покрытий на основе модифицированной полимочевины. *Доклады Российской академии наук. Химия, науки о материалах.* 2021;497(1):29–32. <https://doi.org/10.31857/S2686953521020035>
3. Botvinova O.A., Panov Y.T., Romanov S.V. Producing Bicomponent Sealants Based on Polyaspartate Urea Resins. *Polym. Sci. Ser. D.* 2020;13:407–413. <https://doi.org/10.1134/S1995421220040048>
4. Posey M.L., Hillman K.M., Klein H.P. New Secondary Amine Chain Extenders for Aliphatic Polyurea Materials. *Materials Science.* 2003. Corpus ID: 92430089
5. Akindoyo J., Beg M., Ghazali S., Islam M., Jeyaratnam N., Yuvaraj A.R. Polyurethane types, synthesis and applications-a Review. *RSC Adv.* 2016;6(115):114453–114482. <https://doi.org/10.1039/C6RA14525F>
6. Zilg C., Mulhaupt R. Morphology and toughness/stiffness balance of nanocomposites based upon anhydride-cured epoxy resins and layered silicates. *Macromol. Chem. Phys.* 1999;200(3):661–670. [https://doi.org/10.1002/\(SICI\)1521-3935\(19990301\)200:3<661::AID-MACP661>3.0.CO;2-4](https://doi.org/10.1002/(SICI)1521-3935(19990301)200:3<661::AID-MACP661>3.0.CO;2-4)
7. Умнов А.Е. *Методы математического моделирования.* М.: МФТИ; 2021. 295 p.
8. Закгейм А.Ю. *Введение в моделирование процессов химической инженерии. Серия «Химическая кибернетика».* М.: Химия; 1982. 288 с.
9. Ахназарова С.Л., Кафаров В.В. *Методы оптимизации эксперимента в химической технологии: учебник для химико-технологических специальностей вузов.* М.: Высшая школа; 1985. 327 с.

Dariya A. Rashchupkina, Master Student, Chemical Technologies Department, Alexander and Nikolay Stoletovs Vladimir State University (87, Gor'kogo ul., Vladimir, 600026, Russia). E-mail: dashulka010220002016@gmail.com. <https://orcid.org/0000-0001-7724-6218>

Yuri T. Panov, Dr. Sci. (Eng.), Professor, Head of the Chemical Technologies Department, Alexander and Nikolay Stoletovs Vladimir State University (87, Gor'kogo ul., Vladimir, 600026, Russia). E-mail: tpp_vlgu@mail.ru. Scopus Author ID 54789107500, RSCI SPIN-code 6961-3659, <https://orcid.org/0000-0001-8528-1195>

Об авторах:

Романов Сергей Викторович, к.т.н., директор ООО «Эласт-ПУ» (600026, Россия, Владимир, ул. Гастелло, д. 21а). E-mail: romanov-elastpu@mail.ru. Scopus Author ID 55809569400, SPIN-код РИНЦ 9952-4171, <https://orcid.org/0000-0002-5152-4678>

Ботвинова Ольга Андреевна, к.т.н., начальник исследовательской лаборатории ООО «Эласт-ПУ» (600026, Россия, Владимир, Гастелло, д. 21а). E-mail: ermolaeva_olya@inbox.ru. Scopus Author ID 56907022800, SPIN-код РИНЦ 3933-6884, <https://orcid.org/0000-0003-0217-8446>

Тимаков Евгений Александрович, старший преподаватель кафедры «Химические технологии», ФГБОУ ВО «Владимирский государственный университет им. Александра Григорьевича и Николая Григорьевича Столетовых» (600000, Россия, Владимир, ул. Горького, д. 87). E-mail: okakie@yandex.ru. Scopus Author ID 57219018403, SPIN-код РИНЦ 3178-1477, <https://orcid.org/0000-0003-3312-0810>

Ращупкина Дарья Андреевна, магистрант кафедры «Химические технологии», ФГБОУ ВО «Владимирский государственный университет им. Александра Григорьевича и Николая Григорьевича Столетовых» (600000, Россия, Владимир, ул. Горького, д. 87). E-mail: dashulka010220002016@gmail.com. <https://orcid.org/0000-0001-7724-6218>

Панов Юрий Терентьевич, д.т.н., профессор, заведующий кафедрой «Химические технологии», ФГБОУ ВО «Владимирский государственный университет им. Александра Григорьевича и Николая Григорьевича Столетовых» (600000, Россия, Владимир, ул. Горького, д. 87). E-mail: tpp_vlgu@mail.ru. Scopus Author ID 54789107500, SPIN-код РИНЦ 6961-3659, <https://orcid.org/0000-0001-8528-1195>

The article was submitted: December 21, 2022; approved after reviewing: May 26, 2023; accepted for publication: November 10, 2023.

*Translated from Russian into English by V. Glyanchenko
Edited for English language and spelling by Thomas A. Beavitt*

ISSN 2686-7575 (Online)

<https://doi.org/10.32362/2410-6593-2023-18-6-559-571>



UDC 546-386+54.31+54.057

RESEARCH ARTICLE

A green synthetic method for cobalt(II,III) oxide nanoparticles with high surface activity

Yahya Absalan¹, Rusul Alabada², Mohammad R. Razavi¹, Mostafa Gholizadeh¹, Oksana V. Avramenko^{3,✉}, Irina N. Bychkova⁴, Olga V. Kovalchukova^{3,4}

¹Ferdowsi University of Mashhad, Mashhad, 9177948974 Iran

²Al-Muthanna University, Al-Samawah, 66001 Iraq

³Peoples Friendship University of Russia (RUDN University), Moscow, 117198 Russia

⁴Kosygin Russian State University (Technology, Design, Art), Moscow, 117997 Russia

✉ Corresponding author, e-mail: avramenko-ov@rudn.ru

Abstract

Objectives. To develop a new green method for the synthesis of nanosized materials of cobalt(II,III) oxide, with improved surface activity, using environmentally friendly precursors and solvents.

Methods. A green method was proposed, in order to isolate Co₃O₄ nanoparticles with high surface activity. Instead of the usual organic solvents, three different natural sugars, including glycogen, sucrose, and glucose were used for the first time as templates. Water as a green solvent was used in all the steps. The polymorphic composition of the synthesized samples was determined by means of X-ray phase analysis. The morphology of the obtained crystallites was studied from micrographs of the oxide phases. Image Pro Plus 6 software was used to measure the size of nanoparticles. The surface activity of the isolated samples was studied using the Brunauer–Emmett–Teller method and the Langmuir method. The Barret–Joyner–Halenda method was used to determine the diameter, volume, and distribution of pores.

Results. The crystallite sizes of the samples are 23 nm, 36 nm, and 30 nm for glucose, glycogen, and sucrose templates, respectively. Adsorption-desorption isotherms for samples obtained from complexes of glucose and sucrose correspond to type IV, indicating a strong interaction between the adsorbent and the adsorbed sample. The isotherm for the sample isolated from the complex with glycogen is of a different type and most likely indicates that this sample is almost completely mesoporous. The pore radii are found in the interval 1.2–1.6 nm.

Conclusions. A new green method for the synthesis of nanosized particles of Co(II,III) oxide using natural saccharides and deionized water was developed. The composition, morphology, structure, and surface activity of the samples obtained were studied. It was shown that due to the polymeric structure of their metal complexes and the ability to bind active carbon on the surface of nanoparticles, natural saccharides can be used as matrices in the synthesis of nanosized metal oxides with high surface activity.

Keywords: nanoparticles of cobalt(II,III) oxide, synthesis, surface activity, X-ray phase analysis, Fourier transform IR spectroscopy, electron spectroscopy

For citation: Absalan Ya., Alabada R., Razavi M.R., Gholizadeh M., Avramenko O.V., Bychkova I.N., Kovalchukova O.V. A green synthetic method for cobalt(II,III) oxide nanoparticles with high surface activity. *Tonk. Khim. Tekhnol. = Fine Chem. Technol.* 2023;18(6):559–571. <https://doi.org/10.32362/2410-6593-2023-18-6-559-571>

НАУЧНАЯ СТАТЬЯ

«Зеленый» метод синтеза наночастиц оксида кобальта(II,III) с улучшенной поверхностной активностью

Я. Абсалан¹, Р. Алабада², М.Р. Разави¹, М. Голизадех¹, О.В. Авраменко^{3,✉}, И.Н. Бычкова⁴, О.В. Ковальчукова^{3,4}

¹Мешхедский университет им. Фирдоуси, Мешхед, 9177948974 Иран

²Университет Аль-Мутанна, Самава, 66001 Ирак

³Российский университет дружбы народов (РУДН), Москва, 117198 Россия

⁴Российский государственный университет им. А.Н. Косыгина (Технологии. Дизайн. Искусство), Москва, 115035 Россия

✉ Автор для переписки, e-mail: avramenko-ov@rudn.ru

Аннотация

Цели. Разработать новый «зеленый» метод синтеза наноразмерных материалов оксида кобальта(II,III) с улучшенной поверхностной активностью, используя неопасные для окружающей среды прекурсоры и растворители.

Методы. Предложен новый метод выделения наноразмерных частиц Co_3O_4 с высоко-развитой поверхностью. В качестве матриц впервые применены природные сахара — гликоген, сахароза и глюкоза. В роли экологически чистого растворителя на всех стадиях процесса используется вода. Полиморфный состав синтезированных образцов определяли с помощью рентгенофазового анализа. Морфологию полученных кристаллитов изучали по микрофотографиям оксидных фаз. Для измерения размера наночастиц использовалось программное обеспечение Image Pro Plus 6. Поверхностную активность выделенных образцов изучали методом Брунауэра–Эммета–Теллера и методом Ленгмюра. Для определения диаметра, объема и распределения пор применялся метод Баррета–Джойнера–Халенды.

Результаты. Размеры кристаллитов синтезированных образцов составляют 23, 36 и 30 нм для матриц глюкозы, гликогена и сахарозы соответственно. Изотермы адсорбции–десорбции для образцов, полученных на основе комплексов глюкозы и сахарозы, соответствуют IV типу, что свидетельствует о сильном взаимодействии между адсорбентом и адсорбированным образцом. Изотерма для образца, выделенного на основе комплекса с гликогеном, относится к другому типу и, скорее всего, указывает на то, что этот образец почти полностью мезопористый. Радиус пор составляет 1.2–1.6 нм.

Выводы. Разработан новый «зеленый» метод синтеза наноразмерных частиц оксида кобальта(II,III) с использованием природных сахаридов и деионизированной воды. Исследованы состав, морфология, строение и поверхностная активность полученных образцов. Показано, что природные сахариды благодаря полимерной структуре их металлокомплексов и способности связывать активный углерод на поверхности наночастиц, могут быть использованы в качестве матриц при синтезе наноразмерных оксидов металлов с большой поверхностной активностью.

Ключевые слова: наночастицы оксида кобальта(II,III), синтез, поверхностная активность, рентгенофазовый анализ, ИК-спектроскопия, электронная спектроскопия

Для цитирования: Абсалан Я., Алабада Р., Разави М.Р., Голизадех М., Авраменко О.В., Бычкова И.Н., Ковальчукова О.В. «Зеленый» метод синтеза наночастиц оксида кобальта(II,III) с улучшенной поверхностной активностью. *Тонкие химические технологии*. 2023;18(6):559–571. <https://doi.org/10.32362/2410-6593-2023-18-6-559-571>

INTRODUCTION

At the present time, due to their unique properties, nanoscale materials are widely used in everyday life and various industries, such as medicine, ecology, and the paint and varnish industry [1–4]. However, a significant drawback in their synthesis is the use of environmentally hazardous precursors and solvents. Therefore, an urgent task is to find an environmentally friendly and highly effective method for isolating metal oxide nanoparticles with high surface activity.

Cobalt(II,III) oxide is interesting due to its specific properties. Materials based on Co_3O_4 have the properties of *p*-type semiconductors and exhibit magnetic properties [5, 6]. They are used as molecular detectors, electrochemical storage devices, magnetic storage media, solar energy converters and in the electronics industry, as well as catalytic systems for various purposes, including

organic synthesis and environmental purification from toxic impurities [7–14].

Co_3O_4 nanoparticles are stable structures of various morphologies [15] (rods [16], sheets [17], tubes [11, 18], cubes [19], and spheres [20, 21]). Ordered structures isolated by the hydrothermal method were studied by Hu *et al.* [22], and spinel Co_3O_4 nanoparticles were shown to have lower crystallinity and smaller crystallite size.

Previously we synthesized and studied nanoparticles of 3d metal oxides using organometallic complexes based on alkyl and benzylnitrosohydroxylamines [23], biphenolic compounds [24–26], and polyhydroxybenzoic acids [27, 28] as precursors.

This work reports a new green method for the synthesis of Co_3O_4 nanoparticles using deionized water and natural saccharides and the study of their surface. It is shown that this method can be considered as a promising method for the synthesis of various nanocrystalline materials.

EXPERIMENTAL

The sucrose, glycogen, and glucose used in the work are pure grade, and cobalt(II) chloride hexahydrate is chemical grade purchased from *Sigma-Aldrich*, USA.

Method for the synthesis of Co_3O_4 nanoparticles. 10 g of the corresponding saccharide was dissolved in 50 mL of deionized water and stirred. At the same time, 2.96 g of cobalt(II) chloride hexahydrate was dissolved in deionized water in a second glass and stirred until a homogeneous solution was obtained. The saccharide solution was then slowly poured into the cobalt salt solution and stirred at 75°C for 1 h. The solution was kept at 20°C until a gel formed. The resulting gel was transferred to a pre-calcination oven at 120°C. The dried sample was calcined at 650°C, in order to obtain the corresponding cobalt oxide. The yields of the final products are 60–70%.

Elemental analysis for cobalt content was carried out by means of complexometric titration [29]. Carbon content was determined using micromethods [30]. Elemental analysis results:

Sample 1 (derived from a complex with sucrose). Found: Co — 73.15%; C — traces (<0.5%). For Co_3O_4 it was calculated as: Co — 73.42%.

Sample 2 (derived from a complex with glycogen). Found: Co — 73.38%; C — not detected. For Co_3O_4 it was calculated as: Co — 73.42%.

Sample 3 (derived from a complex with glucose). Found: Co — 73.18 %; C — traces (<0.5%). For Co_3O_4 it was calculated as: Co — 73.42%.

X-ray diffraction patterns of oxide phases were obtained using a GNR automatic diffractometer (*GNR Analytical Instruments Group*, Italy) in continuous mode. Operating wavelength was 1.541 Å (Cu- K_α). X-ray diffraction patterns were interpreted using the GNR Explorer program (*GNR Analytical Instruments Group*, Italy)¹.

The surface activity of the synthesized samples was determined by means of the Brunauer–Emmett–Teller (BET) method at 77 K on a Belsorp-mini II micrometer device (*Microtrac Retsch*, Germany). The Barrett–Joyner–Halenda (BJH) method was used to evaluate mesoporosity and pore size distribution. In order to prepare and dry the material before measuring and removing water vapor, carbon dioxide, or other molecules that may occupy the volume of the material's cavities, the sample was placed in an oven for several hours at high temperature. The dehydration temperature was 393.15 K. The dehydration time

was 2 h at a saturated water vapor pressure of 84.737 kPa.

TEM images were obtained using a model LEO 912AB microscope (*Leitz-Opton*, Germany) in low vacuum mode using ethanol as a dispersant.

FTIR spectra of the samples were recorded using an AVATAR 370 spectrometer (*Thermo Nicolet*, USA) at a temperature of 20°C in the range of 4000–400 cm^{-1} with a resolution of 4 cm^{-1} in KBr pellets.

Electronic absorption spectra were recorded on a Cary-50 spectrophotometer (*Agilent Technologies Inc.*, USA) in the wavelength range 200–800 nm.

RESULTS AND DISCUSSION

Synthesis and Co_3O_4 nanoparticle properties

A diagram of the new green method for the synthesis of Co_3O_4 nanoparticles is shown in Fig. 1.

The polymorphic composition of all synthesized samples was determined using X-ray phase analysis ($15^\circ < 2\theta < 80^\circ$) (Fig. 2). Analysis of X-ray diffraction patterns of samples obtained using various precursors shows that the spinel modification of Co_3O_4 (ICDD: 96-900-5889) of high purity (peaks 19.02° , 31.31° , 36.73° , 44.67° , 59.35° , and 65.02°) is the main crystalline structure of the products obtained from thermolysis of all precursors: the highest purity characteristic of Co_3O_4 being obtained from the decomposition of a solution containing glycogen. Based on the data from literature, the presence of low-intensity peaks in the region of about 26° and 44° in the X-ray diffraction patterns of cobalt oxide samples obtained from glucose and sucrose may indicate the presence of carbon impurities in the samples [31].

The size of crystallites (coherent scattering regions) D_c was calculated using the Scherrer equation (1):

$$D_c = k\lambda/\beta\cos\theta, \quad (1)$$

where k is the shape factor (approximately 0.9), λ is the wavelength of the X-ray source (1.5406 Å), and β is the width of the observed diffraction line at its half-maximum intensity (400).

Based on the results obtained, the sizes of crystallites (coherent scattering regions) of the samples are 23, 36, and 30 nm for precursors based on glucose, glycogen, and sucrose, respectively.

Microphotographs of oxide phases obtained by calcination of cobalt complexes of sucrose,

¹ Explorer: G.N.R. srl – Analytical Instruments Group (gnr.it). Accessed May 23, 2022.

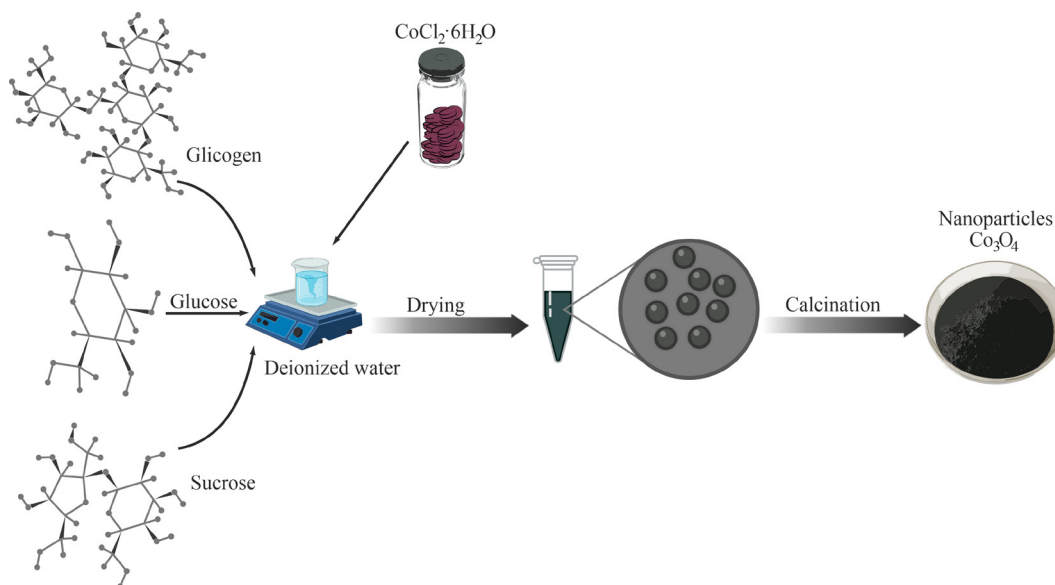


Fig. 1. Synthetic scheme for Co_3O_4 nanoparticles.

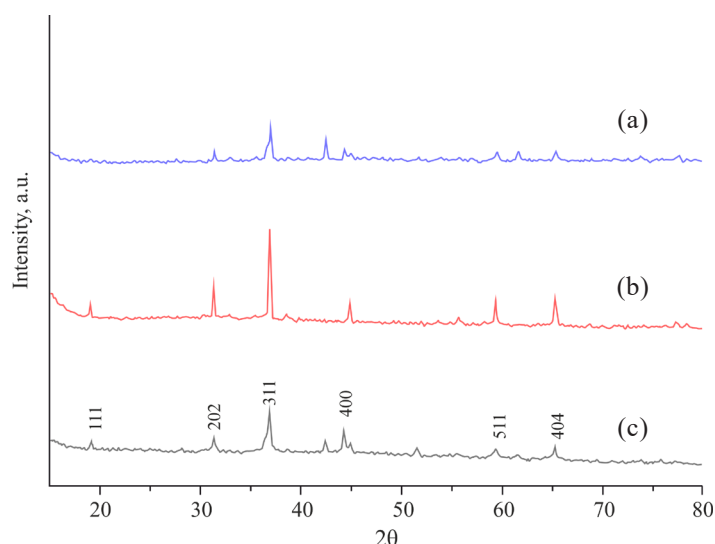


Fig. 2. X-ray diffraction patterns of oxide phases obtained by calcination of cobalt(II) complexes with sucrose (a), glycogen (b), and glucose (c).

glycogen, and glucose are presented in Fig. 3. As can be seen in Fig. 3, the shape of nanoparticles obtained by calcination of cobalt(II) complexes with sucrose, glycogen, and glucose is the same, but they differ in size. The largest size of nanoparticles was observed for the thermolysis product of the complex with sucrose, corresponding to the results obtained from the analysis of X-ray diffraction patterns. Image Pro Plus 6 software (*Media Cybernetics, Inc., USA*)² was used to measure the nanoparticle sizes. It was found that the average particle sizes for all samples were in the range of 5–30 nm.

² <https://mediacy.com/image-pro/>. Accessed July 05, 2022.

Surface properties

The state of the surface of products obtained from solutions containing various sugars was studied by infrared (IR) spectroscopy in the range of 400–4000 cm^{-1} (Fig. 4).

According to the data from literature, the bands at 526 and 561 cm^{-1} correspond to vibrations of the Co_3^+O bonds in the octahedral environment, and Co_2^+O in the *s*-tetrahedral environment in the spinel crystal lattice. The band at 1115 cm^{-1} is associated with stretching vibrations of CO bonds of carbonate anions, formed due to the adsorption of CO_2 on the surface of Co_3O_4 . This is consistent with the basic properties of cobalt(II,III) oxides formed during calcination of saccharides. In the case of Co_3O_4 isolated from a complex with

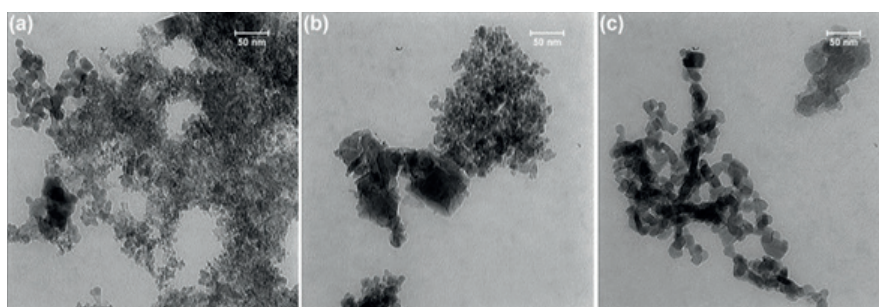


Fig. 3. Micrographs of oxide phases obtained by calcination of cobalt(II) complexes with sucrose (a), glycogen (b), and glucose (c).

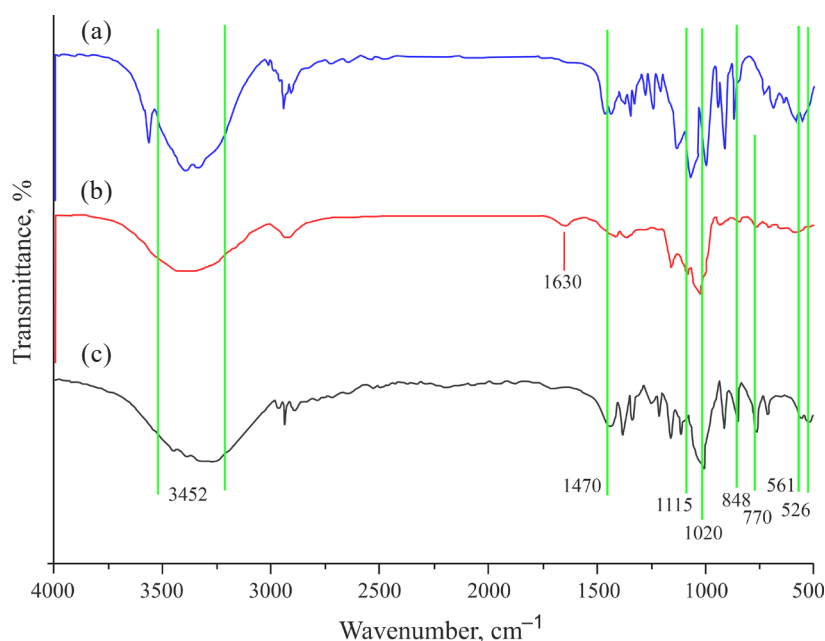


Fig. 4. IR spectra of oxide phases obtained by calcination of cobalt complexes of sucrose (a), glycogen (b), and glucose (c).

glycogen, an additional absorption band at 1630 cm^{-1} is observed in the IR spectrum which can be attributed to bending vibrations of water molecules adsorbed on the surface. In cobalt oxides isolated from solutions containing sucrose and glucose, the $\delta(\text{H}_2\text{O})$ band is also present, but its intensity is much less. The broad band at 3400 cm^{-1} is associated with stretching vibrations of OH groups on the hydrated surface of Co_3O_4 nanoparticles. The absorption at 1470 cm^{-1} is probably due to the stretching vibrations of OCO_2 . The observed band at 848 cm^{-1} can be attributed to bending vibrations of the Co–OH bond. Absorption at 770 cm^{-1} may correspond to $\delta(\text{OCO})$, and the band at 1020 cm^{-1} corresponds to $\delta(\text{C=O})$.

Low-temperature N_2 adsorption–desorption isotherms and the pore distribution curve of the samples are presented in Fig. 5. The surface activity of

the isolated samples was studied by the BET method. The BDC method was used to determine the diameter, volume and distribution of pores. The adsorption–desorption isotherms for samples obtained from glucose and sucrose complexes correspond to type IV, indicating strong interaction between the adsorbent and the adsorbed sample (Fig. 5a and 5c). The isotherm for the sample isolated from the glycogen complex is of a different type and most likely indicates that this sample is almost completely mesoporous.

An important textural characteristic of the resulting material is the pore size distribution. Based on isotherms and average pore diameters, the porosity of nanosized particles is represented by mesopores (see Table). Type IV nanopores are confirmed by the type of adsorption–desorption isotherms and pronounced hysteresis associated with capillary condensation of nitrogen in mesopores.

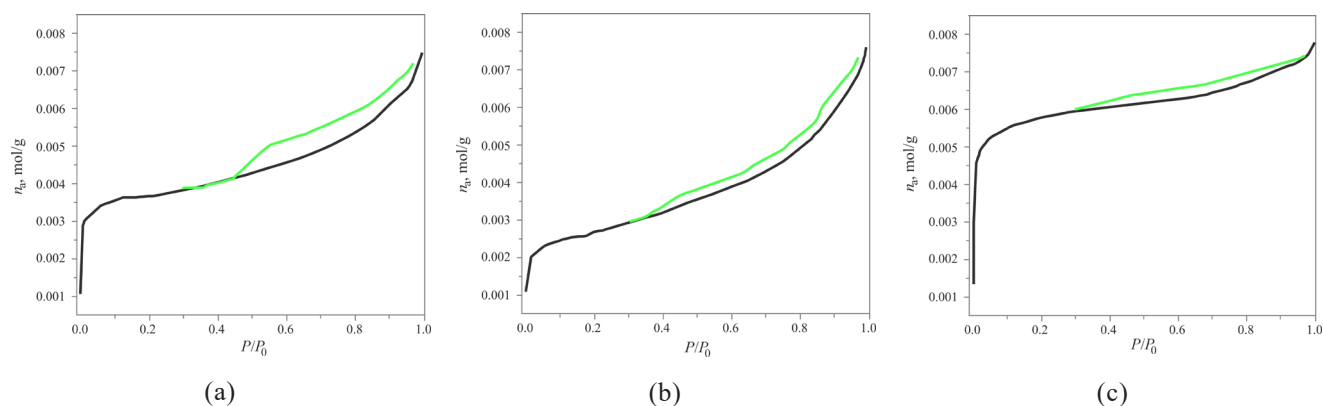


Fig. 5. Adsorption–desorption isotherms of N_2 by nanoparticles isolated from cobalt complexes of glucose (a), glycogen (b), and sucrose (c). n_a is the amount of adsorbed substance, $\text{mol} \cdot \text{g}^{-1}$; P/P_0 is the relative pressure (ratio of system pressure to condensation pressure).

Table. Some characteristics of the surface of Co_3O_4 particles

Parameters	Glucose	Glycogen	Sucrose
BET analysis			
V_m , cm^3/g	71.75	49.39	73.47
$a_{s,\text{BET}}$, m^2/g	312.27	214.96	319.78
C	6366.00	1975.80	9011.80
V , cm^3/g	0.26	0.26	0.17
d , nm	3.30	4.84	2.17
BJH analysis			
V_m , cm^3/g	0.16	0.21	0.06
r_p , nm	1.64	1.64	1.21
a_s , m^2/g	79.64	119.74	41.65
Langmuir plot			
V_m , cm^3/g	65.71	45.54	69.61
a_s , m^2/g	286.00	198.20	302.98

Note: V_m is the specific pore volume, a_s is the specific pore surface area, C is the BET constant, V is the total pore volume, d is the average pore diameter, r_p is the average pore radius.

Based on the analysis of adsorption–desorption isotherms (Fig. 5), it is clear that monolayers are formed at relative pressures P/P_0 equal to 0.076, 0.05 and 0.04, and are completely formed in all samples. There is a known relationship between the shape of the hysteresis loop and the nature of the distribution of mesopores in the joint. The pores of nanoparticles obtained by thermolysis of glucose and glycogen complexes with H_4 type hysteresis are slit-like (glucose and glycogen) and conical (sucrose) [32].

BET analysis of the samples shows that the isolated Co_3O_4 nanoparticles have high surface activity with almost the same amount (Table). The large value of constant C (the ratio of the adsorption equilibrium constants in the first layer and the condensation constant) is probably associated with the nanosize of the resulting oxides, since for micro-sized samples its value usually lies in the range from 50 to 200 [33]. The significant difference in V_m values in the case of the samples obtained on the basis of glucose and sucrose when compared with that for cobalt oxide isolated on the basis of the glycogen complex can be explained by the different nature of the pores.

According to the BDH method, the pore radius of Co_3O_4 nanoparticles obtained from cobalt complexes with glucose and glycogen is the same and equal to 1.64 nm, while for nanoparticles isolated from a complex with sucrose, it is smaller and amounts to 1.21 nm (Fig. 6).

The surface activity of a monolayer of Co_3O_4 nanoparticles obtained using the Langmuir method is consistent with BET analysis; the order of surface activity in both methods is the same (Table). Thus, we can conclude that the new

environmentally friendly synthesis method presented herein makes it possible to obtain nano-sized particles with high surface activity.

Studying the spectral characteristics of photocatalysts is one of the most important factors that determines their activity in a special region of the electromagnetic spectrum. In order to calculate the band gap of the obtained samples, electronic absorption spectra were recorded in the wavelength range from 200 to 800 nm (Fig. 7). All isolated products have optical density in a certain wavelength range: 340 nm, 500 nm, and between 800 and 850 nm, which is consistent with previously published data [34].

To find the best activating region, the Tauc method (2) was used to determine the band gap:

$$\alpha = \alpha_0(h\nu - E_g)n/h\nu, \quad (2)$$

where α is the absorption coefficient of the material, α_0 is the proportionality coefficient, $h\nu$ is the energy of the incident photon (h is the Planck's constant, ν is the frequency of the incident photon), E_g is the optical band gap, n is the refractive index. The band gap is obtained from a plot of $(\alpha h\nu)^2$ versus $h\nu$. The value of $h\nu$ at the point of intersection of the tangent and the x-axis is the band gap. Based on the result, band gap values of 1.53, 2.48, and 3.65 eV were obtained, illustrating the ability of Co_3O_4 nanoparticles to absorb in both the ultraviolet and visible regions of the spectrum.

Co_3O_4 nanoparticles isolated by the proposed synthesis method have high surface activity, exceeding that of nanoparticles obtained by other

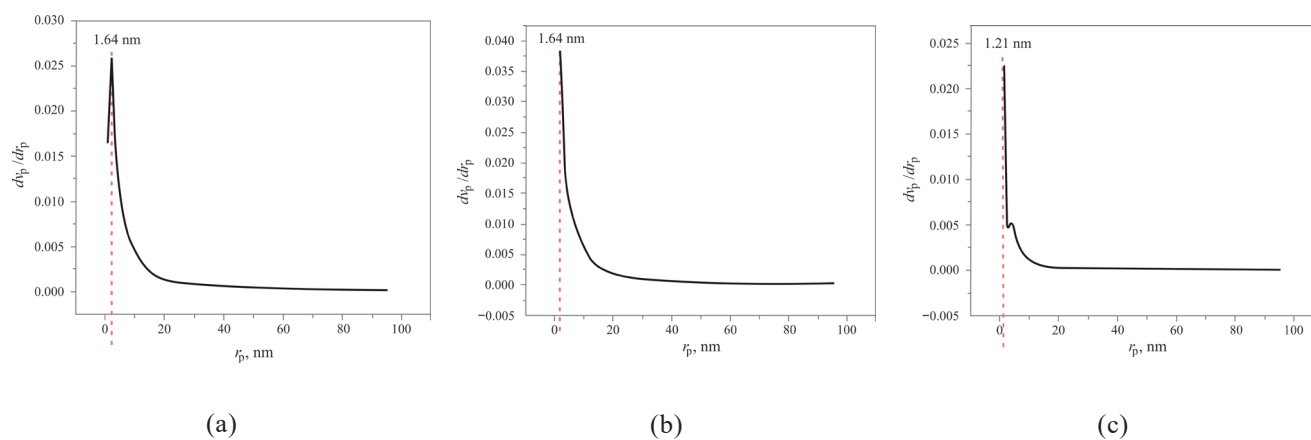


Fig. 6. BJH analysis of Co_3O_4 nanoparticles isolated from cobalt complexes of glucose (a), glycogen (b), and sucrose (c); dV_m/dr_p is the derivative of the ratio of specific volume to average pore radius, r_p is the pore radius, nm.

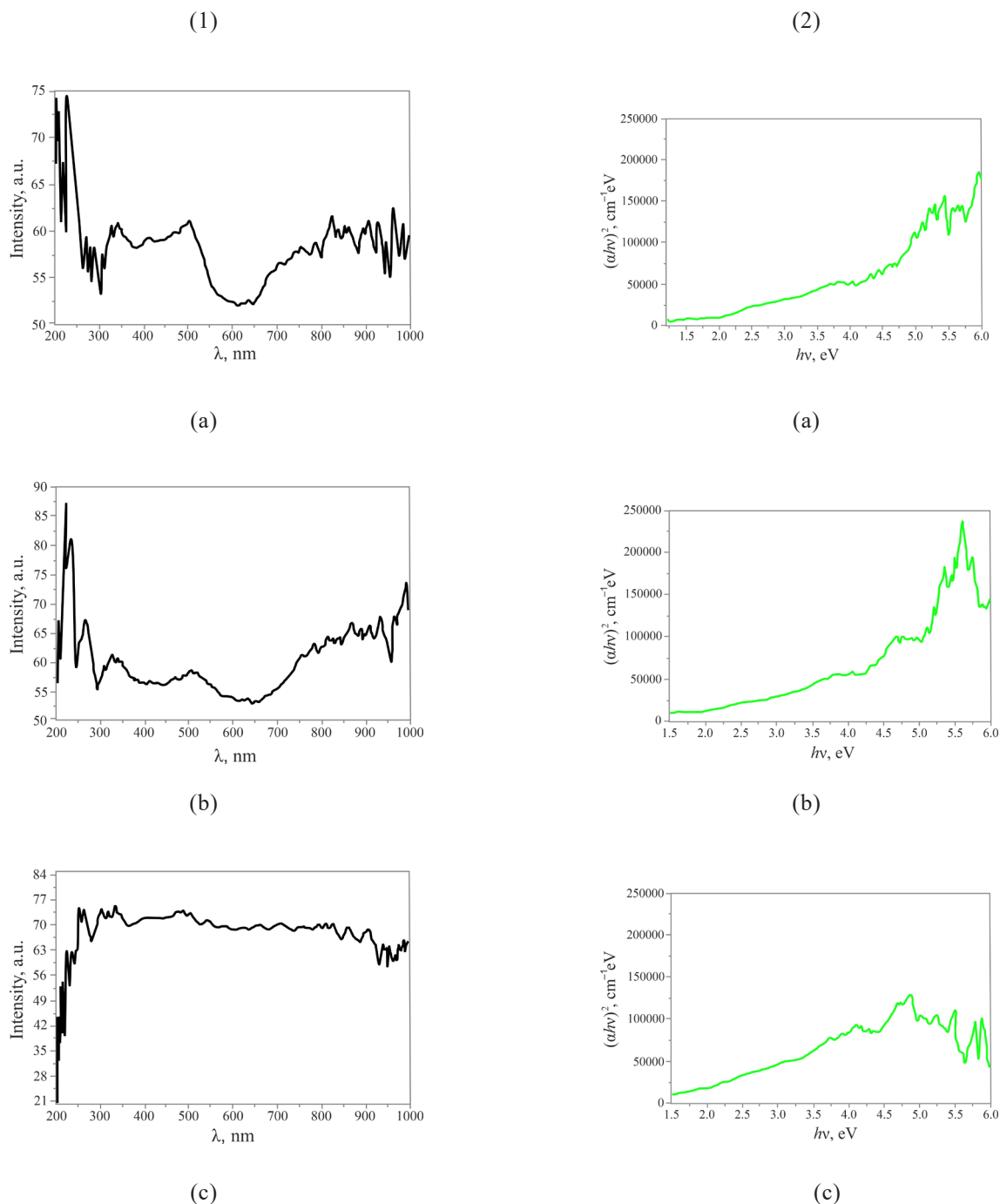


Fig. 7. Electronic absorption spectra (1) and band gap (2) of Co_3O_4 nanoparticles isolated from cobalt complexes of glucose (a), glycogen (b), and sucrose (c); $(\alpha h\nu)^2$ is the absorption coefficient squared, $\text{cm}^{-1}\cdot\text{eV}$; $h\nu$ is the photon energy, eV.

methods. A possible reason is the combustion reaction of natural sugars upon ignition, leading to the formation of carbon and its possible binding with cobalt to form a carbide, the signals of which are observed in X-ray diffraction patterns. The BET constant (C) (see Table), exponentially related to the adsorption energy

of the monolayer, is very high (>200). This also illustrates the presence of active carbon on the surface of the nanoparticles. It has been shown that a natural saccharide with a large amount of carbon in its molecular structure provides greater surface activity of the synthesized cobalt oxide nanoparticles.

CONCLUSIONS

A new green method has been developed for the synthesis of nanosized Co_3O_4 particles using natural saccharides and deionized water. It has been experimentally proven that natural saccharides, due to the polymer structure of their metal complexes and the ability to incorporate carbon on the surface of nanoparticles, can be used as matrices in the synthesis of metal oxide nanoparticles with high surface activity. In addition, natural saccharides, due to their environmental friendliness and low cost, are a good replacement for classical organic compounds used in previously developed methods for the synthesis of nanoparticles.

Acknowledgments

This study was supported by the RUDN University Strategic Academic Leadership Program, Russia, and the Research Council of Ferdowsi University of Mashhad, Iran.

Authors' contributions

Y. Absalan – planning and conducting research, research methodology, conducting research, analyzing research materials, writing the manuscript;

R. Alabada – conducting research, analyzing research materials, obtaining nanoparticles;

M.R. Razavi – conducting research, analyzing research materials, study of spectral characteristics;

M. Gholizadeh – conducting research, analyzing research materials, study of the surface of nanoparticles;

O.V. Avramenko – analyzing research materials, article editing, corresponding author;

I.N. Bychkova – conducting research, validation of research products;

O.V. Kovalchukova – formulation of the scientific concept, general management, analyzing research materials, author's supervision, reviewing and editing the article, scientific consulting.

The authors declare no conflicts of interest.

REFERENCES

1. Sindhwani S., Chan W.C.W. Nanotechnology for modern medicine: next step towards clinical translation. *J. Intern. Med.* 2021;290(3):486–498. <https://doi.org/10.1111/joim.13254>
2. Cao Y., Li S., Chen J. Modeling better *in vitro* models for the prediction of nanoparticle toxicity: a review. *Toxicol. Mech. Methods.* 2021;31(1):1–17. <https://doi.org/10.1080/15376516.2020.1828521>
3. Hsu J.C., Nieves L.M., Betzer O., Sadan T., Noël P.B., Popovtzer R., Cormode D.P. Nanoparticle contrast agents for X-ray imaging applications. *WIREs Nanomed. Nanobiotechnol.* 2020;12(2):e1642. <https://doi.org/10.1002/wnan.1642>
4. Temizel-Sekeryan S., Hicks A.L. Global environmental impacts of silver nanoparticle production methods supported by life cycle assessment. *Resour. Conserv. Recycl.* 2020;156:104676. <https://doi.org/10.1016/j.resconrec.2019.104676>
5. Makhlof S.A. Magnetic properties of Co_3O_4 nanoparticles. *J. Magn. Magn. Mater.* 2002;246(1–2):184–190. [https://doi.org/10.1016/S0304-8853\(02\)00050-1](https://doi.org/10.1016/S0304-8853(02)00050-1)
6. Wang R.M., Liu C.M., Zhang H.Z., Chen C.P., Guo L., Xu H.B., Yang S.H. Porous nanotubes of Co_3O_4 : Synthesis, characterization, and magnetic properties. *Appl. Phys. Lett.* 2004;85:2080–2082. <https://doi.org/10.1063/1.1789577>
7. Rashad M., Rüsing M., Berth G., Lischka K., Pawlis A. CuO and Co_3O_4 nanoparticles: synthesis, characterizations, and Raman spectroscopy. *J. Nanomater.* 2013;2013:Article ID 714853. <https://doi.org/10.1155/2013/714853>

8. Lanje A.S., Ningthoujam R.S., Sharma S.J., Pode R.B., Vatsa R.K. Luminescence properties of $\text{Sn}_{1-x}\text{Fe}_x\text{O}_2$ nanoparticles. *Int. J. Nanotechnol.* 2010;7(9–12):979–988. <https://doi.org/10.1504/IJNT.2010.034703>
9. Duan X., Huang Y., Agarwal R., Lieber C.M. Single-nanowire electrically driven lasers. *Nature.* 2003;421:241–245. <https://doi.org/10.1038/nature01353>
10. Seo Hee J.U., Hong S.K., Jang H.C., Kang Y.C. Fine size cobalt oxide powders prepared by spray pyrolysis using two types of spray generators. *J. Ceramic Soc. Japan.* 2007;115(1344):507–510. <https://doi.org/10.2109/jcersj2.115.507>
11. Lou X.W., Deng D., Lee J.Y., Feng J., Archer L.A. Self-supported formation of needlelike Co_3O_4 nanotubes and their application as lithium-ion battery electrodes. *Adv. Mater.* 2008;20(2):258–262. <https://doi.org/10.1002/adma.200702412>
12. Li Y.G., Tan B., Wu Y.Y. Mesoporous Co_3O_4 nanowire arrays for lithium ion batteries with high capacity and rate capability. *Nano Lett.* 2008;8(1):265–270. <https://doi.org/10.1021/nl0725906>
13. Henglein A. Small-particle research: physicochemical properties of extremely small colloidal metal and semiconductor particles. *Chem. Rev.* 1989;89(8):1861–1873. <https://doi.org/10.1021/cr00098a010>
14. Hagfeldt A., Grätzel M. Light-induced redox reactions in nanocrystalline systems. *Chem. Rev.* 1995;95(1):49–68. <https://doi.org/10.1021/cr00033a003>
15. Zhu X., Bai B., Zhou B., Ji S. Co_3O_4 nanoparticles with different morphologies for catalytic removal of ethyl acetate. *Catal. Commun.* 2021;156:106320. <https://doi.org/10.1016/j.catcom.2021.106320>
16. Nguyen H., El-Safty S.A. Meso- and macroporous Co_3O_4 nanorods for effective VOC Gas sensors. *J. Phys. Chem. C.* 2011;115(17):8466–8474. <https://doi.org/10.1021/jp1116189>
17. Li L.L., Chu Y., Liu Y., Song J.L., Wang D., Du X.W. A facile hydrothermal route to synthesize novel Co_3O_4 nanoplates. *Mater. Lett.* 2008;62(10–11):1507–1510. <https://doi.org/10.1016/j.matlet.2007.09.012>
18. Li W.Y., Xu L.N., Chen J. Co_3O_4 nanomaterials in lithium-ion batteries and gas sensors. *Adv. Funct. Mater.* 2005;15(5):851–857. <https://doi.org/10.1002/adfm.200400429>
19. Xu R., Hua C.Z. Mechanistic investigation on salt-mediated formation of free-standing Co_3O_4 nanocubes at 95°C. *J. Phys. Chem. B.* 2003;107(4):926–930. <https://doi.org/10.1021/jp021094x>
20. Sun X.M., Li Y.D. Colloidal carbon spheres and their core/shell structures with noble-metal nanoparticles. *Angew. Chem. Int. Ed.* 2004;43(5):597–601. <https://doi.org/10.1002/anie.200352386>
21. Sun X.M., Liu J.F., Li Y.D. Use of carbonaceous polysaccharide microspheres as templates for fabricating metal oxide hollow spheres. *Chem. Eur. J.* 2006;12(7):2039–2047. <https://doi.org/10.1002/chem.200500660>
22. Hu L.H., Peng Q., Li Y.D. Selective synthesis of Co_3O_4 nanocrystal with different shape and crystal plane effect on catalytic property for methane combustion. *J. Amer. Chem. Soc.* 2008;130(48):16136–16137. <https://doi.org/10.1021/ja806400e>
23. Kovalchukova O.V., Bostanabad A.Sh., Lobanov N.N., et al. Copper(II) alkyl- and benzylnitrosohydroxylamines as precursors for the synthesis of copper(I) oxide micro- and nanoparticles of various morphologies. *Inorg. Mater.* 2014;50(11):1093–1098. <https://doi.org/10.1134/S0020168514110090>
- [Original Russian Text: Kovalchukova O.V., Bostanabad Ali Sheikh, Lobanov N.N., Rudakova T.A., Strashnov P.V., Skarzhevskii Yu.A., Zyuzin I.N. Copper(II) alkyl- and benzylnitrosohydroxylamines as precursors for the synthesis of copper(I) oxide micro- and nanoparticles of various morphologies. *Neorganicheskie Materialy.* 2014;50(11):1183–1188 (in Russ.). <https://doi.org/10.7868/S0002337X14110098>
24. Absalan Y., Fortalnova E.A., Lobanov N.N., Dobrokhotova E.V., Kovalchukova O.V. Ti (IV) complexes with some diphenols as precursors for TiO_2 nano-sized catalysts. *J. Organomet. Chem.* 2018;859:80–91. <https://doi.org/10.1016/j.jorganchem.2018.02.002>
25. Absalan Y., Kovalchukova O.V., Bratchikova I.G., Lobanov N.N. Novel synthesis method for photo-catalytic system based on some 3d-metal titanates. *J. Mater. Sci.: Mater. Electron.* 2017;28(23):18207–18219. <https://doi.org/10.1007/s10854-017-7769-6>
26. Absalan Y., Ryabov M.A., Kovalchukova O.V. Thermal decomposition of bimetallic titanium complexes: A new method for synthesizing doped titanium nano-sized catalysts and photocatalytic application. *Mater. Sci. Eng. C.* 2019;97:813–826. <https://doi.org/10.1016/j.msec.2018.12.077>
27. Absalan Y., Gholizadeh M., Butusov L., Bratchikova I., Kopylov V., Kovalchukova O. Titania nanotubes (TNTs) prepared through the complex compound of gallic acid with titanium; examining photocatalytic degradation of the obtained TNTs. *Arab. J. Chem.* 2020;13(10):7274–7288. <https://doi.org/10.1016/j.arabj.2020.02.023>
28. Alabada R., Avramenko O.V., Absalan Y., et al. Complex compounds of transition metals with hydroxyaromatic carboxylic acids as precursors for the synthesis of nanosized metal oxides. *Rus. Chem. Bul.* 2020;69(5):934–940. <https://doi.org/10.1007/s11172-020-2851-2>
- [Original Russian Text: Alabada R., Avramenko O.V., Isaeva N.Y., Kovalchukova O.V., Absalan Y. Complex compounds of transition metals with hydroxyaromatic carboxylic acids as precursors for the synthesis of nanosized metal oxides. *Izvestiya Akademii Nauk. Seriya Khimicheskaya.* 2020;(5):934–940 (in Russ.). <https://doi.org/10.1007/s11172-020-2851-2>
29. Shvartsenbakh G., Flashka G. *Kompleksonometricheskoe titrovaniye (Complexonometric Titration)*. Moscow: Khimiya; 1970. 360 p. (in Russ.).
30. Klimova V.A. *Osnovnye mikrometody analiza organicheskikh soedinenii (Basic Micromethods for the Analysis of Organic Compounds)*. Moscow: Khimiya; 1975. 224 p. (in Russ.).
31. Chernyak S.A., Suslova E.V., Ivanov A.S., Egorov A.V., Maslakov K.I., Savilov S.V., Lunin V.V. Co catalysts supported on oxidized CNTs: Evolution of structure during preparation, reduction and catalytic test in Fischer-Tropsch synthesis. *Appl. Catal. A Gen.* 2016;523:221–229. <https://doi.org/10.1016/j.apcata.2016.06.012>
32. Shrestha S., Wang B., Dutta P. Nanoparticle processing: Understanding and controlling aggregation. *Adv. Colloid Interface Sci.* 2020;279:102162. <https://doi.org/10.1016/j.cis.2020.102162>
33. Sathiyamurthy R., Kabeel A.E., Balasubramanian M., Devarajan M., Sharshir S.W., Manokar A.M. Experimental study on enhancing the yield from stepped solar still coated using fumed silica nanoparticle in black paint. *Mater. Lett.* 2020;272:127873. <https://doi.org/10.1016/j.matlet.2020.127873>

34. Arani R.P., Sathyamurthy R., Chamkha A., Kabeel A.E., Deverajan M., Kamalakannan K., Balasubramanian M., Manokar A.M., Essa F., Saravanan A. Effect of fins and silicon dioxide nanoparticle black paint on the absorber plate for augmenting yield from tubular solar still. *Environ. Sci. Pollut. Res.* 2021;28(26):35102–35112. <https://doi.org/10.1007/s11356-021-13126-y>

About the authors:

Yahya Absalan, Cand. Sci. (Chem.), Researcher, Ferdowsi University of Mashhad (Razavi Khorasan Province, Mashhad, 9177948974, Iran). E-mail: yahyaabsalan2014@gmail.com. Scopus Author ID 57195604436, ResearcherID C-1074-2019, <https://orcid.org/0000-0003-2738-9645>

Rusul Alabada, Cand. Sci. (Chem.), Assistant, Al-Muthanna University (Al-Muthanna Province, Al-Samawah, 66001, Iraq). E-mail: ms.rusul@mail.ru. Scopus Author ID 56600857900, <https://orcid.org/0000-0001-7274-6803>

Mohammad Reza Razavi, Student, Ferdowsi University of Mashhad, (Razavi Khorasan Province, Mashhad, 9177948974, Iran). E-mail: yahyaabsalan2014@gmail.com. Scopus Author ID 57448976600.

Mostafa Gholizadeh, Cand. Sci. (Chem.), Researcher, Ferdowsi University of Mashhad, (Razavi Khorasan Province, Mashhad, 9177948974, Iran). E-mail: yahyaabsalan2014@gmail.com. Scopus Author ID 55907553300, ResearcherID E-8281-2017, <https://orcid.org/0000-0002-9947-2248>

Oksana V. Avramenko, Cand. Sci. (Chem.), Associate Professor, Department of General Chemistry, Patrice Lumumba Peoples' Friendship University of Russia (RUDN University) (6, Miklukho-Maklaya Ul., Moscow, 117198, Russia). E-mail: avramenko-ov@rudn.ru. Scopus Author ID 6603223708, ResearcherID E-6124-2018, RSCI SPIN-code 9740-7682, <https://orcid.org/0000-0003-2286-0565>

Olga V. Kovalchukova, Dr. Sci. (Chem.), Head of the Department of Inorganic and Analytical Chemistry, Kosygin State University of Russia (33, Sadovnicheskaya ul., Moscow, 117997, Russia). E-mail: kovalchukova-ov@rguk.ru. Scopus Author ID 6602446862, ResearcherID E-5904-2014, RSCI SPIN-code 7508-4053, <https://orcid.org/0000-0002-6684-5829>

Irina N. Bychkova, Cand. Sci. (Eng.), Director of the Institute of Chemical Technology and Industrial Ecology, Kosygin State University of Russia (33, Sadovnicheskaya ul., Moscow, 117997, Russia). E-mail: bychkova-in@rguk.ru

Об авторах:

Абсалан Яхья, к.х.н., научный сотрудник, Мешхедский университет им. Фирдоуси (9177948974, Иран, Мешхед, провинция Разави Хорасан). E-mail: yahyaabsalan2014@gmail.com. Scopus Author ID 57195604436, ResearcherID C-1074-2019, <https://orcid.org/0000-0003-2738-9645>

Алабада Русул, к.х.н., ассистент, Университет Аль-Мутанна, (66001, Ирак, Самава, провинция Аль-Мутанна). E-mail: ms.rusul@mail.ru. Scopus Author ID 56600857900, <https://orcid.org/0000-0001-7274-6803>

Разави Мохаммад Реза, студент, Мешхедский университет им. Фирдоуси, (9177948974, Иран, Мешхед, Разави Хорасан). E-mail: yahyaabsalan2014@gmail.com. Scopus Author ID 57448976600.

Голизадех Мостафа, к.х.н., научный сотрудник, Мешхедский университет им. Фирдоуси, (9177948974, Иран, Мешхед, Разави Хорасан). E-mail: yahyaabsalan2014@gmail.com. Scopus Author ID 55907553300, ResearcherID E-8281-2017, <https://orcid.org/0000-0002-9947-2248>

Авраменко Оксана Владимировна, к.х.н., доцент кафедры общей химии, ФГАОУ ВО «Российский университет дружбы народов им. Патриса Лумумбы» (РУДН) (117198, Россия, Москва, ул. Миклухо-Маклая, д. 6). E-mail: avramenko-ov@rudn.ru. Scopus Author ID 6603223708, ResearcherID E-6124-2018, SPIN-код РИНЦ 9740-7682, <https://orcid.org/0000-0003-2286-0565>

Ковальчукова Ольга Владимировна, д.х.н., заведующий кафедрой неорганической и аналитической химии, ФГБОУ ВО «Российский государственный университет им. А.Н. Косыгина (Технологии. Дизайн. Искусство)» (115035, Россия, Москва, ул. Садовническая, д. 33). E-mail: kovalchukova-ov@rguk.ru. Scopus Author ID 6602446862, ResearcherID E-5904-2014, SPIN-код РИНЦ 7508-4053, <https://orcid.org/0000-0002-6684-5829>

Бычкова Ирина Николаевна, к.т.н., директор Института химических технологий и промышленной экологии, ФГБОУ ВО «Российский государственный университет им. А.Н. Косыгина (Технологии. Дизайн. Искусство)» (115035, Россия, Москва, ул. Садовническая, д. 33). E-mail: bychkova-in@rguk.ru

The article was submitted: April 10, 2023; approved after reviewing: May 03, 2023; accepted for publication: November 14, 2023.

Translated from Russian into English by H. Moshkov

Edited for English language and spelling by Dr. David Mossop

CHEMISTRY AND TECHNOLOGY OF INORGANIC MATERIALS
ХИМИЯ И ТЕХНОЛОГИЯ НЕОРГАНИЧЕСКИХ МАТЕРИАЛОВ

ISSN 2686-7575 (Online)

<https://doi.org/10.32362/2410-6593-2023-18-6-572-582>



UDC 544.3.01:661.689:661.686

RESEARCH ARTICLE

Fluorination of titanomagnetite concentrate with ammonium bifluoride

Alexander N. D'yachenko

MIREA – Russian Technological University (M.V. Lomonosov Institute of Fine Chemical Technologies),
Moscow, 119571 Russia

✉ Corresponding author, e-mail: dyachenko@mirea.ru

Abstract

Objectives. To study the technological features of a new fluoride technology for the production of titanium dioxide by the decomposition of titanomagnetite concentrate with ammonium fluorides.

Methods. The chemical species of the titanium and iron components in the fluorination of titanomagnetite concentrate and sublimation separation of components were determined by means of X-ray powder diffraction analysis and inductively coupled plasma mass spectrometry. The kinetics of sublimation of the titanium component by the thermal decomposition of ammonium hexafluorotitanate was experimentally studied.

Results. The products of the fluorination of titanomagnetite concentrate with ammonium bifluoride are compounds $(\text{NH}_4)_2\text{TiF}_6$ and $(\text{NH}_4)_3\text{FeF}_6$, as proven by chemical analysis and X-ray powder diffraction analysis. The subsequent sublimation separation of the titanium component produced the target product: a mixture of ammonium fluorotitanates. The desublimation of the titanium-containing fraction gave an NH_4TiF_5 – $(\text{NH}_4)_2\text{TiF}_6$ – $(\text{NH}_4)_3\text{TiF}_7$ mixture, the titanium content of which is 30.6% and the content of impurities (Fe, V, Si) is a minimum (0.45%). The activation energy of the heterogeneous reaction and the rate-limiting step of the process were also determined.

Conclusions. A high-purity titanium product (a mixture of ammonium fluorotitanates) is obtained. This is a valuable commercial product for the industrial production of titanium dioxide pigment from titanomagnetite concentrate and ilmenite.

Keywords: ammonium fluorides, ammonium hexafluorotitanate, titanomagnetite concentrate, titanium dioxide

For citation: D'yachenko A.N. Fluorination of titanomagnetite concentrate with ammonium bifluoride. *Tonk. Khim. Tekhnol. = Fine Chem. Technol.* 2023;18(6):572–582. <https://doi.org/10.32362/2410-6593-2023-18-6-572-582>

НАУЧНАЯ СТАТЬЯ

Исследование процесса фторирования титаномагнетитового концентрата дифторидом аммония

А.Н. Дьяченко

МИРЭА – Российский технологический университет (Институт тонких химических технологий им. М.В. Ломоносова), Москва, 119571 Россия

✉ Corresponding author, e-mail: dyachenko@mirea.ru

Аннотация

Цели. Исследование технологических особенностей новой фторидной технологии производства диоксида титана методом разложения титаномагнетитового концентрата с помощью фторидов аммония.

Методы. Формы нахождения титановых и железистых составляющих в процессе фторирования титаномагнетитового концентрата и сублимационного разделения компонентов определялись рентгенофазовым анализом и масс-спектрометрией с индуктивно-связанной плазмой. Кинетика сублимации титановой составляющей экспериментально изучена термическим разложением гексафторотитаната аммония.

Результаты. В результате фторирования титаномагнетитового концентрата дифторидом аммония образуются продукты реакции в виде соединений $(\text{NH}_4)_2\text{TiF}_6$ и $(\text{NH}_4)_3\text{FeF}_6$, что доказано химическим и рентгенофазовым анализом. С помощью последующего сублимационного отделения титановой составляющей получен целевой продукт, представленный смесью фторотитанатов аммония. Методом десублимации титансодержащей фракции выделена смесь NH_4TiF_5 – $(\text{NH}_4)_2\text{TiF}_6$ – $(\text{NH}_4)_3\text{TiF}_7$, содержание титана в которой находится на уровне 30.6%, а содержание примесей (Fe, V, Si) минимально (0.45%). Определена энергия активации гетерогенной реакции и лимитирующая стадия процесса.

Выводы. Получен высокочистый титановый продукт (смесь фторотитанатов аммония), который является ценным коммерческим продуктом для промышленного производства пигментного диоксида титана из титаномагнетитового концентрата и ильменита.

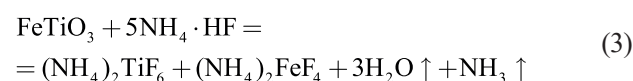
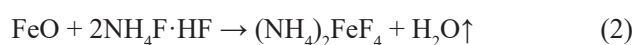
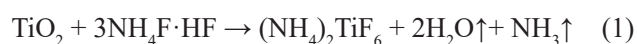
Ключевые слова: фториды аммония, гексафторотитанат аммония, титаномагнетитовый концентрат, диоксид титана

Для цитирования: Дьяченко А.Н. Исследование процесса фторирования титаномагнетитового концентрата дифторидом аммония. *Тонкие химические технологии.* 2023;18(6):572–582. <https://doi.org/10.32362/2410-6593-2023-18-6-572-582>

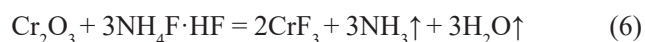
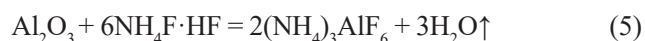
INTRODUCTION

Titanium dioxide is one of the main inorganic products of the chemical industry. It is used as a white pigment in paints and varnishes. Titanium dioxide is produced by two classical processes: the sulfate process and the chloride process whose optimization resource is currently exhausted. In order to reduce production costs, new approaches to processing titanium mineral raw materials are required [1]. Titanomagnetite concentrates (TMC) are refractory minerals, which cannot be processed by the classical sulfuric-acid and chlorine methods for titanium extraction. Our studies investigated the separation of a titanium-containing fraction from TMC fluorinated with ammonium bifluoride. In our previous works, an ammonium fluoride technology for the production of titanium dioxide was patented [2, 3]. However, it can be optimized, in order to reduce the cost of titanium dioxide pigment.

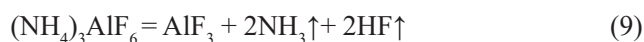
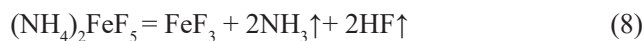
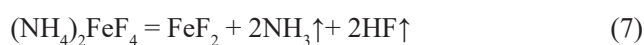
Ammonium fluorides (a commercial technical mixture of ammonium fluoride NH_4F and ammonium bifluoride $\text{NH}_4\text{F} \cdot \text{HF}$ in known ratios) are solid fluorinating agents produced by the chemical industry. They allow the decomposition of ilmenite and TMC by solid-phase sintering followed by thermal distillation of the titanium phase. TMC is a mixture of ilmenite and excess oxidized iron (III) oxide [4]. Ilmenite (FeTiO_3) can be represented as an empirical mixture of titanium dioxide and iron oxide ($\text{FeO} \cdot \text{TiO}_2$). The titanium component of TMC and ilmenite reacts with ammonium fluorides to form ammonium fluorotitanates. Unlike iron fluorides, they are sublimated and separated from the fluorinated mixture [5–8].



Other impurity compounds present in TMC also react with ammonium bifluoride to form ammonium fluoride complexes.



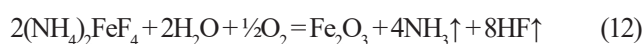
When heated, fluorometalates decompose into metal fluorides, and excess ammonium fluoride enters the gas phase.



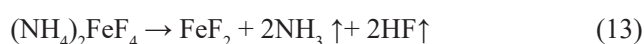
Excess ammonium bifluoride undergoes thermal decomposition.



The iron component of the fluorinated mixture upon heating with access to atmospheric moisture or water vapor formed by reaction (3) undergoes oxidative pyrohydrolysis to form iron(III) oxide.



Upon further heating, ammonium hexafluorotitanate (AHFT) $(\text{NH}_4)_2\text{TiF}_6$ sublimates and is distilled off in the form of a gas phase from the fluorinated mass of ilmenite. The iron component in the form of ammonium tetrafluoroferrate $(\text{NH}_4)_2\text{FeF}_4$ decomposes to form solid iron difluoride with the release of gaseous hydrogen fluoride and water.



The general principles of the fluorination of TMC with ammonium bifluoride are similar in process parameters to the fluorination of ilmenite.

An important economic aspect of this technology is the possibility of the complete regeneration of ammonium fluoride bifluoride, which shows the competitive advantages of the presented technology. Ammonium fluoride is regenerated by the subsequent treatment of the titanium fluoride desublimates with aqueous ammonia. Adding it to an AHFT solution leads to precipitation of hydrated oxy- and oxy-hydroxy compounds with the empirical formulas $\text{TiOF}_2 \cdot n\text{H}_2\text{O}$ and $\text{TiO}(\text{OH})\text{F} \cdot n\text{H}_2\text{O}$. Oxyfluoride monohydrate $\text{TiOF}_2 \cdot \text{H}_2\text{O}$ is known to be released from aqueous solutions. The complex ions existing in aqueous solutions are assigned the formulas TiOF^+ , $[\text{Ti}(\text{OH})_2\text{F}]^+$, TiOF_2 , TiOF_3^- , TiOF_4^{2-} , and TiF_2^{2+} [9–12]. Next, by increasing pH,

these precipitates are converted into titanium hydroxide oxide; then, they are filtered off and, after calcination, transform into titanium dioxide.

The iron component after fluorination of ilmenite with ammonium fluorides is iron tetrafluoroferrate. Upon heating, it transforms into iron difluoride and then undergoes pyrohydrolysis to produce iron(III) oxide, also a commercial product. The closed-loop material flow diagram (Fig. 1) of ammonium fluoride processing of ilmenite into titanium dioxide and iron(III) oxide with the return of all auxiliary reagents enables the so-called ammonium fluoride cycle of ilmenite processing.

This work studied the process parameters of the presented empirical diagram based on the example of the interaction of ammonium bifluoride with titanomagnetite concentrate.

The objects of research were TMC fluorinated with ammonium bifluoride (which was a mixture of AHFT and ammonium tetrafluoroferrate), titanium-containing sublimation products, and a nonsublimating iron-containing residue.

The purpose of the study was to confirm experimentally the above-mentioned chemical sequences of interaction of TMC with ammonium bifluoride, as well as the sublimation separation of the titanium component from the fluorinated mixture. A further aim was to determine the sublimation conditions, and the chemical species

of the iron ferrous and titanium components in the products of the process under study.

EXPERIMENTAL

Table 1. Chemical composition of titanomagnetite concentrate (Baikal-Amur Mining Corporation, Russia)

Substance	TiO ₂	Fe ₂ O ₃	Al ₂ O ₃	SiO ₂	Cr ₂ O ₃	V ₂ O ₅
Content, %	15.2	68.3	5.2	7.0	0.34	0.69

Ammonium bifluoride (*Galogen*, Russia) used in the experiments complied with GOST 9546-75¹.

Chemical analysis was carried out over a wide concentration range by inductively coupled plasma mass spectrometry (ICP-MS) using an Agilent 7500cx mass spectrometer (*Agilent Technologies*, USA; low resolution, generator output power 1500 W, MicroMist nebulizer).

The fluorination of TMC with ammonium bifluoride was studied using an SDT Q600 simultaneous TGA/DSC/DTA² analyzer (*NF Instruments*, USA) with software data processing using the Universal Analysis software (version V4.2E, *TA Instruments*, USA) according to standard ASTM methods³.

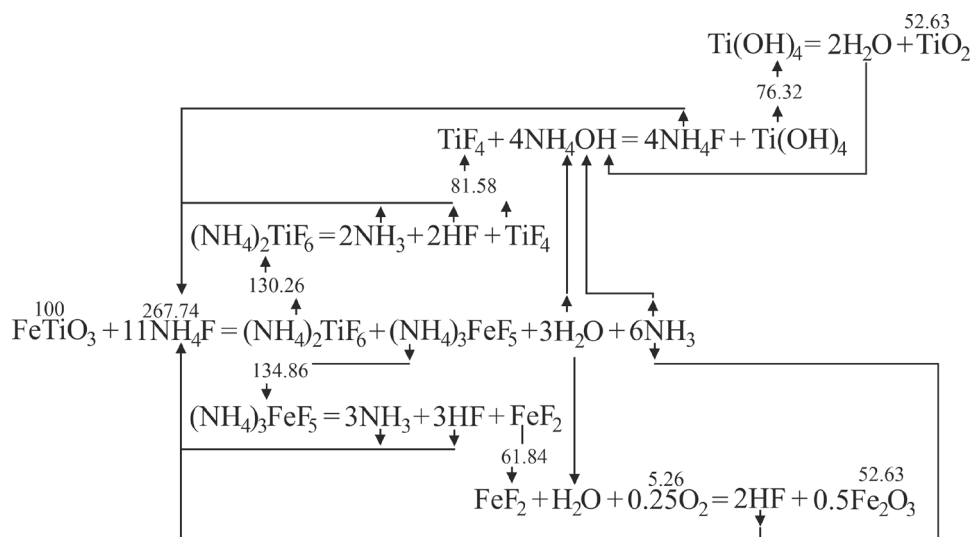


Fig. 1. Material flow diagram of the ammonium fluoride process.

¹ GOST 9546-75. State Standard of the USSR. Reagents. Ammonium fluoride (acid). Specifications. Moscow: Izdatelstvo standartov; 1981.

² TGA/DSC/DTA is the thermogravimetric analysis/differential scanning calorimetry/differential thermal analysis.

³ American Society for Testing and Materials. ASTM E 473-00 (2000). Standard definition of terms relating to thermal analysis. <https://cdn.standards.iteh.ai/samples/7305/ea45d8e86eff4027b88383a80db3c3a8/ASTM-E473-00.pdf>. Accessed October 10, 2023.

The sample weight was up to 25 mg; the sensitivity of the balance, 0.1 μg ; the calorimetric accuracy/reproducibility, $\pm 2\%$ (metal standards); DTA sensitivity, 0.001 $^{\circ}\text{C}$; the thermocouples, Pt/Pt-Rh (type R); the crucibles, platinum (40 μL) and ceramic (Al_2O_3 , 40 μL). The controlled atmosphere over the sample (argon, atmospheric air).

X-ray powder diffraction analysis (XRD) was performed using an XRD 7000S powder diffractometer (Shimadzu, Japan; sample weight, from 10 mg; sensitivity for phase composition, 3–5%).

The sublimation–desublimation process was modeled in a setup specially designed and constructed for these studies (RTU MIREA, Russia) (Fig. 2).

The mixture of the fluorinated TMC was transferred to a corundum boat, placed in a tubular furnace heated to 600 $^{\circ}\text{C}$ and was kept for 5 h. To the outlet of the furnace, a desublimator was hermetically attached. This was a cooled fluoroplastic cup (100 mm in diameter and 300 mm in length) with an internal cooled coil made of a fluoroplastic tube (7 mm in diameter). Upon cooling, the mixture of sublimated titanium ammonium fluoride compounds desublimated again to form AHFT. As a result, the titanium component of TMC was separated from the ferrous component and distilled into the desublimator.

The kinetics of sublimation of the titanium product (containing mainly $(\text{NH}_4)_2\text{TiF}_6$) was studied in a setup (RTU MIREA, Russia) with continuous recording of changes in the weight of the sample. A 3-g AHFT sample in a platinum crucible was placed in a reactor preheated to a given temperature. The crucible diameter was 25 mm; the sublimation surface, 4.9 cm^2 ; the initial thickness of the bulk layer, 0.7 cm. After the completion of the experiment, the residue in the crucible was

weighed and the degree of sublimation was calculated. The average deviation in a series of four experiments was within 3%. The activation energy of the process was calculated according to the published procedure [13].

RESULTS AND DISCUSSION

Study of the fluorination of TMC with ammonium bifluoride

The interaction of ammonium bifluoride with TMC and chemical reactions (1–10) were studied by means of differential thermal analysis (DTA) in a derivatograph with a load of 8 mg of TMC and 24 mg of ammonium bifluoride (Fig. 3).

At temperatures of 103–109 $^{\circ}\text{C}$, the water of crystallization is evaporated from ammonium bifluoride. At 123 $^{\circ}\text{C}$, ammonium bifluoride melts; at 242 $^{\circ}\text{C}$, excess ammonium bifluoride disproportionates to ammonia and hydrogen fluoride. The further changes in the weight of the reacting mixture are characteristic of the sequential formation and destruction of ammonium fluoride complexes of titanium and iron. The latest changes in the TGA and DTA curves in the range 400–450 $^{\circ}\text{C}$ are due to the sublimation of the titanium component. The heat capacity of the system is most significantly affected by the melting and decomposition of ammonium bifluoride in the range 120–200 $^{\circ}\text{C}$, which occur with a total heat absorption of about 1 W/g of charge (300 kW/t of concentrate).

Ammonium bifluoride melts early in the process. This is accompanied by a decrease in the volume of the sample. However, at the same time, solid ammonium fluorometalates and gaseous reaction products begin to form, causing the

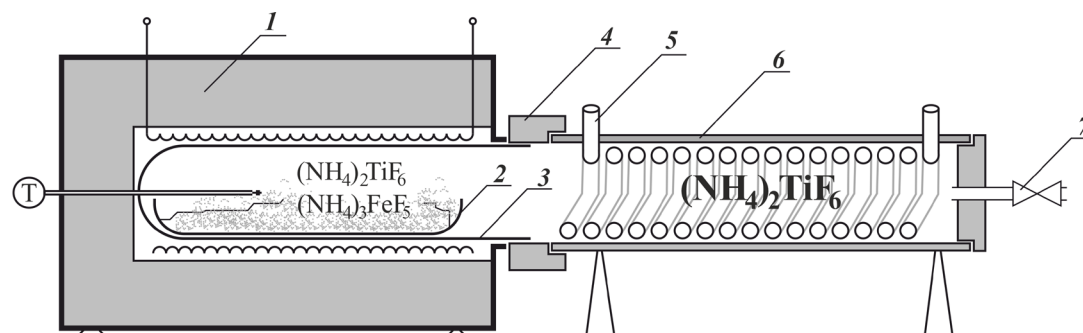


Fig. 2. Setup for separation of the titanium fraction from the ferrous fraction: (1) furnace, (2) boat with a mixture of fluorometallates (corundum or stainless steel), (3) corundum cup, (4) gypsum coupling, (5) water cooling jacket (fluoroplastic), (6) desublimator housing (fluoroplastic), and (7) outlet.

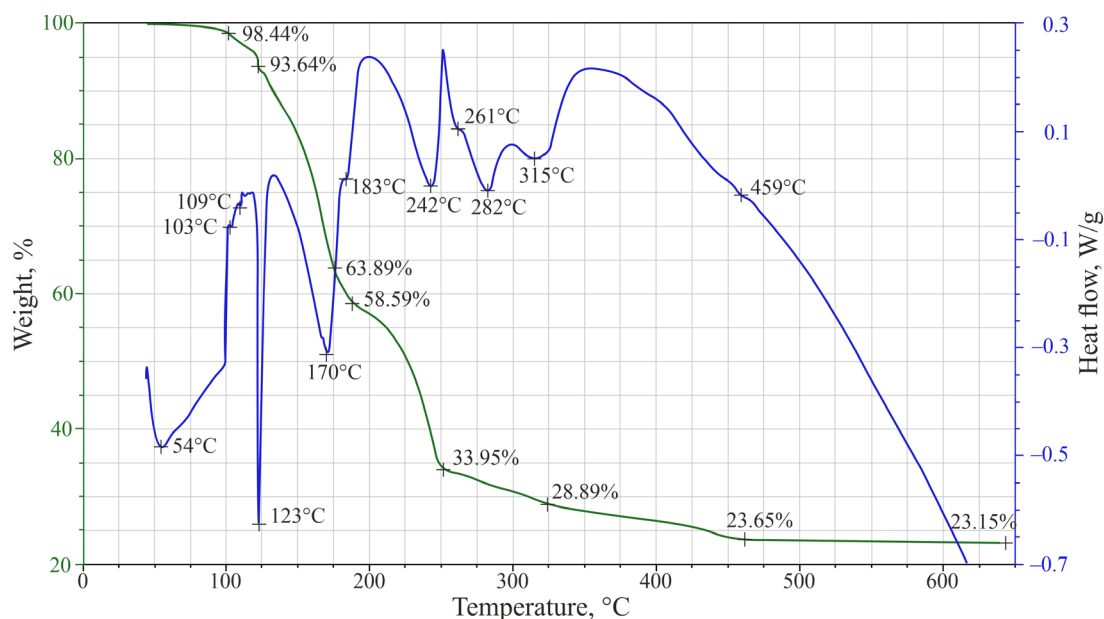


Fig. 3. DTA of the reacting mixture of TMC and ammonium bifluoride.

mixture to foam and leading to an increase in the volume of the sample. Filling the crucible to 80% ensures acceptable accuracy of weight measurements and calculation of observed thermal events, as well as the absence of errors due to sticking to the crucible lid or leakage of part of the reaction mixture.

The chemical composition of the reaction products $(\text{NH}_4)_2\text{TiF}_6$ and $(\text{NH}_4)_3\text{FeF}_6$ was confirmed by XRD (Fig. 4), showing complete agreement between the products and the reference samples. XRD did not detect an unreacted residue, indicating that the reaction had almost completed and the

concentration of the original ilmenite was below the level of determination by XRD, i.e., less than 2%.

The fluorinated mixture was calcined in an atmosphere of natural (undried) air. As expected, ammonium tetrafluoroferrate underwent pyrohydrolysis and was converted into iron(III) oxide which upon calcination transforms into magnetite. XRD (Fig. 5) confirmed the predominance of Fe_3O_4 in the calcined residue, and also detected an admixture of unreacted ilmenite, which fully confirms the occurrence of chemical reaction (4).

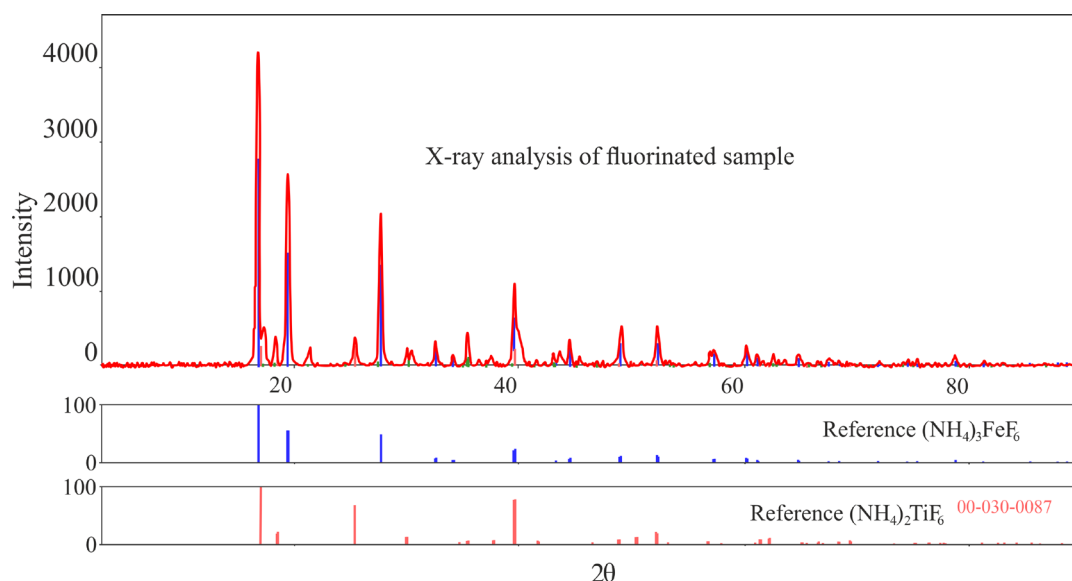


Fig. 4. XRD of the fluorinated sample.

Study of the separation of the titanium-containing fraction of AHFT

With regard to the technological development of the separation of the titanium component from the ilmenite fluorinated with ammonium fluorides, it was necessary to study the rate and completeness of AHFT sublimation. During the experiment, the weight of the residue was recorded and the degree of sublimation was calculated from it (Fig. 6).

The AHFT sublimation rate increases with increasing temperature. Above 650°C, the rate increases significantly, reaching 3.87 and 4.21 g/(h·cm²) at 650 and 700°C, respectively (Table 2). At 700°C, the degree of sublimation of AHFT reaches 85% within 10 min.

The experimental data on the kinetics of AHFT sublimation was mathematically processed using the Crank–Gistling–Brownstein equation.

The calculated activation energy is $E = 52336$ J/mol.

$$1 - \frac{2}{3}\alpha - (1 - \alpha)^{\frac{2}{3}} = 0.183 \cdot \tau \cdot \exp\left(-\frac{52336}{RT}\right).$$

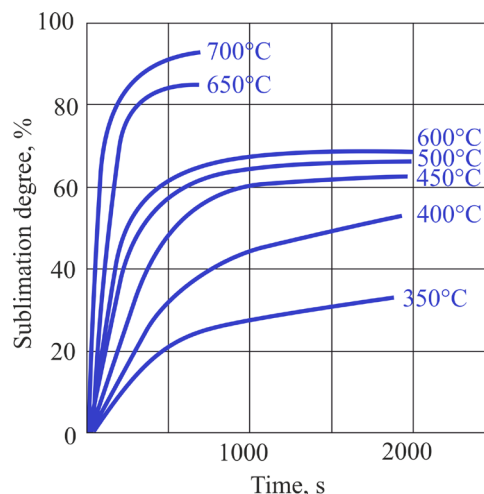


Fig. 6. Dependence of the sublimation degree on temperature and heating time.

The activation energy of the process is 52336 J/mol, indicating that the process is under kinetic (rather than diffusion) control. The process can be enhanced by increasing process temperature.

With a decrease in the AHFT sublimation temperature, the conversion in the pyrohydrolysis

Table 2. AHFT sublimation rate in the temperature range of 350–700°C

Temperature, °C	700	650	600	500	450	400	350
Sublimation rate, g/(h·cm ²)	4.21	3.87	1.55	1.27	0.50	0.31	0.12

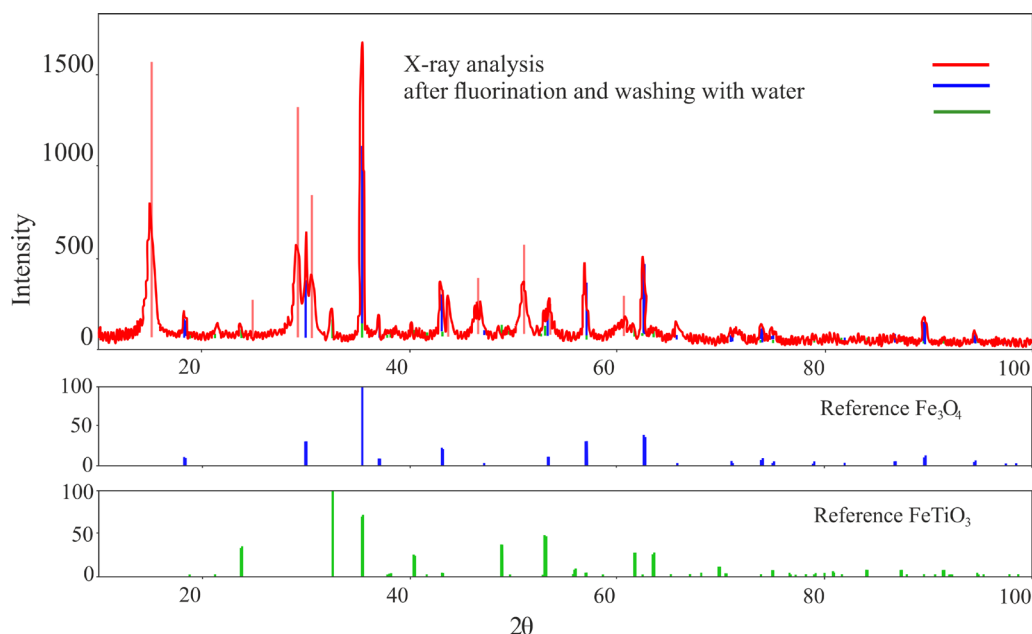
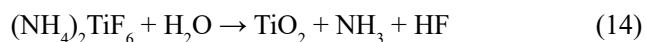


Fig. 5. XRD of the products after fluorination and calcination of the residue.

to form titanium oxide and gaseous products (NH_3 , HF) increases. This increases the loss of titanium in the form of TiO_2 in the residue after sublimation.



The degrees of pyrohydrolysis of AHFT at 650 and 700°C were 17 and 15%, respectively. The conversion and rate of sublimation of AHFT depend on non-linear time and behave differently in the three temperature ranges.

In the temperature range 350–450°C, the increase in the degree of pyrohydrolysis is at its maximum in the first five minutes after the start of the process. During this period of time, the weight loss is 20%. The further weight loss is described by a linear change in the weight of the sample, which characterizes the sublimation of AHFT.

In the temperature range 500–600°C, the sublimation is accompanied by the removal of the water of crystallization. Within 25 min, the weight loss is intense and a high degree of sublimation is achieved: 65 and 73% at 500 and 600°C, respectively.

In the temperature range 650–700°C, AHFT sublimates more intensely in comparison with the low-temperature ranges; the maximum degree of sublimation (83%) is achieved within the first 10 min.

According to previously proposed chemical reaction (1), the products should contain AHFT and

ammonium tetrafluoroferrate. In order to confirm this assumption, experiments were conducted with fluorination of ilmenite under various conditions. Table 3 presents fluorination conditions. These include: fluorination reagent (ammonium fluoride or bifluoride); fluorination temperature; number of fluorination operations (number of passes through the furnace); ratio of ilmenite and ammonium fluoride/bifluoride reagents; and reagent feed rate. Based on the results of ICP-MS chemical analysis of the unreacted ilmenite residue (from the contents of Ti, Fe, and silicon oxide impurity in the residue), the degrees of fluorination were determined (Table 3).

Study of the titanium-containing desublimates

The previously obtained sample of fluorinated TMC, a mixture of $(\text{NH}_4)_2\text{TiF}_6$ and $(\text{NH}_4)_3\text{FeF}_6$, was studied in a sublimation-desublimation apparatus (Fig. 2), in order to determine the quality of the desublimated titanium-containing product. ICP-MS chemical analysis of the desublimates showed minimum contents of impurity elements in the titanium-containing product isolated by sublimation-desublimation from the fluorinated ilmenite (Table 4).

XRD analysis of the desublimated titanium-containing product (Fig. 7) showed that it consists of a mixture of $(\text{NH}_4)_2\text{TiF}_6$, $(\text{NH}_4)_3\text{TiF}_7$, and NH_4TiF_5 . Chemical analysis showed that the titanium content in the desublimates (after with a single sublimation-desublimation cycle) is about 30.6%. The total amount of impurities (Fe, V, Si) is 0.45%,

Table 3. Process parameters and degrees of fluorination of TMC components

No.	Fluorination temperature, °C	Reagent	Time of reaction per operation (total time), min	Number of operations (number of passes through furnace)	Reagent ratio	Feed flow rate of mixture of reagents, g/h	Degree of fluorination, %		
							Ti	Fe	Fe
1	210	NH_4F	60 (240)	4	1:3	900	81	73	95
2	210	$\text{NH}_4\text{F} \cdot \text{HF}$	60 (120)	2	1:3	900	94	92	99
3	210	$\text{NH}_4\text{F} \cdot \text{HF}$	60 (120)	2	1:2.43	900	92	91	99

Table 4. Content of target components in the desublimates

Substance	Ti	Fe	V	Si	Al
Content, %	30.6	0.2	0.16	0.1	0.3

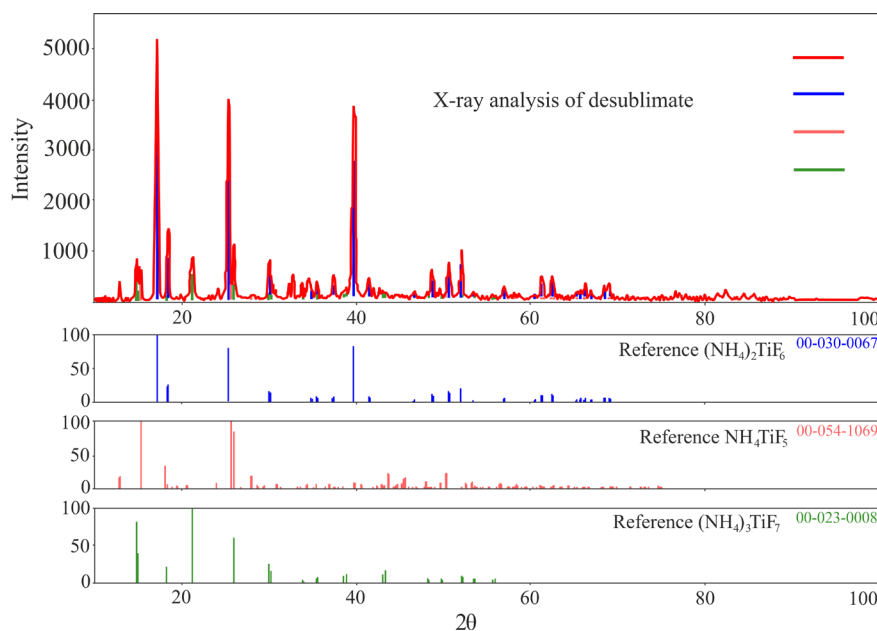


Fig. 7. XRD of the desublimated titanium-containing product.

including only 0.2% Fe. Redistillation of the product reduces the content of impurities in the ammonium fluorotitanate mixture to 0.1%.

Thus, XRF proved that the method of fluorination of TMC with ammonium bifluoride produced a high-purity titanium product: a mixture of ammonium fluorotitanates. The resulting intermediate product—a mixture of NH_4TiF_5 , $(\text{NH}_4)_2\text{TiF}_6$, and $(\text{NH}_4)_3\text{TiF}_7$ —is a valuable commercial product for the industrial production of titanium dioxide pigment from titanomagnetite concentrate and ilmenite.

CONCLUSIONS

The study of the fluorination of TMC by means of ammonium bifluoride followed by the separation of titanium and iron fractions allows us to draw the following conclusions:

(1) The general principles of fluorination of TMC by means of ammonium bifluoride are similar in process parameters to the fluorination of ilmenite.

(2) Chemical analysis and X-ray powder diffraction analysis have proven that the products of the fluorination of TMC with ammonium bifluoride are compounds $(\text{NH}_4)_2\text{TiF}_6$ and $(\text{NH}_4)_2\text{FeF}_4$.

(3) The residue after the fluorination of TMC mainly consists of Fe_2O_3 with an iron content of 40.2% and impurities of unreacted TMC and ilmenite, containing up to 1.1% titanium. This confirms the almost complete fluorination of TMC.

(4) The AHFT sublimation rate increases with increasing temperature, and above 650°C, the rate increases significantly, reaching 3.87 and 4.21 g/(h·cm²) at 650 and 700°C, respectively. At 700°C, the degree of sublimation of AHFT reaches 85% within 10 min.

(5) The titanium-containing fraction separated by sublimation undergoes desublimation. XRD determined that the desublimite consists of a mixture of $(\text{NH}_4)_2\text{TiF}_6$, $(\text{NH}_4)_3\text{TiF}_7$, and NH_4TiF_5 . Chemical analysis showed that the titanium content in the desublimite (after a single sublimation–desublimation cycle) is about 30.6%. The total amount of impurities (Fe, V, Si) is 0.45%, of which 0.2% Fe. Redistillation of the product reduces the amount of impurities in the ammonium fluorotitanate mixture to 0.1%.

(6) The resulting high-purity titanium product (a mixture of ammonium fluorotitanates) is a valuable commercial product for the industrial production of titanium dioxide pigment from titanomagnetite concentrate and ilmenite.

Acknowledgments

This work was conducted using the equipment of the RTU MIREA Center for Collective Use and supported by the Ministry of Education and Science of Russia (Agreement No. 075-15-2021-689 dated September 01, 2021, unique identification number 2296.61321X0010).

The author declares no conflicts of interest.

REFERENCES

1. Dyachenko A.N., Dyachenko E.N., Kraidenko R.I. Titanium dioxide: market, production, new technologies. *Lakokrasochnye materialy i ikh primeneniye* = *Russ. Coating J.* 2021;(7–8):41–50 (in Russ.).
2. Fomina N.N., Ismagilov A.R., Fomin V.G. Titanium pigment dioxide dispersity. *Stroitel'stvo i rekonstruktsiya* = *Building and Reconstruction*. 2020;(2):136–142 (in Russ.).
3. Pavlunenko L.E., Guba L.N. Characterization of the properties of titanium pigments for paints and varnishes. *Stroitel'stvo i tekhnogennaya bezopasnost'* = *Construction and Industrial Safety*. 2013;(46):56–62 (in Russ.).
4. Rakov E.G., Mel'nichenko E.I. The Properties and Reactions of Ammonium Fluorides. *Russ. Chem. Rev.* 1984;53(9):851–869. <https://doi.org/10.1070/rc1984v053n09abeh003126>
[Original Russian Text: Rakov E.G., Mel'nichenko E.I. The Properties and Reactions of Ammonium Fluorides. *Uspekhi Khimii*. 1984;53(9):1463–1492 (in Russ.).]
5. Dyachenko A.N. *Method for Producing Titanium Dioxide from Ilmenite*: RF Pat. 2770576. Publ. 04.18.2022.
6. Kraidenko R.I., Kantaev A.S., Lashur A.L. *Method for Obtaining Titanium Dioxide of Rutile Modification*: RF Pat. 2643555. Publ. 02.02.2018.
7. Dmitriev A.N., Smorokov A.A., Kantaev A.S., Nikitin D.S., Vit'kina G.Yu. Fluoroammonium method of titanium slag processing. *Izvestiya vuzov. Chernaya metallurgiya* = *Izvestiya. Ferrous Metallurgy*. 2021;64(3):178–183 (in Russ.). <https://doi.org/10.17073/0368-0797-2021-3-178-183>
8. Smorokov A.A., Kantaev A.S., Bryankin D.V., Miklashevich A.A. Development of a low-temperature desilicization method for the leucoxene concentrate of the Yarega deposit with a solution of ammonium hydrogen fluoride. *Izv. Vyssh. Uchebn. Zaved. Khim. Khim. Tekhnol.* = *ChemChemTech*. 2022;65(2):127–133 (in Russ.). <https://doi.org/10.6060/ivkkt.20226502.6551>
9. Gordienko, P.S., Pashnina, E.V., Bulanov, S.B., et al. Preparation of Titanium Dioxide from the Ammonium Hexafluorotitanate–Silicon Dioxide System. *Theor. Found. Chem. Eng.* 2022;56(5):819–829. <https://doi.org/10.1134/S0040579522050062>
[Original Russian Text: Gordienko P.S., Pashnina E.V., Bulanov S.B., Dostovalov D.V., Kuryavyy V.G., Shabalin I.A., Karabtsov A.A. Khimicheskaya tekhnologiya. Production of titanium dioxide from the ammonium hexafluorotitanate – silicon dioxide system. *Khimicheskaya Tekhnologiya*. 2021;22(12):530–542 (in Russ.).]
10. Mel'nichenko E.I., Epov D.G., Krysenko G.F. Ammonium oxofluorotitanates. *Russ. J. Inorg. Chem.* 2002;47(2):155–158.
11. Mel'nichenko E.I., Krysenko G.F., Epov D.G., Rakov E.G. Titanium oxyfluorides. *Russ. J. Inorg. Chem.* 2001;46(12):1769–1774.
12. Laptash N.M., Maslennikova I.G. Fluoride processing of titanium-containing minerals. *Adv. Mater. Phys. Chem.* 2013;2(4):21–24. <http://dx.doi.org/10.4236/ampc.2012.24B006>
13. Habashi F. *Kinetics of Metallurgical Processes*. Sainte Foy, Québec City: Métallurgie Extractive Québec, distributed by Laval University Bookstore; 1999. ISBN 2-980-3247-6-0. URL: https://works.bepress.com/fathi_habashi/5/. Accessed October 10, 2023.

СПИСОК ЛИТЕРАТУРЫ

1. Дьяченко А.Н., Дьяченко Е.Н., Крайденко Р.И. Диоксид титана: рынок, производство, новые технологии. *Лакокрасочные материалы и их применение*. 2021;(7–8):41–50.
2. Фомина Н.Н., Исмагилов А.В., Фомин В.Г. Дисперсность пигментного диоксида титана. *Строительство и реконструкция*. 2020;88(2):136–142.
3. Павлуненко Л.Е., Губа Л.Н. Характеристика свойств титановых пигментов для лакокрасочных материалов. *Строительство и техногенная безопасность*. 2013;(46):56–62.
4. Раков Э.Г., Мельниченко Е.И. Свойства и реакции фторидов аммония. *Успехи химии*. 1984;53(9):1463–1492.
5. Дьяченко А.Н. *Способ получения диоксида титана из ильменита*: Пат. 2770576 РФ. Заявка № 2021121156; заявл. 17.07.2021; опубл. 18.04.2022.
6. Крайденко Р.И., Кантаев А.С., Лаштур А.Л. *Способ получения диоксида титана рутильной модификации*: Пат. 2643555 РФ. Заявка № 2017100238; заявл. 09.01.2017; опубл. 02.02.2018.
7. Дмитриев А.Н., Смороков А.А., Кантаев А.С., Никитин Д.С., Витькина Г.Ю. Фтороаммонийный способ переработки титановых шлаков. *Известия вузов. Черная металлургия*. 2021;64(3):178–183. <https://doi.org/10.17073/0368-0797-2021-3-178-183>
8. Смороков А.А., Кантаев А.С., Брянкин Д.В., Миклашевич А.А. Разработка способа низкотемпературного обескремнивания лекоксенового концентрата Ярегского месторождения раствором гидрофторида аммония. *Известия вузов. Химия и химическая технология*. 2022;65(2):127–133. <https://doi.org/10.6060/ivkkt.20226502.6551>
9. Гордиенко П.С., Пашнина Е.В., Буланова С.Б., Достовалов Д.В., Курявый В.Г., Шабалин И.А., Карабцов А.А. Получение диоксида титана из системы аммония гексафторотитанат – диоксид кремния. *Хим. технология*. 2021;22(12):530–542. <https://doi.org/10.31044/1684-5811-2021-22-12-530-542>
10. Mel'nichenko E.I., Epov D.G., Krysenko G.F. Ammonium oxofluorotitanates. *Russ. J. Inorg. Chem.* 2002;47(2):155–158.
11. Mel'nichenko E.I., Krysenko G.F., Epov D.G., Rakov E.G. Titanium oxyfluorides. *Russ. J. Inorg. Chem.* 2001;46(12):1769–1774.
12. Laptash N.M., Maslennikova I.G. Fluoride processing of titanium-containing minerals. *Adv. Mater. Phys. Chem.* 2013;2(4):21–24. <http://doi.org/10.4236/ampc.2012.24B006>
13. Habashi F. *Kinetics of Metallurgical Processes*. Sainte Foy, Québec City: Métallurgie Extractive Québec, distributed by Laval University Bookstore; 1999. ISBN 2-980-3247-6-0. URL: https://works.bepress.com/fathi_habashi/5/. Дата обращения 10.10.2023.

About the author:

Alexander N. Dyachenko, Dr. Sci. (Eng.), Professor, Head of the K.A. Bol'shakov Department of Chemistry and Technology Rare Elements, M.V. Lomonosov Institute of Fine Chemical Technologies, MIREA – Russian Technological University (86, Vernadskogo pr., Moscow, 119571, Russia). E-mail: dyachenko@mirea.ru. Scopus Author ID 7006148917, RSCI SPIN-code 7929-7127, <https://orcid.org/0000-0003-3490-4713>

Об авторе:

Дьяченко Александр Николаевич, д.т.н., профессор, заведующий кафедрой химии и технологии редких элементов им. К.А. Большакова, Институт тонких химических технологий им. М.В. Ломоносова, ФГБОУ ВО «МИРЭА – Российский технологический университет» (119571, Россия, Москва, пр-т Вернадского, д. 86). E-mail: dyachenko@mirea.ru. Scopus Author ID 7006148917, SPIN-код РИНЦ 7929-7127, <https://orcid.org/0000-0003-3490-4713>

The article was submitted: January 24, 2023; approved after reviewing: March 27, 2023; accepted for publication: November 16, 2023.

*Translated from Russian into English by V. Glyanchenko
Edited for English language and spelling by Dr. David Mossop*

ISSN 2686-7575 (Online)

<https://doi.org/10.32362/2410-6593-2023-18-6-583-594>



UDC 546.6

RESEARCH ARTICLE

Coordination compounds of indium, gadolinium, and erbium nitrates with low urea content

Elena V. Savinkina^{1,✉}, Igor A. Karavaev¹, Elizaveta K. Bettels¹, Grigorii A. Buzanov², Aleksei S. Kubasov²

¹MIREA – Russian Technological University (M.V. Lomonosov Institute of Fine Chemical Technologies), Moscow, 119571 Russia

²Kurnakov Institute of General and Inorganic Chemistry, Russian Academy of Sciences, Moscow, 119991 Russia

✉ Corresponding author, e-mail: savinkina@mirea.ru

Abstract

Objectives. To date, compounds of rare earth nitrates with urea in a ratio of 1:4 and indium in a ratio of 1:6 have been synthesized and structurally characterized. However, there is a lack of research into similar compounds having a lower urea content. The purpose of this work was to continue the search for regularities of structure formation for complexes of various elements with urea.

Methods. Novel coordination compounds were synthesized and characterized by powder- and single-crystal X-ray diffraction analysis, as well as infrared spectroscopy.

Results. The interaction of indium, gadolinium and erbium nitrates with urea (Ur) in an aqueous solution under conditions of ligand deficiency produces the previously unknown coordination compounds $\text{cis-[In(Ur)}_4\text{(NO}_3\text{)}_2\text{]NO}_3$, $[\text{Gd(H}_2\text{O)}_2\text{(Ur)}_2\text{(NO}_3\text{)}_3]$, and $[\text{Er(H}_2\text{O)}_2\text{(Ur)(NO}_3\text{)}_3]$. The indium complex is shown to have an ionic structure, whereas the gadolinium and erbium

complexes have a molecular structure. In the indium complex, the coordination number is 6; the cation has an octahedral structure; it involves two cis-arrange monodentate nitrate groups and four monodentate urea molecules. The coordination number of gadolinium is 10; here, the coordination polyhedron is a distorted pentagonal bipyramid at the vertices of which there are two water molecules, while in the internal polygonal base there are two monodentate urea molecules and three bidentate chelating nitrate groups oriented perpendicular to the polygonal base of the bipyramid. The coordination number of erbium is 9; the coordination polyhedron is a distorted tricapped trigonal prism.

Conclusions. In contrast with the gadolinium complex, one urea molecule is coordinated in the erbium complex instead of two, decreasing the coordination number from 10 to 9. In the indium complex cation, the coordination number is 6; unlike the gadolinium and erbium complexes, the cation does not contain water, and the nitrate groups are monodentate.

Keywords: indium nitrate, gadolinium nitrate, erbium nitrate, urea, complexes, crystal structure, X-ray diffraction analysis

For citation: Savinkina E.V., Karavaev I.A., Bettels E.K., Buzanov G.A., Kubasov A.S. Coordination compounds of indium, gadolinium, and erbium nitrates with low urea content. *Tonk. Khim. Tekhnol. = Fine Chem. Technol.* 2023;18(6):583–594. <https://doi.org/10.32362/2410-6593-2023-18-6-583-594>

НАУЧНАЯ СТАТЬЯ

Координационные соединения нитратов индия, гадолиния и эрбия с низким содержанием мочевины

Е.В. Савинкина^{1,✉}, И.А. Караваев¹, Е.К. Беттельс¹, Г.А. Бузанов²,
А.С. Кубасов²

¹МИРЭА – Российский технологический университет (Институт тонких химических технологий им. М.В. Ломоносова), Москва, 119571 Россия

²Институт общей и неорганической химии им. Н.С. Курнакова Российской академии наук, Москва, 119991 Россия

✉ Corresponding author, e-mail: savinkina@mirea.ru

Аннотация

Цели. В настоящее время синтезированы и структурно охарактеризованы соединения нитратов редкоземельных элементов с мочевиной в соотношении 1:4 и индия — в соотношении 1:6, однако практически не изучены подобные соединения с меньшим содержанием мочевины. Целью настоящей работы является продолжение поиска закономерностей образования и строения комплексов различных элементов с мочевиной.

Методы. Новые координационные соединения синтезированы и охарактеризованы методами рентгенофазового анализа, инфракрасной спектроскопии и рентгеноструктурного анализа.

Результаты. Взаимодействие нитратов гадолиния и эрбия с карбамидом (мочевиной, Ur) в водном растворе в условиях недостатка лиганда приводит к образованию ранее неизвестных координационных соединений $\text{cis-[In(Ur)}_4(\text{NO}_3)_2]\text{NO}_3$, $[\text{Gd}(\text{H}_2\text{O})_2(\text{Ur})_2(\text{NO}_3)_3]$ и $[\text{Er}(\text{H}_2\text{O})_2(\text{Ur})(\text{NO}_3)_3]$. Показано, что комплекс индия имеет ионное, а комплексы гадолиния и эрбия — молекулярное строение. Координационное число индия равно 6; комплексный катион имеет октаэдрическое строение с *цис*-расположением двух монодентатных нитратных групп. Вершины октаэдра заняты атомами кислорода четырех

монодентатных молекул карбамида. Координационное число гадолиния равно 10, координационный полиэдр можно представить как искаженную пентагональную пирамиду, в вершинах которой расположены две молекулы воды, а в плоскости — две мондентатные молекулы мочевины и три бидентатно-хелатирующие нитратные группы, ориентированные перпендикулярно плоскости бипирамиды. Координационное число эрбия равно 9, координационный полиэдр — искаженная трехшапочная тригональная призма.

Выводы. При переходе от гадолиния к эрбию наблюдается координация одной молекулы мочевины вместо двух, координационное число уменьшается от 10 до 9. В комплексе индия координационное число равно шести; в отличие от комплексов гадолиния и эрбия комплексный катион не содержит воды, а нитратные группы являются не бидентатными, а монодентатными.

Ключевые слова: нитрат индия, нитрат гадолиния, нитрат эрбия, карбамид, комплексы, кристаллическая структура, рентгеноструктурный анализ

Для цитирования: Савинкина Е.В., Караваев И.А., Беттельс Е.К., Бузанов Г.А., Кубасов А.С. Координационные соединения нитратов индия, гадолиния и эрбия с низким содержанием мочевины. *Тонкие химические технологии*. 2023;18(6):583–594. <https://doi.org/10.32362/2410-6593-2023-18-6-583-594>

INTRODUCTION

Complexes of nitrates of various elements with urea are attracting attention in the context of the development of self-propagating high-temperature synthesis (SHS) methods, in particular, the solution combustion synthesis (SCS) method. The SCS method has been successfully used to obtain a wide range of functional materials, whose components or precursors are oxides, sulfides, nitrides, and silicates of metals [1–6] in nanosized states.

According to this method, nitrates serve as oxidizing agents, while urea (Ur , $\text{CH}_4\text{N}_2\text{O}$) is a fuel. Under conditions of synthesis from solution, complex compounds of the corresponding metal cations with urea should be formed as intermediate compounds, whose compositions should vary according to the nitrate/urea ratio. A study of rare earth element (REE) nitrate–urea–water ternary systems showed that, in

most cases, several compounds with REE nitrate/urea ratios from 1:1 to 1:7 crystallize in each system [7]. In particular, in systems involving gadolinium and erbium compounds at 30°C, compounds $\text{Gd}(\text{NO}_3)_3 \cdot 4\text{Ur}$, $\text{Gd}(\text{NO}_3)_2 \cdot 2\text{Ur}$ [8], $\text{Er}(\text{NO}_3)_3 \cdot 4\text{Ur}$, $\text{Er}(\text{NO}_3)_3 \cdot 3\text{Ur} \cdot 2\text{H}_2\text{O}$ were reported to be formed [9]. Compounds with a REE nitrate/urea ratio of 1:4 for these elements, as well as those for the entire series of REEs, were isolated and structurally characterized [10–12]. Their compositions, which turned out to include water, have the coordination formula $[\text{Ln}(\text{H}_2\text{O})_2(\text{Ur})_4(\text{NO}_3)_2]\text{NO}_3$ ($\text{Ln} = \text{Gd}, \text{Er}$). For indium, an 1:6 complex $[\text{In}(\text{Ur})_6](\text{NO}_3)_3$ was described, which was used as a precursor for the SHS preparation of gallium indium zinc oxide [13]. When using complexes with a high urea content under SCS conditions, complete oxidation of all urea by the reduction of nitrate ions may not be achieved [14]. In this regard, a question arose

concerning the possibility of forming complexes containing a lower urea content. The aim of this work was to continue the search for patterns of formation and structure of metal complexes with urea, namely, the isolation and structural study of complexes of indium-, gadolinium-, and erbium nitrates having a low urea content.

EXPERIMENTAL

In the work, we used urea (special purity grade, *REAKhIM*, Russia), as well as $\text{In}(\text{NO}_3)_3 \cdot 5\text{H}_2\text{O}$, $\text{Gd}(\text{NO}_3)_3 \cdot 5\text{H}_2\text{O}$, and $\text{Er}(\text{NO}_3)_3 \cdot 4\text{H}_2\text{O}$, which were obtained by dissolving the corresponding carbonates (reagent grade, *REAKhIM*) in concentrated nitric acid (special purity grade), followed by concentrating the solution until the formation of crystals.

Compounds $[\text{Gd}(\text{H}_2\text{O})_2(\text{Ur})_2(\text{NO}_3)_3]$ (**I**), $[\text{Er}(\text{H}_2\text{O})_2(\text{Ur})(\text{NO}_3)_3]$ (**II**), and $[\text{In}(\text{Ur})_4(\text{NO}_3)_2]\text{NO}_3$ (**III**) were synthesized by reacting the corresponding nitrates with urea in ratios from 1:1 to 1:3 in acetonitrile at 30–40°C. After 6 days, crystals formed, which were separated from the mother liquor and dried. The yield was 65–70%.

The contents of C, H, and N in the produced compounds were determined with a CHNS Flash EA 1112 elemental analyzer (*Thermo Finnigan*, Italy) at the Center for Shared Use,

MIREA – Russian Technological University, Moscow, Russia. The indium content in compound **III** was determined by inductively coupled plasma atomic emission spectroscopy (ICP-MS) with an iCAP 6300 Duo spectrometer (*Thermo Fisher Scientific*, USA) at the Center for Shared Use, Kurchatov Institute National Research Center—IREA, Moscow, Russia. The gadolinium and erbium contents were determined by complexometric titration.

The phase purity of compounds **I–III** was confirmed by X-ray powder diffraction analysis. X-ray powder diffraction patterns were recorded with a Bruker D8 ADVANCE X-ray diffractometer (*Bruker*, Germany: radiation — CuK_α ; filter — Ni; detector — LYNXEYE; reflection geometry — $2\theta = 5^\circ\text{--}50^\circ$; scan step size — 0.01125° ; signal accumulation time — 0.25 s) at the Research Equipment Sharing Center of Physical Methods for Studying Substances and Materials, Kurnakov Institute of General and Inorganic Chemistry, Russian Academy of Sciences (IGIC RAS), Moscow, Russia. Since the prepared complexes are sensitive to air components, the diffraction patterns were recorded using fluoroplastic cells with clamp rings for holding a 7.6- μm -thick Capton protective polyimide film for X-ray studies (*Safetystep*, Russia). Sample preparation was carried out in a SPEKS GB22M sealed glove box (*Spectroscopicheskie sistemy*, Russia) with a residual water vapor content of no more than 10 ppm.

Table 1. Elemental analysis of complexes **I**, **II**, and **III**

Complex	Elemental content, %			
I	C	H	N	Gd
Found	5.00	2.35	19.80	31.66
Calculated	4.81	2.20	19.62	31.48
II	C	H	N	Er
Found	2.93	2.01	15.73	37.43
Calculated	2.67	1.79	15.59	37.22
III	C	H	N	In
Found	8.65	3.16	26.14	21.33
Calculated	8.87	2.96	25.87	21.23

Infrared (IR) spectroscopic studies were performed with an FSM 2201 FTIR spectrometer (*Infraspek*, Russia; 4000–500 cm^{-1} , KBr pellets, 25°C). The error in measuring the frequencies of absorption bands was no more than 3–4 cm^{-1} .

Single-crystal X-ray diffraction analysis of the complexes **I**, **II**, and **III** was performed with a Bruker SMART APEX II diffractometer (*Bruker*, Germany; graphite monochromator, MoK_α radiation) at IGIC RAS. The unit cell parameters were refined over the whole dataset. The experimental intensities were corrected for absorption using SADABS program [Sheldrick G.M., *SADABS*, Madison, Wisconsin, USA: Bruker AXS, 2008]. The structure was solved by a direct method (SHELXS97) and refined by the full-matrix least squares method (SHELXL-2018/3) using all data in the anisotropic approximation for all non-hydrogen atoms. The H atoms of the water molecule were localized by difference Fourier synthesis and refined without any constraints. The H atoms of NH_2 groups were introduced in geometrically calculated positions with thermal parameters $U_{\text{H}} = 1.2U_{\text{eq}}(\text{N})$, where $U_{\text{eq}}(\text{N})$ are the equivalent isotropic thermal parameters of nitrogen atoms.

RESULTS AND DISCUSSION

The coordination compounds of indium, gadolinium, and erbium nitrates with urea were synthesized at metal/ligand molar ratios from 1:1 to 1:3. These ratios were chosen from the data of the solubility diagrams of the $\text{M}(\text{NO}_3)_3\text{--Ur--H}_2\text{O}$ systems [7–9]. Compounds having metal/ligand ratios of 1:4, 1:2, and 1:1 for indium, gadolinium, and erbium, respectively, were isolated from saturated aqueous solutions. The complex compounds of gadolinium and erbium, which additionally included water, had the coordination formulas $[\text{Gd}(\text{H}_2\text{O})_2(\text{Ur})_2(\text{NO}_3)_3]$ (**I**) and $[\text{Er}(\text{H}_2\text{O})_2(\text{Ur})(\text{NO}_3)_3]$ (**II**). The indium complex was anhydrous: $[\text{In}(\text{Ur})_4(\text{NO}_3)_2]\text{NO}_3$ (**III**).

The IR spectroscopy study confirmed the presence of coordinated water molecules in the gadolinium and erbium complexes: broad bands are observed in the range of 3500–3200 cm^{-1} . The broadening of these absorption bands was explained by the formation of a developed system of hydrogen bonds. It was shown that, in complexes **I–III**, the urea molecule is coordinated through the donor oxygen atom of the carbonyl group, as evidenced by the shift of the amide I stretching vibrations ($\nu(\text{CO})$ 1641–1654 cm^{-1}) toward longer wavelengths in comparison with free urea (1675 cm^{-1}). The coordination of nitrate ions

as bidentate cyclic ligands in complexes **I** and **II** was confirmed by the absorption bands at 1490 ($\nu(\text{N--O})$), 1353 ($\nu_{\text{as}}(\text{NO}_2)$), 1041 ($\nu_{\text{s}}(\text{NO}_2)$), and 805 ($\pi(\text{NO}_3)$) cm^{-1} [15]. Complex **III** contains both monodentate coordinated and non-coordinated nitrate ions, which results in the splitting of the absorption bands of nitrate groups: 1498 and 1453 ($\nu(\text{N--O})$), 1389 and 1287 ($\nu_{\text{as}}(\text{NO}_2)$), 1151 and 1033 ($\nu_{\text{s}}(\text{NO}_2)$), and 824 and 800 ($\pi(\text{NO}_3)$) cm^{-1} .

The X-ray powder diffraction analysis confirmed the formation of new compounds in the $\text{M}(\text{NO}_3)_3\text{--Ur--H}_2\text{O}$ systems, where $\text{M} = \text{Er, Gd, In}$ (Fig. 1). Reflections of the initial compounds are not found in the presented diffraction patterns of complex compounds. In addition, the X-ray powder diffraction analysis confirmed that the obtained compounds are not isostructural to each other.

The crystal and molecular structures of the obtained compounds were determined by the single-crystal X-ray diffraction analysis. Table 2 presents the crystallographic characteristics of the complexes.

Table 3 summarizes the bond lengths and bond angles in the presented complexes.

The gadolinium complex $[\text{Gd}(\text{H}_2\text{O})_2(\text{Ur})_2(\text{NO}_3)_3]$ (**I**) is isostructural to the previously described praseodymium compound $[\text{Pr}(\text{H}_2\text{O})_2(\text{Ur})_2(\text{NO}_3)_3]$ [12]. It has a molecular structure; two water molecules, two urea molecules, and three nitrate ions are bound to the central ion. Water molecules and urea molecules in this compound are monodentate ligands and are coordinated to the central atom through donor oxygen atoms, and nitrate groups are bidentate

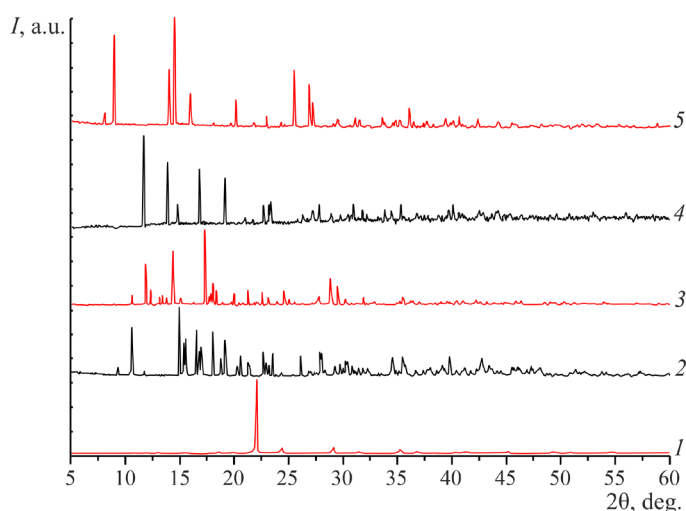


Fig. 1. X-ray powder diffraction patterns of (1) Ur, (2) $\text{Er}(\text{NO}_3)_3 \cdot 4\text{H}_2\text{O}$, (3) $[\text{Er}(\text{H}_2\text{O})_2(\text{Ur})(\text{NO}_3)_3]$, (4) $[\text{Gd}(\text{H}_2\text{O})_2(\text{Ur})_2(\text{NO}_3)_3]$, and (5) $[\text{In}(\text{Ur})_4(\text{NO}_3)_2]\text{NO}_3$.

Table 2. Crystallographic characteristics, details of the X-ray diffraction experiment, and refinement of structures **I–III**

Parameters	I	II	III
Empirical formula	C ₂ H ₁₂ GdN ₇ O ₁₃	CH ₈ ErN ₅ O ₁₂	C ₄ H ₁₆ InN ₁₁ O ₁₃
<i>M</i>	499.44	449.38	541.10
Crystal system	monoclinic	monoclinic	monoclinic
Space group	<i>C2/c</i>	<i>P2₁/n</i>	<i>C2/c</i>
Unit cell parameters:			
<i>a</i> , Å	10.685(6)	7.756(4)	11.232(2)
<i>b</i> , Å	8.756(4)	10.265(5)	21.869(4)
<i>c</i> , Å	15.367(8)	14.449(7)	7.341(2)
β, °	97.34(3)	98.33(3)	99.44(3)
<i>V</i> , Å ³	1425.8(13)	1138.2(9)	1778.7(7)
<i>Z</i>	4	4	4
Temperature <i>T</i> , K	150	150	100
Density ρ, g/cm ³	2.327	2.622	2.021
Number of independent reflections	2073	3304	1864
Goodness of fit	1.131	1.087	1.235
<i>R</i> ₁ / <i>wR</i> ₂ [<i>I</i> ≥ 2σ(<i>I</i>)]	0.0544/0.0553	0.0492/0.0517	0.1012/0.0995

Note: *a*, *b*, *c* are the lengths of the edges of the unit cell; β is the angle between the edges of the unit cell; *V* is the volume of the unit cell; *Z* is the number of formula units per unit cell; and *R* is the reliability factor.

chelating ligands. Thus, the coordination number of the central ion is 10. If all nitrate ions are represented as points, then the coordination polyhedron can be described as a distorted pentagonal bipyramid with water molecules in the axial position (Fig. 2). The gadolinium atom lies in the plane of the internal polygonal base formed by the nitrogen atoms of the nitrate ligands. The planar nitrate groups are oriented perpendicular to the polygon base. The almost planar urea molecules are turned about the polygon base at an angle of 44.60°, while the angle between their planes is 86.06°.

The somewhat shorter metal–oxygen bonds in **I** than those in the similar praseodymium compound are due to the decrease in the radius of the central atom.

In the erbium complex [Er(H₂O)₂(Ur)(NO₃)₃] (**II**), the erbium/urea ratio is 1:1. This is the first example of a structurally characterized complex compound of rare earth nitrate with urea of such composition. This complex, as complex **I**, has a molecular structure.

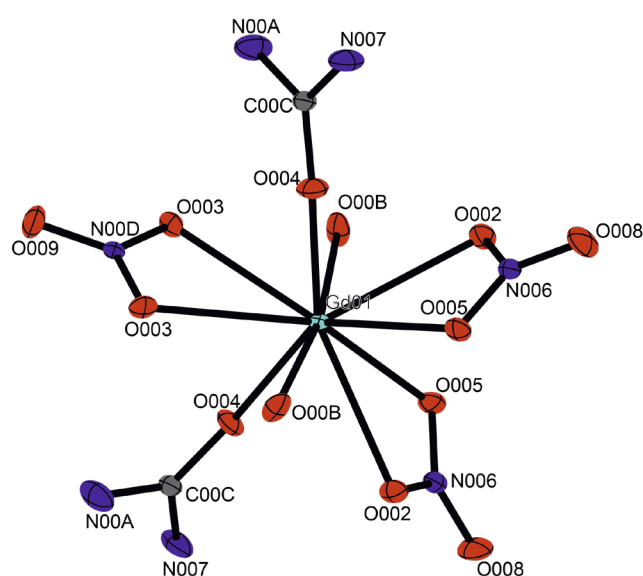
**Fig. 2.** Structure of [Gd(H₂O)₂(Ur)₂(NO₃)₃] (**I**).

Table 3. Bond lengths and bond angles in complexes I–III

Bond length, Å	Bond angle, °	Torsion angle, °
I		
Gd01 O002 2.6482(19)	O002 Gd01 O002 93.38(9)	Gd01 O002 N006 O005 7.5(2)
Gd01 O003 2.665(2)	O002 Gd01 O003 144.46(6)	Gd01 O002 N006 O008 –171.9(2)
Gd01 O004 2.283(2)	O002 Gd01 O003 116.17(6)	Gd01 O003 N00D O003 –0.002(0)
Gd01 O005 2.513(2)	O003 Gd01 O003 47.72(8)	Gd01 O003 N00D O009 180.000(0)
Gd01 O00B 2.411(2)	O004 Gd01 O002 71.21(7)	Gd01 O004 C00C N007 –151.7(3)
	O004 Gd01 O002 138.39(6)	Gd01 O004 C00C N00A 29.7(5)
	O004 Gd01 O003 73.50(6)	Gd01 O005 N006 O002 –8.0(2)
	O004 Gd01 O003 73.55(6)	Gd01 O005 N006 O008 171.4(2)
	O004 Gd01 O004 143.86(10)	
	O004 Gd01 O005 74.34(7)	
	O004 Gd01 O005 137.95(6)	
	O004 Gd01 O00B 87.42(8)	
	O004 Gd01 O00B 90.07(8)	
	O005 Gd01 O002 49.32(6)	
	O005 Gd01 O002 66.85(7)	
	O005 Gd01 O003 123.17(6)	
	O005 Gd01 O003 147.80(6)	
	O005 Gd01 O005 80.76(9)	
	O00B Gd01 O002 119.66(7)	
	O00B Gd01 O002 66.55(7)	
	O00B Gd01 O003 62.10(6)	
	O00B Gd01 O003 109.81(6)	
	O00B Gd01 O005 115.77(6)	
	O00B Gd01 O005 70.90(7)	
	O00B Gd01 O00B 171.91(9)	
II		
Er01 O003 2.462(3)	O003 Er01 O00A 143.26(8)	Er01 O003 N008 O004 179.1(3)
Er01 O005 2.341(3)	O003 Er01 O00G 106.50(9)	Er01 O003 N008 O007 –1.5(3)
Er01 O006 2.400(3)	O005 Er01 O003 72.67(9)	Er01 O007 N008 O003 1.5(3)
Er01 O007 2.422(3)	O005 Er01 O006 78.83(10)	Er01 O007 N008 O004 –179.1(3)
Er01 O00A 2.478(3)	O005 Er01 O007 125.19(8)	Er01 O00B N00E O009 –169.0(3)
Er01 O00B 2.393(3)	O005 Er01 O00A 79.57(9)	Er01 O00B N00E O00G 10.6(3)
Er01 O00D 2.198(2)	O005 Er01 O00B 76.14(9)	Er01 O00D C00I N00F 8.0(7)
Er01 O00G 2.585(3)	O005 Er01 O00G 121.81(9)	Er01 O00D C00I N00J –172.3(3)

Table 3. Continued

Bond length, Å	Bond angle, °	Torsion angle, °
II		
Er01 O00H 2.293(2)	O006 Er01 O003 139.70(9)	
	O006 Er01 O007 143.24(9)	
	O006 Er01 O00A 52.20(9)	
	O006 Er01 O00G 65.83(9)	
	O007 Er01 O003 52.54(8)	
	O007 Er01 O003 52.54(8)	
	O007 Er01 O00G 77.46(9)	
	O00A Er01 O00G 108.46(8)	
	O00B Er01 O003 72.21(9)	
	O00B Er01 O006 73.73(10)	
	O00B Er01 O007 85.00(10)	
	O00B Er01 O00A 123.89(9)	
	O00B Er01 O00G 50.98(8)	
	O00D Er01 O003 78.22(10)	
	O00D Er01 O005 82.40(10)	
	O00D Er01 O006 125.78(9)	
	O00D Er01 O007 87.76(9)	
	O00D Er01 O00A 74.61(9)	
	O00D Er01 O00B 147.44(9)	
	O00D Er01 O00G 155.77(8)	
	O00D Er01 O00H 85.80(10)	
	O00H Er01 O003 128.16(9)	
	O00H Er01 O005 153.13(9)	
	O00H Er01 O006 88.81(10)	
	O00H Er01 O007 78.13(9)	
	O00H Er01 O00A 74.03(9)	
	O00H Er01 O00B 123.33(8)	
	O00H Er01 O00G 72.54(9)	
III		
In1 O1 2.169(9)	O1 In1 O1 103.6(5)	In1 O1 N1 O2 18.0(14)
In1 O1 2.169(9)	O4 In1 O1 170.9(3)	In1 O1 N1 O3 –164.9(11)
In1 O4 2.127(8)	O4 In1 O1 85.5(3)	In1 O4 C1 N2 –2.4(18)
In1 O4 2.127(8)	O4 In1 O1 85.5(3)	In1 O4 C1 N3 –179.5(8)
In1 O5 2.114(8)	O4 In1 O1 170.9(3)	In1 O5 C2 N4 170.4(9)

Table 3. Continued

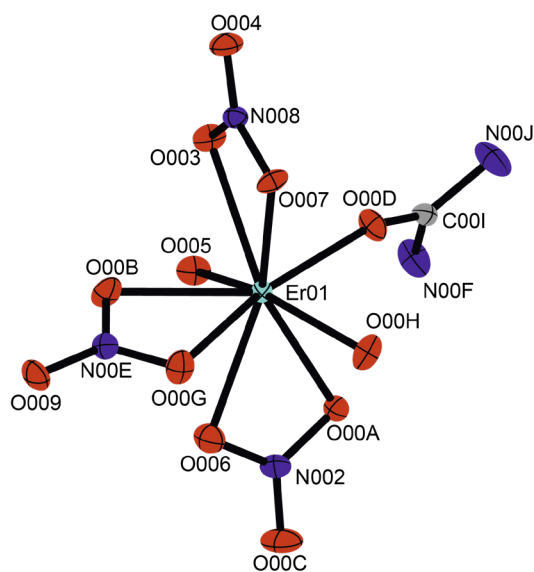
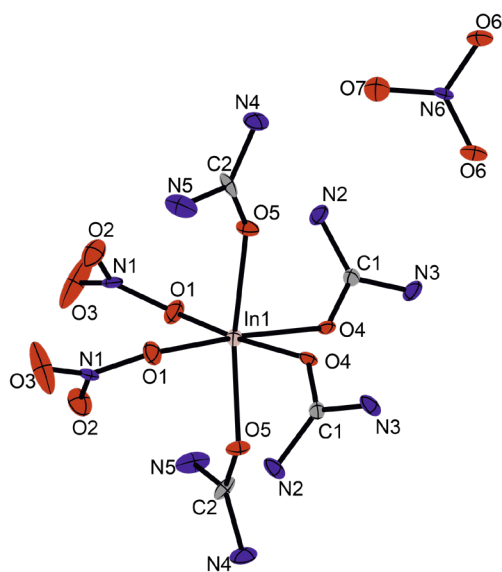
Bond length, Å	Bond angle, °	Torsion angle, °
III		
In1 O5 2.114(8)	O4 In1 O4 85.5(5)	In1 O5 C2 N5 –8(2)
	O5 In1 O1 92.4(3)	
	O5 In1 O1 92.4(3)	
	O5 In1 O1 93.2(3)	
	O5 In1 O1 93.2(3)	
	O5 In1 O4 87.3(3)	
	O5 In1 O4 86.1(3)	
	O5 In1 O4 87.3(3)	
	O5 In1 O4 86.1(3)	
	O5 In1 O5 171.0(5)	

Two water molecules, one urea molecule, and three bidentate chelating nitrate ions are bound to the central ion. The coordination number of the central ion is 9. The coordination polyhedron is a tricapped trigonal prism (Fig. 3). The planar nitrate ligands are located in three mutually perpendicular planes (the angles between them are 72.33°, 85.82°, and 89.36°). The almost planar urea molecule is located at angles of 40.89°, 67.48°, and 79.43° with respect to these planes.

In erbium complex **II** in comparison with gadolinium complex **I**, the radius of the central atom is much smaller resulting in the shorter lengths of metal–oxygen bonds, as well as the number of

coordinated urea molecules (one instead of two). In complexes **I** and **II**, there are no intramolecular hydrogen bonds, but numerous intermolecular hydrogen bonds between coordinated urea molecules, nitrate ions and water molecules of neighboring molecular complexes.

In indium complex *cis*-[In(Ur)₄(NO₃)₂]NO₃ (**III**), the indium/urea ratio is 1:4. The complex has an ionic structure. Four urea molecules and two monodentate nitrate ions occupying *cis* positions are bound to the central atom. One nitrate ion is located in the outer sphere. The coordination number of the central ion is 6. The coordination polyhedron is a distorted octahedron (Fig. 4). The structure is stabilized by hydrogen bonds. Each urea molecule

Fig. 3. Structure of [Er(H₂O)₂(Ur)(NO₃)₃] (**II**).Fig. 4. Structure of [In(Ur)₄(NO₃)₂]NO₃ (**III**).

forms hydrogen bonds of the N–H...O type with the neighboring urea molecule and with inner-sphere or outer-sphere nitrate ions.

CONCLUSIONS

The analysis of the structures of the complexes of gadolinium and erbium nitrates with urea demonstrated, that they are molecular with monodentate water and urea molecules and bidentate chelating nitrate groups in the inner sphere. The decrease in the radius of the central atom leads to a decrease in the number of ligands in the inner sphere of the erbium complex in comparison with the gadolinium complex. Although both complexes contain two water molecules and three nitrate groups, the gadolinium complex contains two coordinated urea molecules, whereas the erbium complex contains one. This leads to a decrease in the coordination number from 10 to 9 and a significant change in the coordination polyhedron. Thus, complex compounds of gadolinium and erbium with a low urea content differ in composition and structure, in contrast to the isostructural compounds $[\text{Ln}(\text{Ur})_4(\text{H}_2\text{O})(\text{NO}_3)_2]\text{NO}_3$ (Ln = Gd, Er) containing four urea molecules. This may be due to the fact that urea loses its structure-forming role with a decrease in the number of coordinated urea molecules. In this case, steric factors determined primarily by the size of the central REE ion become more important.

REFERENCES

1. Varma A., Mukasyan A.S., Rogachev A.S., Manukyan K.V. Solution Combustion Synthesis of Nanoscale Materials. *Chem. Rev.* 2016,116(23):14493–14586. <https://doi.org/10.1021/acs.chemrev.6b00279>
2. Stojanovic B.D., Dzunuzovic A.S., Ilic N.I. Review of methods for the preparation of magnetic metal oxides. In: *Magnetic Ferroelectric, and Multiferroic Metal Oxides*. 2018. P. 333–360. <https://doi.org/10.1016/B978-0-12-811180-2.00017-7>
3. Zhuravlev V.D., Bamburov V.G., Beketov A.R., Perelyaeva L.A., Baklanova I.V., Sivtsova O.V., Vasil'ev V.G., Vladimirova E.V., Shevchenko V.G., Grigorov I.G. Solution combustion synthesis of $\alpha\text{-Al}_2\text{O}_3$ using urea. *Ceram. Int.* 2013;39(2):1379–1384. <https://doi.org/10.1016/j.ceramint.2012.07.078>
4. Abu-Zied B.M. Controlled synthesis of praseodymium oxide nanoparticles obtained by combustion route: Effect of calcination temperature and fuel to oxidizer ratio. *Appl. Surf. Sci.* 2019;471:246–255. <https://doi.org/10.1016/j.apsusc.2018.12.007>

Complex **III** differs from $[\text{In}(\text{Ur})_6](\text{NO}_3)_3$ by the smaller number of coordinated urea molecules. The typical coordination number 6 for indium is achieved by additional coordination of nitrate ions, rather than water molecules, as is usually observed in urea complexes. In this case, a *cis* isomer is formed, and nitrate ions are coordinated as monodentate ligands, which is quite rare.

Acknowledgments

The study was performed using the equipment of the Center for Shared Use at the MIREA – Russian Technological University, the Research Equipment Sharing Center of Physical Methods for Studying Substances and Materials at the Kurnakov Institute of General and Inorganic Chemistry, Russian Academy of Sciences, and the Center for Shared Use at the Kurchatov Institute National Research Center—IREA with the support of the Ministry of Science and Higher Education of the Russian Federation.

Authors' contributions

E.K. Bettels – synthesis;
I.A. Karavaev – IR spectroscopy;
G.A. Buzanov – X-ray powder diffraction;
A.S. Kubasov – X-ray single-crystal diffraction;
E.V. Savinkina – overall supervision, literature review, analysis of results, and writing the text of the article.

The authors declare no conflicts of interest.

СПИСОК ЛИТЕРАТУРЫ

1. Varma A., Mukasyan A.S., Rogachev A.S., Manukyan K.V. Solution Combustion Synthesis of Nanoscale Materials. *Chem. Rev.* 2016,116(23):14493–14586. <https://doi.org/10.1021/acs.chemrev.6b00279>
2. Stojanovic B.D., Dzunuzovic A.S., Ilic N.I. Review of methods for the preparation of magnetic metal oxides. In: *Magnetic Ferroelectric, and Multiferroic Metal Oxides*. 2018. P. 333–360. <https://doi.org/10.1016/B978-0-12-811180-2.00017-7>
3. Zhuravlev V.D., Bamburov V.G., Beketov A.R., Perelyaeva L.A., Baklanova I.V., Sivtsova O.V., Vasil'ev V.G., Vladimirova E.V., Shevchenko V.G., Grigorov I.G. Solution combustion synthesis of $\alpha\text{-Al}_2\text{O}_3$ using urea. *Ceram. Int.* 2013;39(2):1379–1384. <https://doi.org/10.1016/j.ceramint.2012.07.078>
4. Abu-Zied B.M. Controlled synthesis of praseodymium oxide nanoparticles obtained by combustion route: Effect of calcination temperature and fuel to oxidizer ratio. *Appl. Surf. Sci.* 2019;471:246–255. <https://doi.org/10.1016/j.apsusc.2018.12.007>

5. Get'man E.I., Oleksii Yu.A., Radio S.V., Ardanova L.I. Determining the phase stability of luminescent materials based on the solid solutions of oxyorthosilicates ($(\text{Lu}_{1-x}\text{Ln}_x)[(\text{SiO}_4)_{0.5}\text{O}_{0.5}]$, where $\text{Ln} = \text{La}-\text{Yb}$. *Fine Chem. Technol.* 2020;15(5):54–62. <https://doi.org/10.32362/2410-6593-2020-15-5-54-62>
6. Lupin M.S., Peters G.E. Thermal decomposition of aluminum, iron and manganese complexes of urea. *Thermochim. Acta.* 1984;73(1–2):79–87. [https://doi.org/10.1016/0040-6031\(84\)85178-3](https://doi.org/10.1016/0040-6031(84)85178-3)
7. Siekierski S., Salomon M., Mioduski T. (Eds.). *Solubilities Data Series. V. 13. Scandium, Yttrium, Lanthanum and Lanthanide Nitrates*. London: Pergamon; 1983. 514 p.
8. Khudaibergenova N., Sulaimankulov K. Gadolinium nitrate–urea–water and ytterbium nitrate–urea–water systems at 30°C. *Russ. J. Inorg. Chem.* 1980;25(8):1249–1255.
[Original Russian Text: Khudaibergenova N., Sulaimankulov K. Gadolinium nitrate–urea–water and ytterbium nitrate–urea–water systems at 30°C. *Zhurnal Neorganicheskoi Khimii.* 1980;25(8):2254–2260 (in Russ.).]
9. Aitimbetov K., Sulaimankulov K.S., Batyuk A.G., Ismailov V. Systems erbium chloride–urea–water and erbium nitrate–urea–water at 30°C. *Russ. J. Inorg. Chem.* 1975;20(9):1391–1395.
[Original Russian Text: Aitimbetov K., Sulaimankulov K.S., Batyuk A.G., Ismailov V. Systems erbium chloride–urea–water and erbium nitrate–urea–water at 30°C. *Zhurnal Neorganicheskoi Khimii.* 1975;20(9):2510–2515 (in Russ.).]
10. Savinkina E.V., Karavaev I.A., Grigoriev M.S., Buzanov G.A., Davydova M.N. A series of urea complexes with rare-earth nitrates: Synthesis, structure and thermal decomposition. *Inorg. Chim. Acta.* 2022;532:120759. <https://doi.org/10.1016/j.ica.2021.120759>
11. Karavaev I.A., Savinkina E.V., Grigor'ev M.S., Buzanov G.A., Kozerozhets I.V. New Coordination Compounds of Scandium Nitrate with Carbamide: Precursors for the Preparation of Nanosized Scandium Oxide. *Russ. J. Inorg. Chem.* 2022;67(8):1178–1183. <https://doi.org/10.1134/S0036023622080186>
[Original Russian Text: Karavaev I.A., Savinkina E.V., Grigor'ev M.S., Buzanov G.A., Kozerozhets I.V. New Coordination Compounds of Scandium Nitrate with Carbamide: Precursors for the Preparation of Nanosized Scandium Oxide. *Zhurnal neorganicheskoi khimii.* 2022;67(8):1178–1183 (in Russ.). <https://doi.org/10.31857/S0044457X22080189>]
12. Savinkina E.V., Karavaev I.A., Grigoriev M.S. Crystal structures of praseodymium nitrate complexes with urea, precursors for solution combustion synthesis of nanoscale praseodymium oxides. *Polyhedron.* 2020;192:114875. <https://doi.org/10.1016/j.poly.2020.114875>
13. Sanctis S., Hoffmann R.C., Koslowski N., Foro S., Bruns M., Schneider J.J. Aqueous Solution Processing of Combustible Precursor Compounds into Amorphous Indium Gallium Zinc Oxide (IGZO) Semiconductors for Thin Film Transistor Applications. *Chem. Asian J.* 2018;13:3912. <https://doi.org/10.1002/asia.201801371>
14. Ullah S., Branquinho R., Mateus T., Martins R., Fortunato E., Rasheed T., Sher F. Solution Combustion Synthesis of Transparent Conducting Thin Films for Sustainable Photovoltaic Applications. *Sustainability.* 2020;12:10423. <https://doi.org/10.3390/su122410423>
5. Get'man E.I., Oleksii Yu.A., Radio S.V., Ardanova L.I. Determining the phase stability of luminescent materials based on the solid solutions of oxyorthosilicates ($(\text{Lu}_{1-x}\text{Ln}_x)[(\text{SiO}_4)_{0.5}\text{O}_{0.5}]$, where $\text{Ln} = \text{La}-\text{Yb}$. *Fine Chem. Technol.* 2020;15(5):54–62. <https://doi.org/10.32362/2410-6593-2020-15-5-54-62>
6. Lupin M.S., Peters G.E. Thermal decomposition of aluminum, iron and manganese complexes of urea. *Thermochim. Acta.* 1984;73(1–2):79–87. [https://doi.org/10.1016/0040-6031\(84\)85178-3](https://doi.org/10.1016/0040-6031(84)85178-3)
7. Siekierski S., Salomon M., Mioduski T. (Eds.). *Solubilities Data Series. V. 13. Scandium, Yttrium, Lanthanum and Lanthanide Nitrates*. London: Pergamon; 1983. 514 p.
8. Худайбергенова Н., Сулайманкулов К. Системы нитрат гадолиния–карбамид–вода и нитрат иттербия–карбамид–вода при 30°C. *Журн. неорган. химии.* 1980;25(8):2254–2260.
9. Aitimbetov K., Sulaimankulov K.S., Batyuk A.G., Ismailov V. Systems erbium chloride–urea–water and erbium nitrate–urea–water at 30°C. *Russ. J. Inorg. Chem.* 1975;20(9):1391–1395.
10. Savinkina E.V., Karavaev I.A., Grigoriev M.S., Buzanov G.A., Davydova M.N. A series of urea complexes with rare-earth nitrates: Synthesis, structure and thermal decomposition. *Inorg. Chim. Acta.* 2022;532:120759. <https://doi.org/10.1016/j.ica.2021.120759>
11. Караваев И.А., Савинкина Е.В., Григорьев М.С., Бузанов Г.А., Козерожец И.В. Новые координационные соединения нитрата скандия с карбамидом – предшественники для получения наноразмерного оксида скандия. *Журн. неорган. химии.* 2022;67(8):1080–1086. <https://doi.org/10.31857/S0044457X22080189>
12. Savinkina E.V., Karavaev I.A., Grigoriev M.S. Crystal structures of praseodymium nitrate complexes with urea, precursors for solution combustion synthesis of nanoscale praseodymium oxides. *Polyhedron.* 2020;192:114875. <https://doi.org/10.1016/j.poly.2020.114875>
13. Sanctis S., Hoffmann R.C., Koslowski N., Foro S., Bruns M., Schneider J.J. Aqueous Solution Processing of Combustible Precursor Compounds into Amorphous Indium Gallium Zinc Oxide (IGZO) Semiconductors for Thin Film Transistor Applications. *Chem. Asian J.* 2018;13:3912. <https://doi.org/10.1002/asia.201801371>
14. Ullah S., Branquinho R., Mateus T., Martins R., Fortunato E., Rasheed T., Sher F. Solution Combustion Synthesis of Transparent Conducting Thin Films for Sustainable Photovoltaic Applications. *Sustainability.* 2020;12:10423. <https://doi.org/10.3390/su122410423>

About the authors:

Elena V. Savinkina, Dr. Sci. (Chem.), Professor, A.N. Reformatskii Department of Inorganic Chemistry, M.V. Lomonosov Institute of Fine Chemical Technologies, MIREA – Russian Technological University (86, Vernadskogo pr., Moscow, 119571, Russia). E-mail: savinkina@mirea.ru. Scopus Author ID 8419176500, ResearcherID G-2949-2013, RSCI SPIN-code 2302-3375, <https://orcid.org/0000-0002-2088-5091>

Igor A. Karavaev, Cand. Sci. (Chem.), Senior Lecturer, A.N. Reformatskii Department of Inorganic Chemistry, M.V. Lomonosov Institute of Fine Chemical Technologies, MIREA – Russian Technological University (86, Vernadskogo pr., Moscow, 119571, Russia). E-mail: karavaev@mirea.ru. Scopus Author ID 57214990536, ResearcherID HNP-2255-2023

Elizaveta K. Bettels, Postgraduate Student, A.N. Reformatskii Department of Inorganic Chemistry, M.V. Lomonosov Institute of Fine Chemical Technologies, MIREA – Russian Technological University (86, Vernadskogo pr., Moscow, 119571, Russia). E-mail: bettels@mirea.ru. <https://orcid.org/0009-0007-5009-2299>

Grigori A. Buzanov, Cand. Sci. (Chem.), Senior Researcher, Kurnakov Institute of General and Inorganic Chemistry, Russian Academy of Sciences (31, Leninskii pr., Moscow, 119071, Russia). E-mail: gbuzanov@yandex.ru. Scopus Author ID 26026544800, ResearcherID N-8207-2015, RSCI SPIN-code 5945-4169, <https://orcid.org/0000-0003-2676-8774>

Aleksei S. Kubasov, Cand. Sci. (Chem.), Senior Researcher, Kurnakov Institute of General and Inorganic Chemistry, Russian Academy of Sciences (31, Leninskii pr., Moscow, 119071, Russia). E-mail: fobosax@mail.ru. Scopus Author ID 56118634600, ResearcherID J-5588-2016, RSCI SPIN-code 8266-8605, <https://orcid.org/0000-0002-0156-5535>

Об авторах:

Савинкина Елена Владимировна, д.х.н., профессор кафедры неорганической химии им. А.Н. Реформатского, Институт тонких химических технологий им. М.В. Ломоносова, ФГБОУ ВО «МИРЭА – Российский технологический университет» (119571, Россия, Москва, пр-т Вернадского, д. 86). E-mail: savinkina@mirea.ru. Scopus Author ID 8419176500, ResearcherID G-2949-2013, SPIN-код РИНЦ 2302-3375, <https://orcid.org/0000-0002-2088-5091>

Караваяев Игорь Александрович, к.х.н., преподаватель кафедры неорганической химии им. А.Н. Реформатского, Институт тонких химических технологий им. М.В. Ломоносова, ФГБОУ ВО «МИРЭА – Российский технологический университет» (119571, Россия, Москва, пр-т Вернадского, д. 86). E-mail: karavaev@mirea.ru. Scopus Author ID 57214990536, ResearcherID HNP-2255-2023

Беттельс Елизавета Карстеновна, аспирант кафедры неорганической химии им. А.Н. Реформатского, Институт тонких химических технологий им. М.В. Ломоносова, ФГБОУ ВО «МИРЭА – Российский технологический университет» (119571, Россия, Москва, пр-т Вернадского, д. 86). E-mail: bettels@mirea.ru. <https://orcid.org/0009-0007-5009-2299>

Бузанов Григорий Алексеевич, к.х.н., старший научный сотрудник, Институт общей и неорганической химии им. Н.С. Курнакова, Российская академия наук (ИОНХ РАН) (119071, Россия, Москва, Ленинский пр-т, д. 31). E-mail: gbuzanov@yandex.ru. Scopus Author ID 26026544800, ResearcherID N-8207-2015, SPIN-код РИНЦ 5945-4169, <https://orcid.org/0000-0003-2676-8774>

Кубасов Алексей Сергеевич, к.х.н., старший научный сотрудник, Институт общей и неорганической химии им. Н.С. Курнакова, Российская академия наук (ИОНХ РАН) (119071, Россия, Москва, Ленинский пр-т, д. 31). E-mail: fobosax@mail.ru. Scopus Author ID 56118634600, ResearcherID J-5588-2016, SPIN-код РИНЦ 8266-8605, <https://orcid.org/0000-0002-0156-5535>

The article was submitted: February 28, 2023; approved after reviewing: April 10, 2023; accepted for publication: November 06, 2023.

Translated from Russian into English by V. Glyanchenko

Edited for English language and spelling by Thomas A. Beavitt

MIREA – Russian Technological University
78, Vernadskogo pr., Moscow, 119454, Russian Federation.
Publication date *December 31, 2023*.
Not for sale

МИРЭА – Российский технологический университет
119454, РФ, Москва, пр-т Вернадского, д. 78.
Дата опубликования *31.12.2023*.
Не для продажи

www.finechem-mirea.ru

